Doctoral Dissertation

Study on biomimetic locomotion using oscillatory paired limbs

by

Xiaoqian Sun
July 2013

Department of Naval Architecture and Ocean Engineering
Graduate School of Engineering
Osaka University

The Dissertation Committee for Xiaoqian Sun Certifies that this is the approved version of the following dissertation:

Study on biomimetic locomotion using oscillatory paired limbs

Committee:

Professor Naomi Kato, Supervisor

Professor Yasuyuki Toda

Associate Professor Hiroyoshi Suzuki

Abstract

The utilization of paired biomimetic oscillatory limbs can be taken into account as a means of improving the maneuverability of underwater vehicles concurrently with either fully providing or assisting propulsion. Past researches on mechanical pectoral fins of fish and fore flippers of sea turtle concentrate on certain aspects of them (hydrodynamics, material or shape, for instance) and less work has been done on the compatibility between underwater vehicles and paired oscillating limbs.

In this thesis centering on how to apply paired flexible biomimetic flapping limbs onto underwater vehicles and how to investigate the effects of their locomotion on the swimming performance of their attached bodies, a united methodology is proposed to evaluate the performance of flexible artificial pectoral fins and prosthetic fore flippers from the aspects of (1) material properties and manufacturing of the paired oscillating limbs; (2) 3D kinematics of their movement; (3) the fluid dynamics characteristics. Furthermore, as an extension, this dissertation also discusses the characteristics of pectoral fins from the viewpoint of the effect of fin form and flexibility on the motion control of underwater vehicles by allowing the vehicle to carry out a specific task. On the one hand flexible prosthetic flippers are developed for an injured sea turtle “Yu”; on the other hand a series of flexible pectoral fin research is done specific to PLATYPUS, a biomimetic underwater vehicle. The main conclusions are summarized as below:

a) On prosthetic fore flippers of sea turtles

By observing the motion trajectories of fore flippers, it can be seen that on the horizontal plane parallel to the body of sea turtles, the fore flippers of Sho (a healthy sea turtle) and Yu depict a circular arc with large curvature, but in case of Yu equipped with prosthetic flippers, the projecting trajectory on this plane is a circular arc with small

curvature; on the vertical plane from the side view of sea turtles, the projecting trajectories of the fore flippers of Sho and Yu are ovals but in case of Yu equipped with prosthetic flippers the trajectory is similar to an oval with twist at the posterior position for the left prosthetic flipper and at the middle position for the right prosthetic flipper.

The proposed 3D hydrodynamic analysis method based on wing element theory can to some extent evaluate the hydrodynamics of sea turtles' forelimb motion. It shows prosthetic flippers can assist generating thrust but the thrust generated by the right flipper is larger than that generated by the left one. Therefore from the viewpoint of the compatibility between fore flippers and sea turtles, it is better to improve present prosthetic flippers to make both flippers generate equal thrust to make sure that Yu's swimming motion become smooth.

b) On pectoral fins of Fish

Straight forward and backward swimming experiments of PLATYPUS verify that flexible pectoral fins can propel the vehicle faster than rigid ones do within the same fin controlling parameters. Iterative computation of spanwise deformation of asymmetric pectoral fins between Finite Element software and wing theory shows that flexible softer fin can generate larger thrust compared to flexible harder fin and rigid fin; lift force plays an important role in generating thrust; the investigation of tip deformation clarifies that spanwise deformation has positive influence on the generation of thrust for pectoral fins.

Point-to-point (PTP) control tests in still water and water currents are employed to investigate the effects of fin form and flexibility on the motion control of PLATYPUS. From turning ability test of PLATYPUS using only rear fins the azimuth fuzzy control range is selected; from swimming ability test of PLATYPUS using only fore fins the distance fuzzy control range is selected. From the PTP control tests in still water and in water currents, it can be said that the compatibility between underwater vehicles and

pectoral fins changes under different given conditions. First, for different pectoral fins the suitable controlling scheme of the propulsor is different. Second, asymmetric flexible harder fin can propel PLATYPUS faster in straight forward and backward swimming in still water than asymmetric rigid fin and symmetric rigid fin do, and therefore it also does better in PTP control in still water. But during PTP control in water currents the symmetric rigid one has an advantage over the other two.

Acknowledgement

First and foremost, I would like to express my deep gratitude to my academic supervisor—Professor Naomi Kato. He has been always readily available for research guidance and discussions, and in the past five years I have been trained to become a true researcher from identifying research and writing research proposals, to executing research ideas, organizing experiments and carrying out simulation, to writing concise papers and time management during my master and doctoral candidate life. Without his guidance and support, this dissertation would not have been completed.

I am also grateful to Associate Professor Hiroyoshi Suzuki for his kindly guiding and discussing in the area of hydrodynamic calculation. He can always provide very insightful advice and comments. Thanks are also given to Assistant Professor Hidetaka Senga and the past and current students in Kato's laboratory for the technical discussions and friendly support they have provided.

Also I would like to express appreciate to Professor Yasuyuki Toda for agreeing to serve in my PhD committee despite his very full schedule, and for his precious comments and discussions.

I acknowledge Japan Ministry of Education, Culture, Sports, Science and Technology (MEXT) for providing Japanese Government (Monbukagakusho) scholarship for both my master and doctoral course in the past five years.

Finally, and most importantly, I am indebted to the love and support that I have received from my family members. In special, I am thankful to my parents and elder sister, who made several sacrifices to ensure that I could pursue my dream of furthering the education abroad to master and PhD. Deepest gratitude is given to my mother for her immense emotional support and constant encouragement.

Nomenclature

In Chapter 2

$\gamma,\ \varphi$	Euler angles
β	The relative pitch angle
$\alpha_{1/4}$	Geometric angle of attack
C_L, C_D	Geometric lift and drag coefficients
α_{eff}	Effective angle of attack
$(C_L)_{eff}, (C_D)_{eff}$	Effective lift and drag coefficients
C_{Di}	Induced drag coefficient
AR	Aspect ratio of fore flipper of sea turtles
L'', D''	Actual lift and drag force acting on the wing segment in $o''-x''y''z''$
T'', Z''	Thrust and lateral force acting on the wing segment in $o''-x''y''z''$
T, Z	Thrust and vertical force acting on the wing segment in $O-XYZ$
δ, ψ	The upper view projecting value and the side view projecting value of the angle between the line located at the spanwise middle of the flipper and the carapace line of sea turtle

In Chapter 3, 4

μ	The shear modulus of the material in the undeformed stress-free configuration
$\Phi_R, \Phi_{FL}, \Phi_{FE}$	The instant rowing angle, the instant flapping angle and the instant flapping angle of pectoral fin
$\Phi_{R0}, \Phi_{FL0}, \Phi_{FE0}$	The initial rowing angle, the initial flapping angle and the initial feathering angle of pectoral fin

$\Phi_{RA}, \Phi_{FLA}, \Phi_{FEA}$	The amplitude of rowing angle, the amplitude of flapping angle and the amplitude of feathering angle of pectoral fin
$\Delta\Phi_{FL}$	Phase difference between flapping motion and rowing motion of pectoral fin
$\Delta\Phi_{FE}$	Phase difference between feathering motion and rowing motion of pectoral fin
ω_{fin}	Circular frequency of fin motion
f	Frequency of fin motion
c	Maximum chord length of pectoral fin
b	Span of pectoral fin
AR	Aspect ratio of pectoral fin
φ	The azimuth of underwater vehicle
$E\varphi, \Delta E\varphi$	Input variables in fuzzy rule of azimuth control
$\delta E\varphi$	Output variable in fuzzy rule of azimuth control
X	Current distance of the underwater vehicle
$Ex, \Delta Ex$	Input variables in fuzzy rule of distance control
δEx	Output variable in fuzzy rule of distance control

Abbreviations

Sym-rigid	Symmetric rigid pectoral fin
Asym-rigid	Asymmetric rigid pectoral fin
Asym-harder	Asymmetric harder flexible pectoral fin
Asym-softer	Asymmetric softer flexible pectoral fin
PTP	Point-to-point control test

Table of Contents

List of Tables

List of Figures

Chapter 1 Introduction

1.1 Background and Challenges

Natural selection has ensured that the locomotion mechanisms employed by aquatic animals, although not necessarily optimal, are highly efficient with regard to their habitats and modes of life for each species [1]. Their often remarkable agilities [2] have been inspiring innovative designs to improve the ways that man-made systems operate in and interact with the underwater environment. Hence by mimicking the swimming of marine animals, many biomimetic underwater vehicles were developed. Significant work in this area was initiated in the 1990s by Triantafyllou et al., who developed the Robo-Tuna [3] and its descent, the Vorticity Control Unmanned Undersea Vehicle [4], both of which have a flexible, tuna-f shaped hull and are propelled by an oscillating caudal fin. Following that, many other robotic fish were manufactured, such as PF200-700 and UPF2001 robots (NMRI, Japan) [5], G1-G5 and MT1 robots (Essex Univ., England) [5], and so on. The propulsion systems of the first biomimetic underwater vehicles mentioned above focuses on cruising/sprinting specialists or acceleration specialists that necessarily move by axial undulation [6, 7].

However, the existing underwater robots, the motion of which is usually controlled by screw-type thrusters and wings, exhibit poor performance not only in hovering and turning over intricate seabed terrain in strong currents, but also in dexterous manipulation under floating conditions. Based on the fact that many aquatic animals employ one or more pairs of oscillating pectoral fins (fish) or flippers (sea turtles, penguins, whales, seals, dolphins and so on.) to increase both stability and maneuverability, it is reasonable to believe that the utilization of paired biomimetic

oscillating limbs can be taken into account as a means of improving the maneuverability of underwater vehicles concurrently with either fully providing propulsion or assisting propulsion.

Because of the frequent usage of pectoral fins of fish and forelimbs of sea turtles as the models of paired oscillating propulsors, here these two are compared. From the view of anatomy, pectoral fins and fore flippers are completely different, as pectoral fins are comprised of membranous appendages and connective tissue or fragile bony spines protruding from the body but fore flippers, which contain bones similar to a human hand with cartilage and connective tissue surrounding the bones in a thicker manner, are evolved from legs and become flat broad limbs specialized for an aquatic animal's swimming. Another difference is that fore flippers can be used as legs to walk on the land, but pectoral fins usually do not possess this function. But in fact pectoral fins and flippers possess many similarities: firstly morphologically most fore flippers and pectoral fins are located at both sides of the front end of a marine animal's body. Secondly from the viewpoint of functionalism fore flippers can provide propulsion and maneuvering forces, and so can pectoral fins of fishes in the Labriform swimming mode. Thirdly from the view of kinematics, for both the fore flippers and pectoral fins, the propulsive forces are generated by two primary kinematic modes: flapping and rowing. In flapping locomotion, the propulsive appendages reciprocate in a stroke plane largely orthogonal to the resultant force vector and the lift force is the predominant component [8, 9]. In rowing, propulsive forces are produced during the power stroke by both the drag force acting on a translating appendage and the reaction forces generated by the acceleration of fluid relative to the body [9].

Although so many similarities shared by pectoral fins of fish and the fore flippers of sea turtles, most researchers in the past studied these two propulsors separately.

1.1.1 Reviews on Fore Flippers of Sea Turtles

Turtle species exhibit a diversity of kinematic patterns in their forelimbs during swimming. Generally speaking, the flapping forelimb strokes are usually employed by marine turtles and the rowing forelimb strokes are usually used by most freshwater turtles, which have been documented in an extensive range of previous studies [10, 11, 12, 13, 14]. In the case of turtles, flapping strokes are characterized by predominantly dorsoventral forelimb movements, whereas rowing strokes are characterized by predominantly anteroposterior forelimb movements combined with rotation of the foot (perpendicular to flow during thrust and feathered during recovery) [15].

Inspired by the fore flipper motion of sea turtles, Konno et al. developed a turtle-like submersible vehicle, which is propelled by fore fins flapping and maneuvered by a combination of flapping and feathering motion. The two fore fins are rigid and have two degrees of freedom: flapping and feathering motions [16]. Long et al. constructed an aquatic robot named Madeleine with four flexible flippers in Vassar College, but each of them can only carry out pitching motion [17]. By implementing the kinematics of the live sea turtle on the biomimetic vehicle Finnegan, Licht et al. developed four independently controlled high aspect ratio rigid fins with two-degree of freedom angular motion, which enabled them to simulate the animal's function to some degree [18]. Kato group designed and developed an amphibious robot RT-I equipped with two pairs of rigid fin actuators by combining the swimming of sea turtles and the walking of tortoise, and each of the fin can carry out four-degree of freedom: flapping, rowing, feathering and elbow rotating [19]. Zhao et al. constructed a turtle-like underwater robot with four rigid mechanical flippers, and each flipper consists of two joints generating a rowing motion by a combination of lead-lag and feathering motions [20]. In order to mimic the soft-morphing deformation of a marine animal's movement, Kim et al. fabricated a turtle-like swimming

robot with a novel actuating mechanism. The two fore flippers are made of smart soft composite structure and can realize smooth soft flapping motion [21]. Font et al. presented the design and implementation of a rigid turtle hydrofoil for an autonomous underwater vehicle, and four alternative hydrofoil propulsion mechanisms (four bar mechanism, differential mechanism, ball-and-socket mechanism and pulley mechanism) were proposed and evaluated in terms of compactness, motion amplitude, sealing and torque requirements [22].

1.1.2 Reviews on Pectoral Fins of Fish in Labriform Propulsion Mode

Kinematic studies of fish swimming indicate that pectoral fin propulsion can be utilized for underwater vehicles in the drag-based labriform swimming mode at low swimming speeds and in the lift-based labriform swimming mode at high cruising speeds [23, 24]. The former is characterized by the rowing action of pectoral fins forming a large angle with the horizontal axis of the fish body. The latter is characterized by the flapping action of pectoral fins forming a small angle with the horizontal axis of the fish body.

Rigid pectoral fins have been documented in many papers. But recent studies of fish locomotion reveal that fish fins exhibit much greater flexibility than previously suspected and that there is considerable deformation of fin surface during locomotion [25]. Many aquatic organisms exploit the flexibility of their fins/wings to achieve high maneuverability at low speeds. It is probable that flexible fin actuators should have an advantage over the rigid ones in both efficiency and maneuverability.

On the one hand, many researchers developed different kinds of flexible pectoral fins to investigate their performance or to propel underwater vehicles. Kato group constructed Active Pneumatic Actuator Fin and Passive Flexible Fin to investigate their load characteristics [26, 27]. With the pectoral fins of the bird wrasse as the prototype,

Palmisano et al. manufactured a pair of flapping fins with actively controlled curvature for an unmanned underwater vehicle, each of which is comprised of five independent compliant ribs connected by a flexible skin of thickness 0.4mm [28]. By learning from the kinematics of bluebill sunfish, Tangorra et al. developed a series of biorobotic fins, each of which uses five flexible fin rays attached to hinges mounted in curved, rigid base and interconnected by webbings of thin polyester and elastane weaves, and the effects of fin stiffness and the shape of fin rays on hydrodynamics were investigated [29]. Geder et al. described the tradeoffs between performance and produceability during the bio-inspired design of an actively controlled curvature pectoral fin and the incorporation of it into both two-fin and four-fin swimming underwater flight vehicles [30].

On the other hand, the collaboration with experimentalists (biologists and engineers), through a multi-disciplinary effort, has enabled high-fidelity data to be used in the computational analysis, which is helpful in elucidating the role of flexibility in fin motions. Liu et al. studied the effect of spanwise flexibility to the performance of oscillating propulsors [31]. Bose [32] and Prempraneerach et al. [33]] investigated the effect of chordwise flexibility on the performance of a flapping foil separately. Shoele and Zhu carried out fluid-structural interaction analysis of skeleton-reinforced fins and concluded that structural flexibility of the fin rays leads to passive deformation of the fin, which could increase the thrust generation and the propulsion efficiency [34]. Taft et al. proposed that the pectoral fin is divided into functional as well as morphological regions and that the fin rays in each functional region have distinct roles during steady swimming in sculpin [35]. Ramakrishnan et al. reinforced the notion that the dorsal leading edge of the bluegill's pectoral fin dominates the overall performance during steady swimming propulsion and further put forward the proposition that besides the dorsal region, the ventral region of the pectoral fin also plays an important role in modulating maneuvering

forces [36]. Tangorra et al. studied how fins are regulated in response to external disturbances and concluded that the response of pectoral fins to large deformation is not reflexible and that fin motions are regulated when it is necessary to correct for disturbances to the motion of the fish [37].

1.1.3 Objective of This Dissertation

Close scrutiny of the previous research on mechanical fore flippers of sea turtles shows that there are two drawbacks: One is that most of them are rigid ones, while the actual flippers are flexible; the other is that its motion is constrained in the certain degree(s) of freedom, because the use of conventional actuators, such as motors and pistons, can restrict synthesizing the movements and scales of biological mechanisms, therefore it cannot mimic biological movements exactly [38].

As for the case of pectoral fin, many more types of rigid and flexible fin were developed than mechanical fore flippers. And also the implementation of its motion has fewer constraints than that of mechanical fore flippers. But most of the researches were concentrated on the hydrodynamics study of fin, only a little work was done on how flexible fins apply to underwater vehicle propulsion, and even less work on the compatibility between underwater robots and flexible pectoral fins.

Although it seems there should be much more work need to be done for flexible mechanical fore flippers than flexible pectoral fin, they possess the some future problem—how to apply them onto and how to evaluate the effect of their locomotion on the swimming performance of biomimetic underwater vehicles. According to the similarities shared by the two, one idea comes up: does any universal methodology exist for investigating the performance of both flexible fore flippers and flexible pectoral fins, or further other flexible paired oscillating propulsors.

In this dissertation a united way is narrated to evaluate the performance of flexible artificial pectoral fins and prosthetic fore flippers. A full understanding of the effect of flexible paired oscillating limbs on the swimming performance of the attached body can be achieved by incorporating descriptions of (1) material properties and manufacturing of the propulsors; (2) 3D kinematics of propulsor movement; (3) the fluid dynamics effects of propulsor motion on the attached body. In addition, as an extension, the characteristics of pectoral fins is also investigated from the viewpoint of the effect of fin form and flexibility on the motion control of the attached underwater vehicles by allowing the vehicle to carry out a specific task. The duplication of these three components would allow for further experimental investigation of changes to propulsor design and for testing of hypothesized relationships between movement and force production. Such a comprehensive suite of data is not yet available for any flexible paired flapping propulsors.

Here it should be emphasized that the prosthetic fore flippers study concentrates on the swimming locomotion of marine turtles and that the pectoral fin study here concentrates on the pectoral fins of fish relying on labriform propulsion for sustained cruising. On the one hand many flexible prosthetic fore flippers are developed for an injured sea turtle “Yu” in order to find the most suitable type; One the other hand, a series of flexible pectoral fin research is done specific to PLATYPUS, a biomimetic underwater vehicle developed by Kato Laboratory in Osaka University.

1.2 Overview and Contribution of This Dissertation

This dissertation summarizes our research program with the goal of producing a comprehensive data set for each of the three components noted above through evaluating the flapping of flexible prosthetic fore flippers on the swimming performance of sea

turtles and the flapping of flexible pectoral fins on the swimming performance of PLATYPUS.

It is constructed with five chapters, acknowledgements, appendix and bibliography. The background and objectives of this dissertation have already been shown in this chapter. The other chapters are summarized as follows:

Chapter 2 illustrates the research on forelimb propulsion of sea turtles with prosthetic flippers. Firstly, template matching method is adopted to track and compare the 3D movements of fore flippers in three cases respectively: that of a healthy turtle named "Sho", that of Yu without prosthetic flippers and that of Yu with prosthetic flippers. The trajectories of three cases are discussed and the effect of prosthetic flippers on flipper kinematics is clarified. Secondly, 3D hydrodynamic analysis for three cases based on quasi-steady wing element theory are carried out to investigate the hydrodynamic effects of prosthetic flippers on the swimming performance of the sea turtle comparing with the other two cases. Some mechanisms of forelimb propulsion of sea turtle are clarified and also remarks for the design of next generation's prosthetic flippers in the future are given.

Chapter 3 and Chapter 4 investigate the effects of flexibility and chordwise crosssection of pectoral fins on the swimming performance of PLATYPUS by designing and making new types of pectoral fins. In Chapter 3 fundamental experiments show the roles of both fin flexibility and chordwise crosssection in propelling underwater vehicle, and in the meantime iterative computation of spanwise deformation between Finite Element software and wing theory analyzes the hydrodynamic characteristics of these new pectoral fins. In Chapter 4 Point-to-Point control tests in still water and water currents check the different performances of each fin in carrying out specific task and the fuzzy control rules are revised to find the most suitable one for each fin respectively.

Finally, in Chapter 5, based on the results of the previous chapters, the manufacturing, kinematics and hydrodynamics of flexible prosthetic fore flippers of sea turtles and flexible mechanical pectoral fins are concluded and the united method of evaluating the performance of flexible paired flapping appendages is concluded. Also the future works are listed sequentially.

Chapter 2 Analysis of Forelimb Propulsion of Sea Turtles with Prosthetic Flippers

2.1 Introduction

An injured female loggerhead sea turtle (*Caretta caretta*) named “Yu” was found and rescued by Sea Turtle Association of Japan at Kiisuido in the summer of 2008. Her swimming speed was just 60% of that of healthy adult sea turtle because only a half of the left forelimb and two thirds of the right forelimb were left after being attacked by a shark. Realizing that we could not put her back into the sea under such a condition, “Yu Project” has begun since 2009 to develop prosthetic flippers for her in cooperation with veterinarians, a prosthetic company, aquariums, universities and a public administration.

Yu, as a sea turtle, belongs to the flapping stroke types. But specifically speaking, sea turtle species display considerable diversity in their styles of forelimb flapping. So quantifying the exact forelimb kinematics and the corresponding thrust forces during turtles’ swimming is a key, which is a significant challenge because direct measurements of force generated by the free turtles’ flapping are not feasible.

Davenport et al. estimated the thrust force by attaching a force transducer to the shells of turtles [39]. But this still puts some restriction on the free swimming of turtles. Walker et al. documented the changes in velocity and acceleration in aquatic locomotion by tracking the center of mass of an animal through an artificial locomotor cycle [40]. Some other reaearchers tried to obtain the thrust force by examining the properties of the flow field around the aquatic animals. For example Drucker et al. employed digital particle image velocimetry (DPIV) to examine the vortex wake shed by freely swimming fish and then evaluated the thrust force [41].

Chapter 2. Analysis of forelimb propulsion of sea turtle

This chapter introduces a new method to quantify the forelimb kinematics and the corresponding thrust force by directly observing the forelimb movements of sea turtles and calculating the corresponding hydrodynamic forces. Previously Isobe et al. [42] compared the 2D (two-dimensional) and 3D (three-dimensional) motions of fore flippers between Yu itself, Yu equipped with prosthetic flippers and a healthy sea turtle in a pool of an aquarium, an artificial lagoon and a water circulating tank. At the same time assuming the flipper consists of a rigid wing with uniform flapping, rowing and feathering motion from root to tip, they analyzed 2D hydrodynamic characteristics of different flippers under uniform flow.

On account of the 3D motion of fore flippers, it is thought that 2D hydrodynamic analysis cannot accurately evaluate the swimming performance of sea turtles. In the following 3D hydrodynamic analyses, the flipper is treated as flexible in spanwise direction and consists of several wing segments with different flapping, rowing and feathering motion from root to tip. The purpose is to contribute to design and development of prosthetic flippers from the viewpoint of 3D hydrodynamic analysis of the forelimb propulsion of marine turtles.

2.2 Sea Turtles and Prosthetic Flippers

2.2.1 Specifications of Sea Turtles

Specifications of the injured sea turtle Yu and the healthy sea turtle Sho, used as comparison, are given in Table 2.1 and Figure 2.1.

Table 2.1 Specifications of Yu and Sho

Name	Carapace length	Body mass	Area (left flipper)	Area (right flipper)
Yu	0.797 [m]	100.5 [kg]	0.039 [m^2]	0.026 [m^2]
Sho	0.751 [m]	84.8 [kg]	0.063 [m^2]	0.067 [m^2]

Figure 2.1 Photographs of Yu (left) and Sho (right)

2.2.2 Manufacturing of Prosthetic Flippers

The prosthetic flippers for Yu are made of a kind of copolymers by Kawamura Gishi Co. Ltd. The left and right ones are shown in Figure 2.2. At first we let Yu put on the specially designed jacket (Figure 2.3). And then the prosthetic flippers are installed onto the corresponding forelimb of Yu. Finally Velcro tape is used to tighten the prosthetic flippers around each sleeve of the jacket. Honestly speaking, the present shape of prosthetic flippers and the procedure of installing them onto the forelimbs are the results of many trials and errors in the past. The specially designed jacket has the function of avoiding the prosthetic flippers coming off the forelimb.

Chapter 2. Analysis of forelimb propulsion of sea turtle

Figure 2.2 Left and right prosthetic flippers for Yu

Figure 2.3 Specially designed jacket for Yu equipped with both prosthetic flippers

Figure 2.4 Upper view of Yu with prosthetic flippers

2.3 3D Kinematic Analysis of Sea Turtle's Fore Flippers

2.3.1 Method of 3D Kinematic Analysis

A motion capturing software using template matching method was utilized to observe forelimb movements in the form of time variation of the prescribed points on the forelimbs. As Sho is healthy and possesses symmetric fore flippers, only the movements of its left fore flipper during swimming is analyzed. But as for the case of Yu, because its actual left flipper and actual right flipper show different shapes, the movements of both flippers is needed to be analyzed in the following context. Locations of the targeted points on Sho's left flipper, Yu's flipper and the prosthetic flippers are shown in Figure 2.5, Figure 2.6 and Figure 2.7 respectively. Two targeted points located in the spanwise middle of the flipper are used to obtain the feathering motion of the flipper. The body fixed coordinate is defined in Figure 2.8. In the following context Lroot, LM and Ltip denote the root, the middle and the tip of left flipper, respectively; Rroot, RM and Rtip denote the root, the middle and the tip of right flipper respectively.

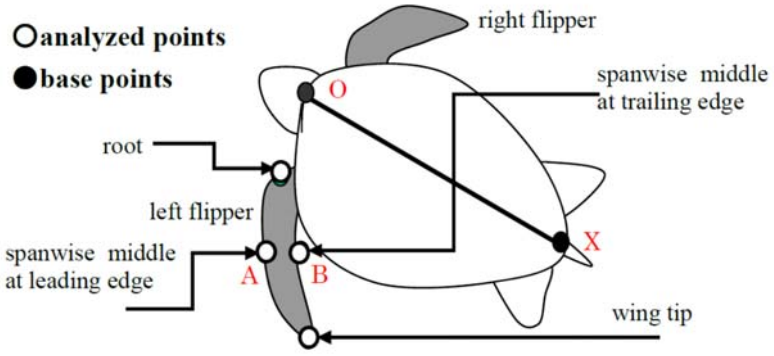

Figure 2.5 Motion captured points on Sho's left flipper

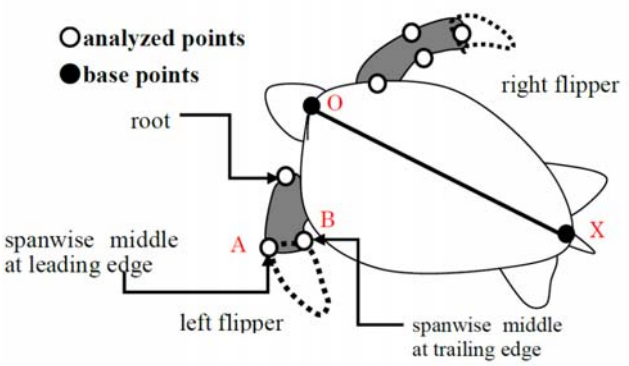

Figure 2.6 Motion captured points on Yu's fore flippers

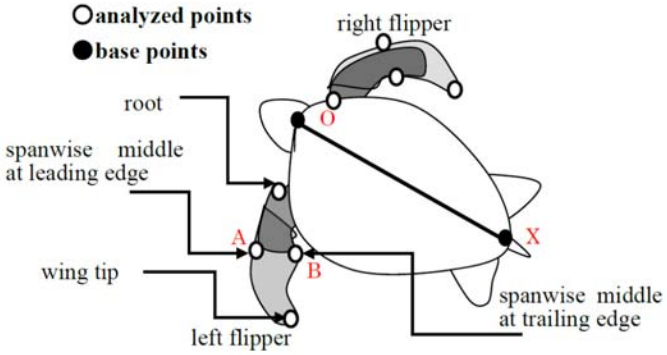

Figure 2.7 Motion captured points on the prosthetic flippers

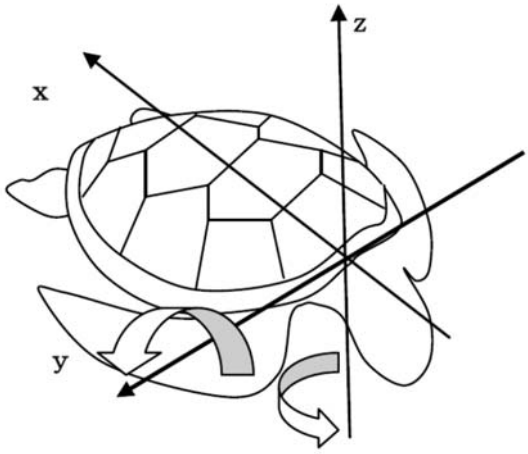

Figure 2.8 Body fixed coordinates during motion analysis

2.3.2 Experimental Condition

Three videos were taken simultaneously from the left side, the right side and the upper side of Sho, Yu without prosthetic flippers and Yu with prosthetic flippers at the water tank of Suma Aqualife Park KOBE.

2.3.3 Results of 3D Kinematic Analysis

Figure 2.9 shows the trajectories of the motion captured points on the left flipper of Sho in x-y plane of the body fixed coordinate. The period of motion is 3.0s. Figure 2.10 shows the trajectories of the motion captured points on the left and right flippers of Yu without prosthetic flippers in x-y plane of the body fixed coordinate separately. The period is 2.4s. Figure 2.11 shows the trajectories of the motion captured points on the left and right prosthetic flippers of Yu in x-y plane of the body fixed coordinate separately. The period is 2.93s. First of all it is observed that Yu swims with a bigger frequency of flipper movements than Sho does, but if the prosthetic flippers are installed, the flipper movement frequency of Yu decreases. From these figures it can be seen that the flippers of Sho and Yu describe a circular arc with large curvature in both the power stroke (from anterior position to posterior position) and the recovery stroke (from posterior position to anterior position). On the other hand, in the case of Yu equipped with prosthetic flippers, the trajectory of flippers in x-y plane is a circular arc with small curvature.

Figure 2.12 shows the trajectories of the motion captured points on the left flipper of Sho in x-z plane of the body fixed coordinate. Figure 2.13 shows the trajectories of the motion captured points on the left and right flippers of Yu without prosthetic flippers in x-z plane of the body fixed coordinate. Figure 2.14 shows the trajectories of the motion captured points on the left and right prosthetic flippers of Yu in x-z plane of the body fixed coordinate. The trajectories of the flippers of Sho and Yu are ovals but in the case

of Yu equipped with prosthetic flippers the trajectory of the flippers is similar to an oval with twist at the posterior position for the left prosthetic flipper and at the middle position for the right prosthetic flipper.

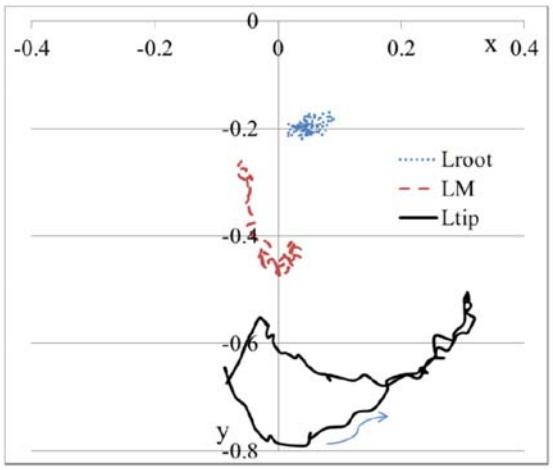

Figure 2.9 Trajectories of motion captured points on the left flipper of Sho in x-y plane (period: 3.0s)

(The arrows in Figure 2.9-2.14 denote trajectory direction with time variation)

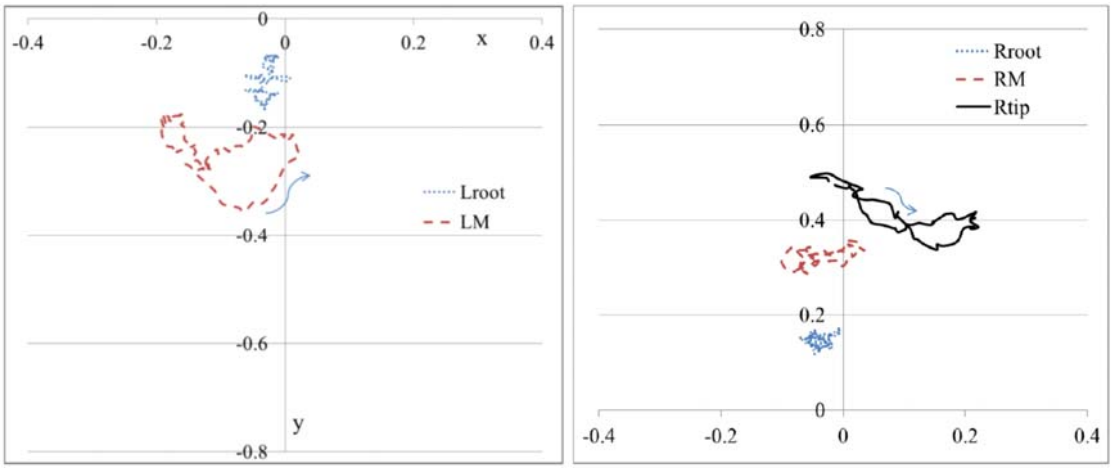

Figure 2.10 Trajectories of motion captured points on the left flipper (left panel) and the right flipper (right panel) of Yu without prosthetic flippers in x-y plane (period: 2.4s)

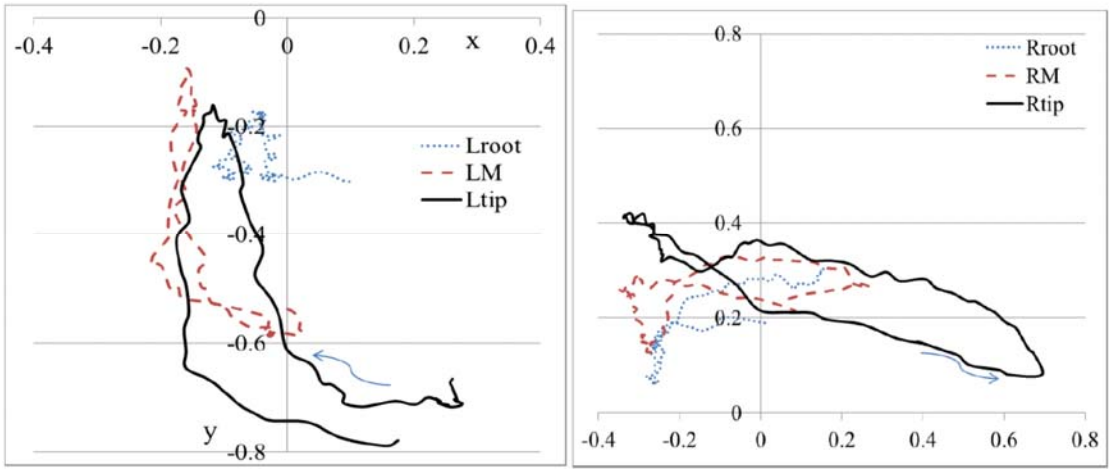

Figure 2.11 Trajectories of motion captured points on the left prosthetic flipper (left panel) and the right prosthetic flipper (right panel) of Yu in x-y plane (period:2.93s)

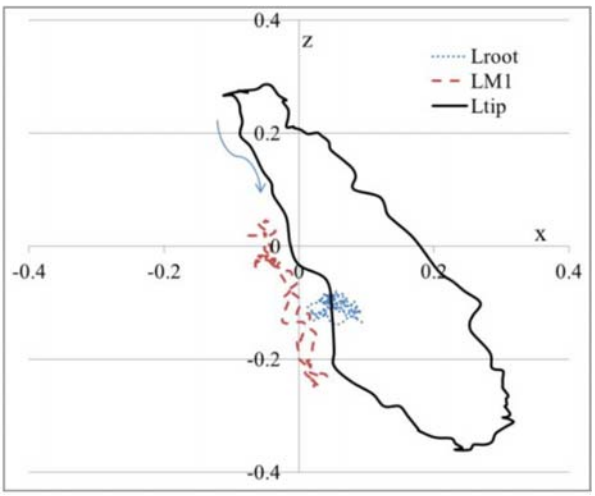

Figure 2.12 Trajectories of motion captured points on the left flipper of Sho in x-z plane

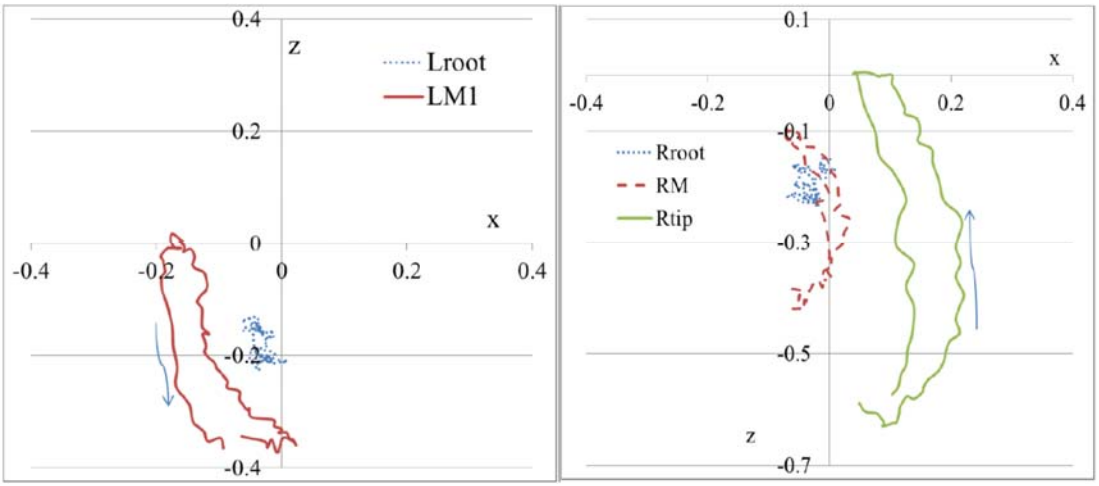

Figure 2.13 Trajectories of motion captured points on the left flipper (left panel) and the right flipper (right panel) of Yu without prosthetic flippers in x-z plane

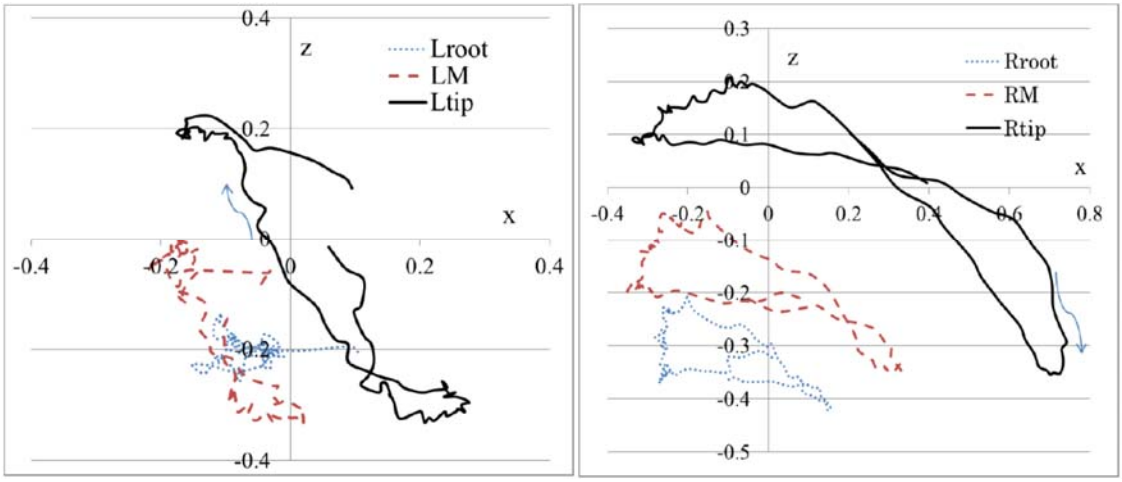

Figure 2.14 Trajectories of motion captured points on the left prosthetic flipper (left panel) and right prosthetic flipper (right panel) of Yu in x-z plane

2.4 Method of Hydrodynamic Analysis of Turtles' Forelimb Propulsion

2.4.1 Coordinates Definition

Chapter 2. Analysis of forelimb propulsion of sea turtle

Altogether four coordinates are defined during hydrodynamic analysis (Figure 2.15).

$O-XYZ$: The front point of the carapace is set as the origin and the centerline of the carapace as the X-axis.

$o-xyz$: The origin is located at the leading point of one cross section of the forelimb. The three axes are parallel to the axes of $O-XYZ$ respectively.

$o'-x'y'z'$: The origin is located at the leading point of the same cross section of the forelimb. $o'-x'y'z'$ can be obtained by rotating $o-xyz$ around axis $o-z$ with the angle of γ.

$o''-x''y''z''$: The origin is also located at the leading point of the same cross-section. Plane $o''-x''z''$ coincides with the cross section. $o''-x''y''z''$ can be got by rotating $o'-x'y'z'$ around $o'-x'$ with the angle of φ.

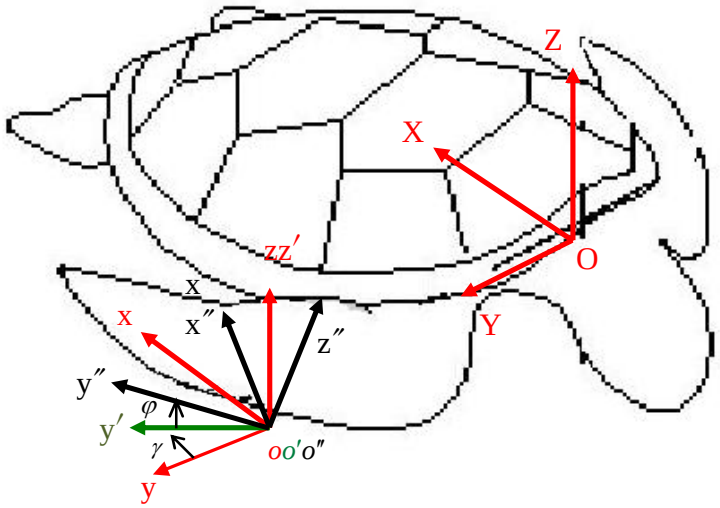

Figure 2.15 Coordinates definition during hydrodynamics analysis

Assume an arbitrary $\vec{r}$ has different Cartesian components in different coordinates:

$O-XYZ:\ (\vec{r})_{O-XYZ}=(r_X,r_Y,r_Z)$

$o-xyz:\ (\vec{r})_{o-xyz}=(r_x,r_y,r_z)$

$o'-x'y'z':\ (\vec{r})_{o'-x'y'z'}=(r_{x'},r_{y'},r_{z'})$

$o''-x''y''z'':\ (\vec{r})_{o''-x''y''z''}=(r_{x''},r_{y''},r_{z''})$

Then the following relationships can be given:

$$\begin{pmatrix} x \\ y \\ z \end{pmatrix}=\begin{pmatrix} X \\ Y \\ Z \end{pmatrix}-\begin{pmatrix} X_o \\ Y_o \\ Z_o \end{pmatrix} \tag{2.1}$$

$$\begin{pmatrix} x' \\ y' \\ z' \end{pmatrix}=R_Z(\gamma)\begin{pmatrix} x \\ y \\ z \end{pmatrix}=\begin{pmatrix} \cos\gamma & \sin\gamma & 0 \\ -\sin\gamma & \cos\gamma & 0 \\ 0 & 0 & 1 \end{pmatrix}\begin{pmatrix} x \\ y \\ z \end{pmatrix} \tag{2.2}$$

$$\begin{pmatrix} x'' \\ y'' \\ z'' \end{pmatrix}=R_X(\varphi)\begin{pmatrix} x' \\ y' \\ z' \end{pmatrix}=\begin{pmatrix} 1 & 0 & 0 \\ 0 & \cos\varphi & \sin\varphi \\ 0 & -\sin\varphi & \cos\varphi \end{pmatrix}\begin{pmatrix} x' \\ y' \\ z' \end{pmatrix} \tag{2.3}$$

2.4.2 Determination of Euler Angle γ and φ

During flipper movement, the shape of forelimb changes instantly as a combination of flapping, rowing and feathering motions and its flexibility. In order to reflect the direction variation as accurately as possible, each forelimb is divided into four sections. Every moment inside each section all the body fixed coordinates can be assumed to possess the same direction properties, namely at each moment inside each section the values of γ and φ for different cross sections are uniquely determined separately. The division of Sho's left flipper is taken as example below (Figure 2.16).

The values of γ and φ of Section Lroot-LI2-LI1 can be calculated by considering the direction of Triangle Lroot-LI2-LI1, which can be assumed to be included in the

representative surfaces of this section. For the other three sections the same method is adopted.

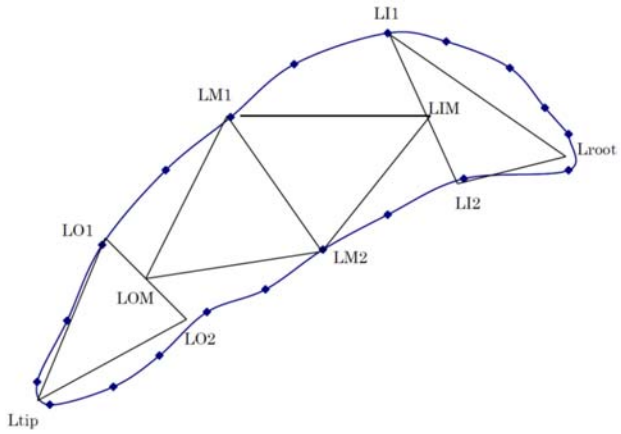

Figure 2.16 Division of Sho's left forelimb during the determination of Euler angles

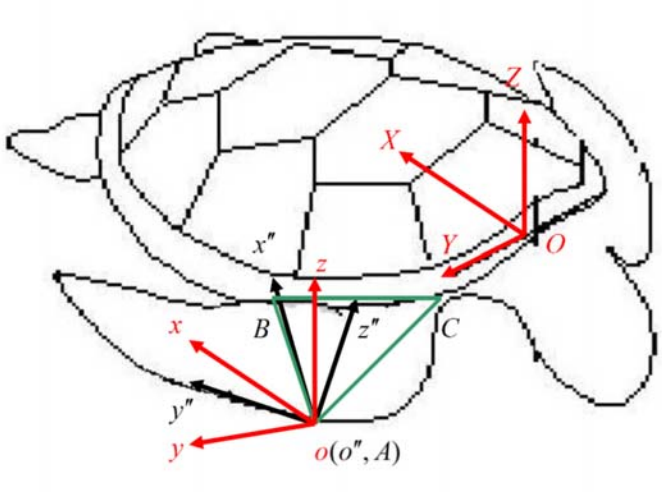

Figure 2.17 Determination of Euler angle γ and φ

Next only one section is concentrated to get the values of γ and φ for that section (Figure 2.17). Line segment AB denotes the chord of one cross section (LI1-LI2, LM1-LM2 or LO1-LO2 in Figure 2.16) that lies in the plane $o''-x''z''$, and that C denotes one point (Lroot, LIM, LOM or Ltip in Figure 2.16) of the triangles above.

Chapter 2. Analysis of forelimb propulsion of sea turtle

In coordinate $O-XYZ$, the values of $A(X_A,Y_A,Z_A)$, $B(X_B,Y_B,Z_B)$ and $C(X_C,Y_C,Z_C)$ can be obtained by movement analysis. Then the expression of surface ABC can be given as follows:

$$\begin{vmatrix} X-X_A & Y-Y_A & Z-Z_A \\ X_B-X_A & Y_B-Y_A & Z_B-Z_A \\ X_C-X_A & Y_C-Y_A & Z_C-Z_A \end{vmatrix} = 0 \tag{2.4}$$

In coordinate $o-xyz$ according to (2.1), (2.4) can be converted to the expression:

$$\begin{vmatrix} x & y & z \\ x_B & y_B & z_B \\ x_C & y_C & z_C \end{vmatrix} = 0 \tag{2.5}$$

This determinant can be expanded as follows:

$$\left(y_B z_C - y_C z_B\right)x - \left(x_B z_C - x_C z_B\right)y + \left(x_B y_C - x_C y_B\right)z = 0 \tag{2.6}$$

Therefore $\vec{m}$, a normal vector to surface ABC, should have the following expression:

$$\vec{m} = \begin{pmatrix} y_B z_C - y_C z_B \\ x_C z_B - x_B z_C \\ x_B y_C - x_C y_B \end{pmatrix} \tag{2.7}$$

On the other hand, the unit vector of axis $o''-y''$ is given as:

$$\vec{n}_{(o''-x''y''z'')} = \begin{pmatrix} 0 & 1 & 0 \end{pmatrix} \tag{2.8}$$

The expression of this unit vector in coordinate $o-xyz$ can be got by using (2.2) and (2.3).

$$\vec{n}_{(o-xyz)} = R_Z^{-1}(\gamma)R_X^{-1}(\varphi)\begin{pmatrix} 0 \\ 1 \\ 0 \end{pmatrix} = \begin{pmatrix} -\sin\gamma\cos\varphi \\ \cos\gamma\cos\varphi \\ \sin\varphi \end{pmatrix} \tag{2.9}$$

If we assume $o''-y''$ is in the plane ABC, we have that $\vec{m}$ is perpendicular to $\vec{n}$:

$$\vec{m}\cdot\vec{n} = 0 \tag{2.10}$$

Because AB is also perpendicular to $\vec{n}$, it also has

$$\overrightarrow{AB}\cdot\vec{n} = 0 \tag{2.11}$$

Substituting (2.7) and (2.9) into (2.10) and (2.11), finally it is obtainedthat:

$$\tan\gamma = \frac{y_B(x_B y_C - x_C y_B) - z_B(x_C z_B - x_B z_C)}{x_B(x_B y_C - x_C y_B) - z_B(y_B z_C - y_C z_B)} \tag{2.12}$$

$$\tan\varphi = (x_B \sin\gamma - y_B \cos\gamma) / z_B \tag{2.13}$$

Up to here, the values of γ and φ can be obtained.

2.4.3 Hydrodynamic Force Calculation

In the water the fore flippers serve as wings. The movement of forelimb is unsteady, but here we use two-point hinge oscillating wing theory, which is a quasi-steady theory developed by Nagai [43].

There are altogether three important forces during hydrodynamic analysis: lift force, drag force and added mass force. During the calculation of lift and drag force, 2D wing theory is modified by using lifting line theory. The vortex wake consists of streamwise vortices due to the spanwise circulation gradient and transverse vortices due to the variation of the circulation with time. Given the large aspect ratio of flippers and the low frequency of flipper motion, it is assumed that the transverse vortices are very small, the flow within each chordwise cross section of the flipper can be dealt with 2D wing theory and 3D effect is only considered by the difference of induced velocities and induced angles of attack. As for the calculation of added mass, given the density of water is much larger than that of air, it is chosen to obtain the corresponding value of each segment along the spanwise direction without any assumption on the flow because of its simplicity. By this way the hydrodynamic calculation is simplified.

Because the chord length of cross sections varies greatly in different positions of the forelimbs, in order to reflect this variation each section of the flipper in the previous part is subdivided into three segments respectively, which is shown in Figure 2.18.

Chapter 2. Analysis of forelimb propulsion of sea turtle

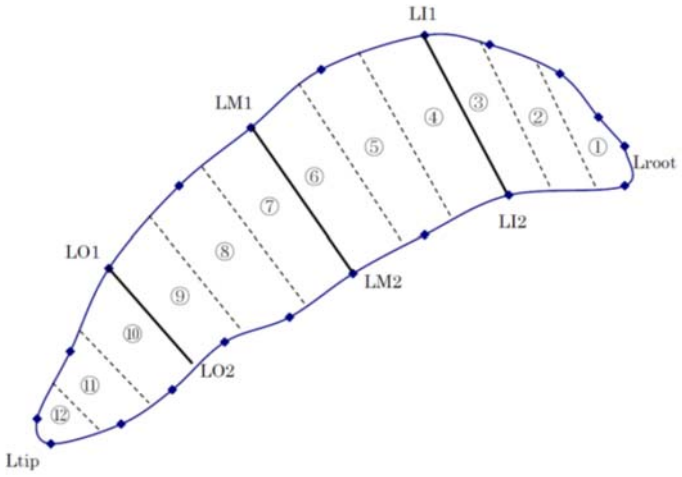

Figure 2.18 Subdivisions of each segment of Sho's left flipper

Considering each subsection as a regular 3D wing, each subsection can be represented with the middle chord length of each subsection as the representative chord length of the 3D wing, with the width of each subsection as the span length of the 3D wing.

For each segment the two-point hinge oscillating wing theory is adopted to simulate cross section motion, which is coupled with heaving and pitching motions. Then the corresponding thrust in each segement can be calculated. Finally the resultant force can be obtained by adding all the thrust forces in each subsection.

In one cross section of the fore flipper, schematic compositions of velocities are given in Figure 2.19.

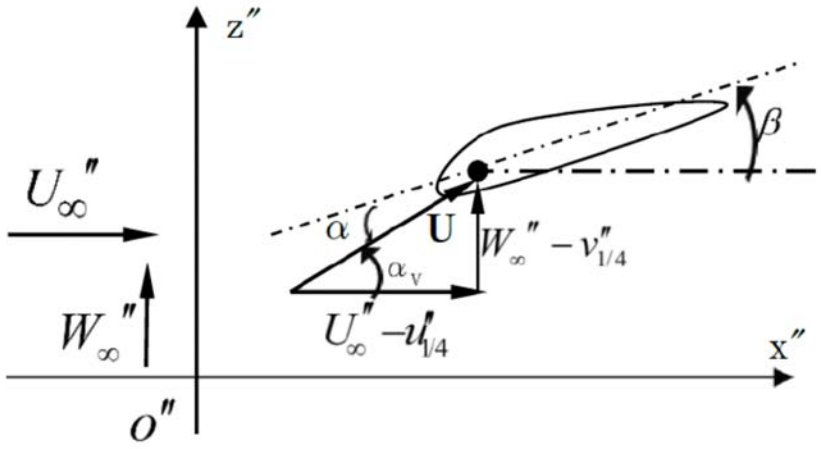

Figure 2.19 Velocity compositions in one cross section

Here the origin o'' is actually the leading point of each cross section. U_∞'' and W_∞'' are the incoming flow velocity components in the $o''-x''$ and $o''-y''$ direction. β is the relative pitch angle.

Here the motion of one quarter point on the chord of wing is used to represent wing movement. Assuming that (x_1'', z_1'') is the coordinate of the leading point in $o''-x''z''$, the coordinate of the one-quarter point on the chord of wing can be given as:

$$x_{1/4}'' = x_1'' + \frac{c}{4}\cos\beta \qquad z_{1/4}'' = z_1'' + \frac{c}{4}\sin\beta \tag{2.14}$$

Then the velocity at the one-quarter point can be got:

$$u_{1/4}'' = \frac{dx_{1/4}''}{dt} = u_1'' + d\left(\frac{c}{4}\cos\beta\right)/dt \qquad w_{1/4}'' = \frac{dz_{1/4}''}{dt} = w_1'' + d\left(\frac{c}{4}\sin\beta\right)/dt \tag{2.15}$$

u_1'' and w_1'' are the velocity components of the leading point A of the cross section in $o-x''y''z''$, which can be calculated by movement analysis.

At the one-quarter point of chord,

$$\begin{aligned} U_{1/4}'' &= \sqrt{\left(U_\infty'' - u_{1/4}''\right)^2 + \left(W_\infty'' - w_{1/4}''\right)^2} \\ (\alpha_v)_{1/4} &= \tan^{-1}\frac{W'' - w_{1/4}''}{U_\infty'' - u_{1/4}''} \end{aligned} \tag{2.16}$$

The geometric angle of attack is calculated as:

$$\alpha_{1/4} = (\alpha_v)_{1/4} - \beta \tag{2.17}$$

The geometric lift coefficient C_L and the geometric drag coefficient C_D can be obtained from the curves in Figure 2.20, which is referred from the paper by Okamoto and Jinba [44].

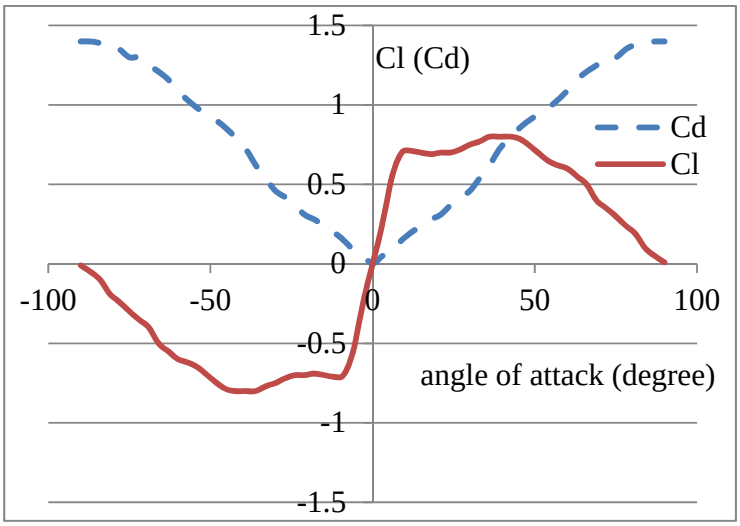

Figure 2.20 Curves between C_L (C_D) and angles of attack

Taking into account the downwash phenomenon of 3D wing, the effective angle of attack can be calculated according to [45]:

$$\alpha_{eff} = \alpha_{1/4} - \varepsilon, \quad \varepsilon = C_L / (\pi \cdot AR), \quad AR = b^2 / S \tag{2.18}$$

Where ε is induced angle of attack, AR is the aspect ratio of wing, b is the span of wing and S is the projecting area of wing. Next the effective lift coefficient $(C_L)_{eff}$ can be got from Figure 2.20. The effective drag coefficient is the sum of geometric drag coefficient C_D and induced drag coefficient C_{Di}.

$$(C_D)_{eff} = C_D + C_{Di}, \qquad C_{Di} = \varepsilon C_L = C_L^2 / (\pi \cdot AR) \tag{2.19}$$

Finally actual lift and drag acting on the wing are:

$$L'' = \frac{1}{2}(C_L)_{eff}\,\rho U_{1/4}''^2 S_N, \qquad D'' = \frac{1}{2}(C_D)_{eff}\,\rho U_{1/4}''^2 S_N \tag{2.20}$$

Here ρ denotes fluid density and S_N is the projecting area of each segment.

The added mass can be approximated by the added mass of the fluid of the column of which diameter is equal to the chord length of the wing c, and of which length is the same as the wing span b. Then added mass force can be obtained as below:

$$F_n'' = \frac{\pi}{4}\rho b c^2 \frac{d(U_{1/4}'' \sin\alpha_{1/4})}{dt} \tag{2.21}$$

Up to now, according to the force analysis in Figure 2.21, the expressions of thrust force and lateral force in coordinate $o''-x''y''z''$ are given below:

$$\begin{aligned} T'' &= -L''\sin(\alpha_v)_{1/4} + D''\cos(\alpha_v)_{1/4} - F_n''\sin\beta \\ Z'' &= L''\cos(\alpha_v)_{1/4} + D''\sin(\alpha_v)_{1/4} + F_n''\cos\beta \end{aligned} \tag{2.22}$$

The expressions of lift force and vertical force in coordinate $o-xyz$ and $O-XYZ$ can be obtained:

$$T = T''\cos\gamma + Z''\sin\gamma\sin\varphi, \quad Z = Z''\cos\varphi \tag{2.23}$$

T is thrust force along O-X direction and Z is vertical force along O-Z direction.

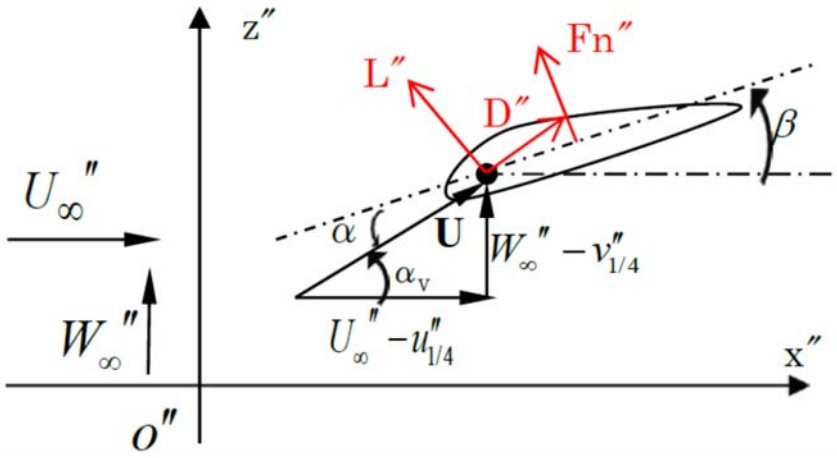

Figure 2.21 Force analysis of one segment

2.4.4 The Determination of the Relative Pitch Angle β

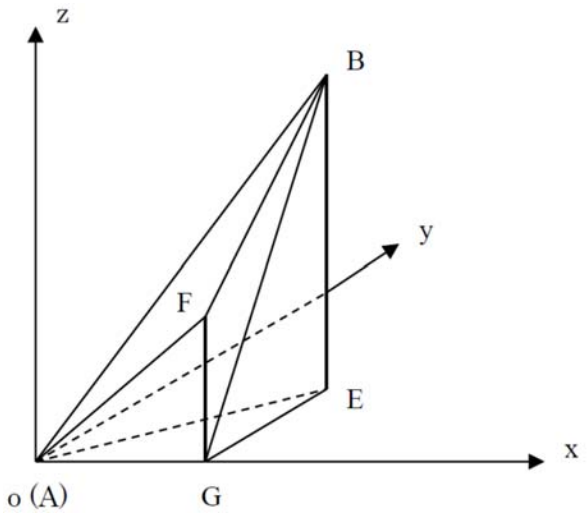

Figure 2.22 Geometric relationship between β and δ , ψ

During previous part, parameters except the relative pitch angle β were introduced. So in this part the process of how to get the values of β will be explained.

In Figure 2.22, it is assumed that AB is the chord of one cross section. BE and BF are perpendicular to plane $o-xy$ and $o-xz$ respectively. G is the intersecting point between plane BEF and line $o-x$. Assume that $\angle FAG=\delta$ and $\angle EAG=\psi$. δ and ψ are defined as the upper view projecting value and the side view projecting value separately of the angle between the line of the flipper located at the spanwise middle (line segment AB in Figure 2.5) and the carapace line (line segment OX in Figure 2.5). Their values can be obtained by movement analysis.

Assume that the coordinates of point B is (x_B, y_B, z_B), and then the relationship below can be got:

$$y_B = x_B \tan\psi, \quad z_B = x_B \tan\delta \tag{2.24}$$

Then the vector parallel to $\overrightarrow{OB}$ can be written as:

$$\vec{c}_{o-xyz} = (1, \tan\psi, \tan\delta) \tag{2.25}$$

According to (2.2) and (2.3), the expression of $\vec{c}$ at coordinate $o''-x''y''z''$ is:

$$\vec{c}_{o''-x''y''z''} = \begin{pmatrix} \cos\gamma + \sin\gamma\tan\psi \\ -\sin\gamma\cos\varphi + \cos\gamma\cos\varphi\tan\psi + \sin\varphi\tan\delta \\ \sin\gamma\sin\varphi - \cos\gamma\sin\varphi\tan\delta + \cos\varphi\tan\delta \end{pmatrix} = \begin{pmatrix} c_{x''} \\ c_{y''} \\ c_{z''} \end{pmatrix} \tag{2.26}$$

β can be considered as the angle between $\vec{c}_{o''-x''y''z''}$ and $o''-x''$. And then the value of β can be obtained:

$$\beta = \arccos\frac{c_{x''}}{\sqrt{c_{x''}^2 + c_{y''}^2 + c_{z''}^2}} \tag{2.27}$$

2.5 Results of Hydrodynamic Analysis

2.5.1 Hydrodynamic Analysis of Sho's Left Flipper

Using the theoretical analysis method mentioned above, the relationship between drag force acting on the body of sea turtle and thrust force produced by the left forelimb of Sho is discussed.

Figure 2.23 shows time variation of swimming velocity components of Sho in coordinate $O-XYZ$. Figure 2.24 gives the time variation of angles of attack of the 7th segment of Sho's left flipper in Figure 2.18. On the other hand, hydrodynamic drag coefficients on turtle body were referred from the paper by Watson and Granger [46]. It is plotted the time variation of total thrust force generated by left flipper and body drag force in Figure 2.25. The average thrust force generated by the left flipper is -0.9873N, the average total thrust force can be got as twice of the thrust generated by left flipper and the average body drag force is 2.0114N. Consequently the total thrust force and body drag force can be balanced.

Chapter 2. Analysis of forelimb propulsion of sea turtle

In order to verify the validity of the method in this dissertation in carrying out the hydrodynamic analysis of sea turtle's swimming, some further calculation was performed. The average total thrust force (twice of the thrust force generated by the left flipper) and the average body drag force in different swimming velocities were calculated and then the tendency of both forces were compared (Figure 2.26). The velocity of the intersecting point is 0.269 m/s and the actual swimming velocity during Sho's calculation is 0.278m/s. So it can be said that the method in this dissertation can almost predict the hydrodynamic analysis of Sho's forelimb movements.

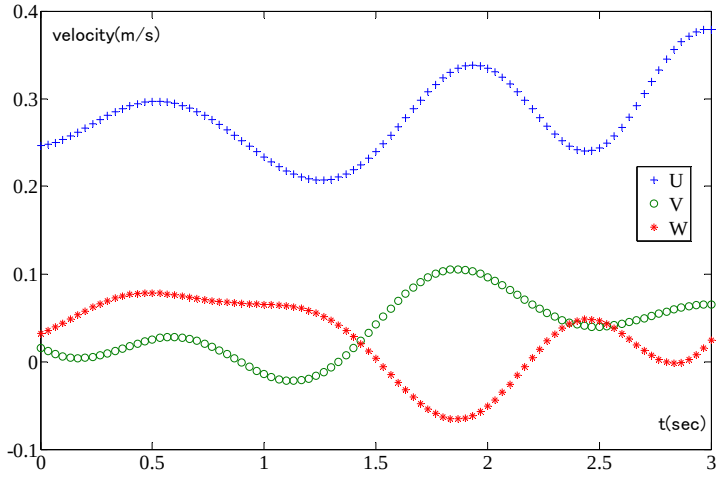

Figure 2.23 Time variation of swimming velocity components of Sho in $O-XYZ$

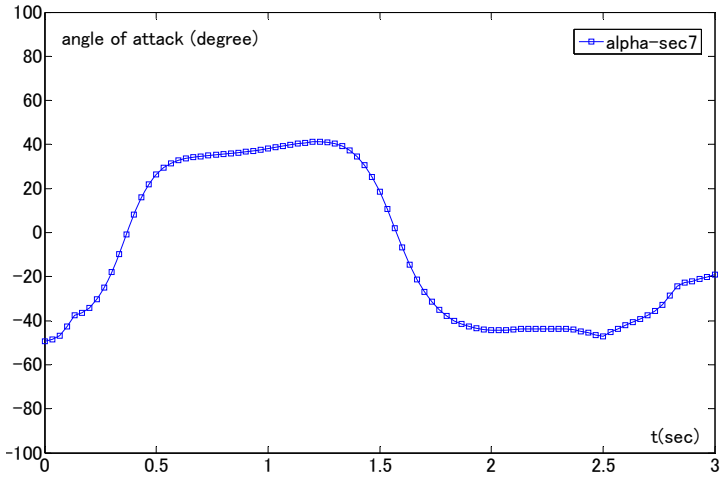

Figure 2.24 Time variation of angles of attack of the 7th segment for Sho's left flipper

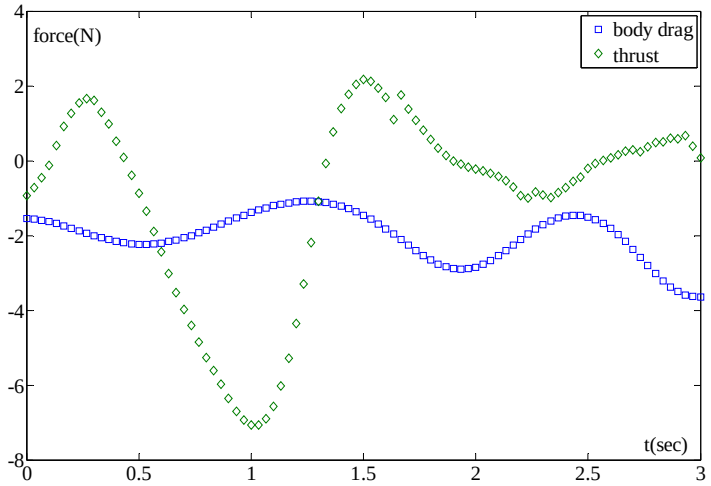

Figure 2.25 Time variation of total thrust force generated by left flipper and total body drag force of Sho (Here the sing of body drag force is set as minus to compare easily with total thrust force)

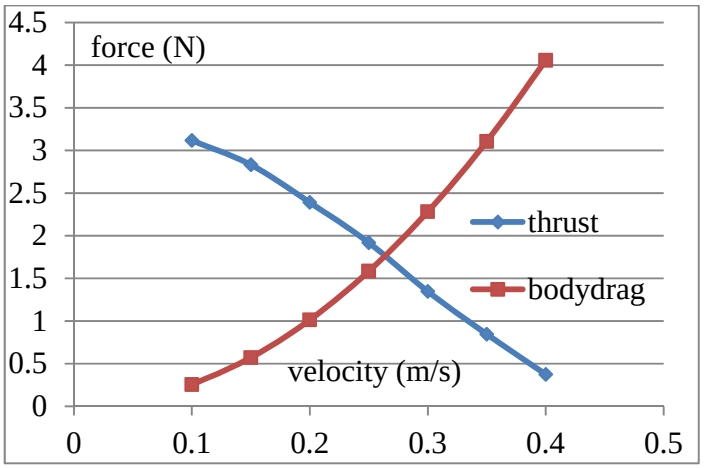

Figure 2.26 Average total thrust force and body drag force of Sho in different swimming velocities (the sign of both forces is set as plus here)

2.5.2 Hydrodynamic Analysis of Yu's Forelimbs Without Prosthetic Flippers

Figure 2.27 shows the time variation of swimming velocity components of Yu with actual flippers. Figure 2.28 gives the time variation of angles of attack of the 8th segment for Yu's actual left flipper (left panel) and actual right flipper (right panel). Figure 2.29 is the time variation of total thrust force generated by both actual flippers and body drag force. The average thrust force generated by left flipper is -0.3789N, the average thrust force generated by right flipper is -0.5381N, and the average body drag force is 0.9228N. Consequently the total thrust force and body drag force can be almost balanced.

The verification calculations in different swimming velocities were also done (Figure 2.30). The total thrust force is the sum of the thrust force generated by the left and right actual flippers. The velocity of the intersecting point is 0.203m/s and the actual swimming velocity during Yu's calculation is 0.187m/s. Although there exist some

discrepancies, the method in this dissertation can predict the hydrodynamic analysis of Yu's forelimb movements.

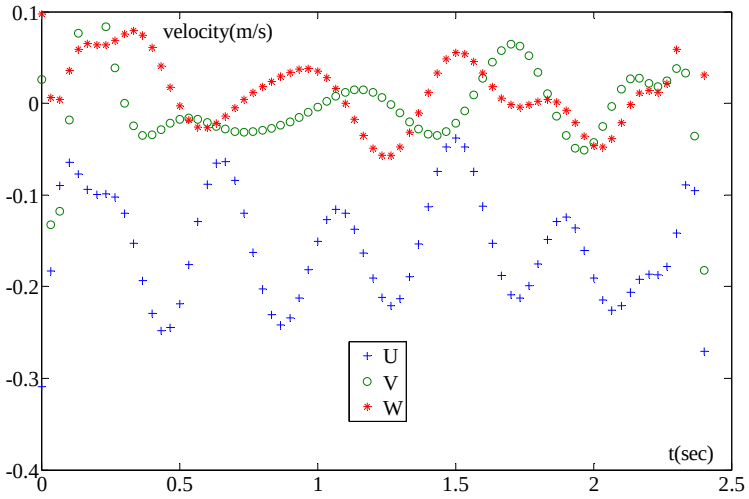

Figure 2.27 Time variation of swimming velocity components of Yu with actual flippers

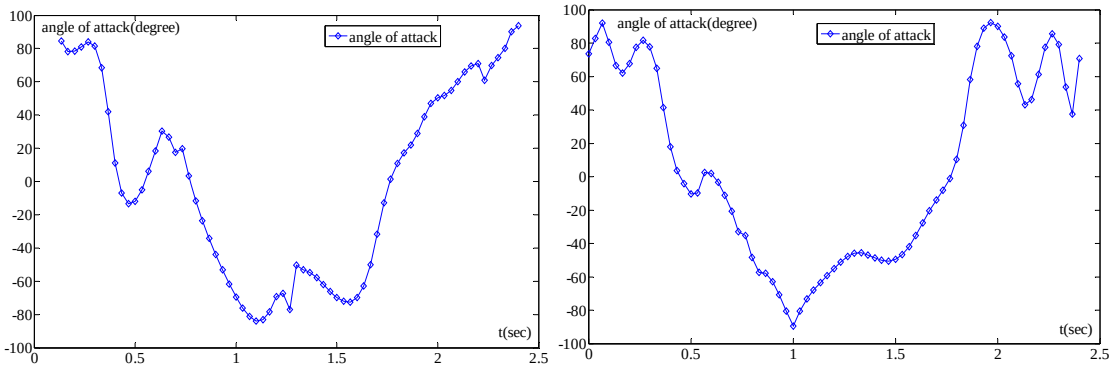

Figure 2.28 Time variation of angles of attack of the 8th segment for Yu's left actual flipper (left panel) and Yu's right actual flipper (right panel)

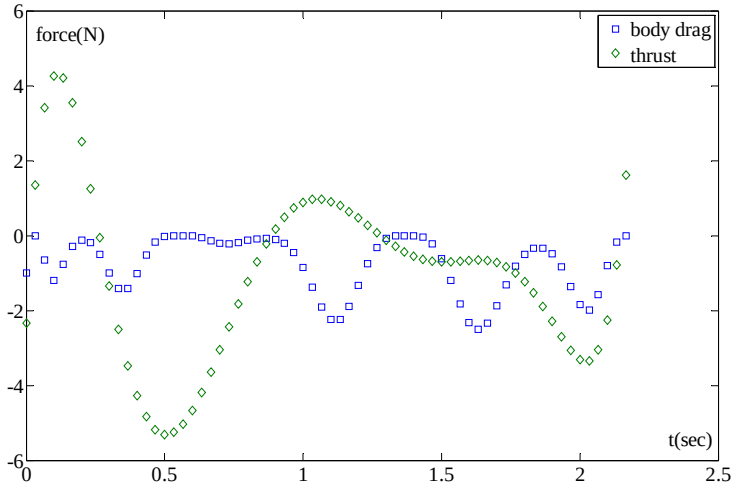

Figure 2.29 Time variation of total thrust force generated by Yu's both actual flippers and total body drag of Yu (Here the sing of body drag force is set as minus to compare easily with total thrust force)

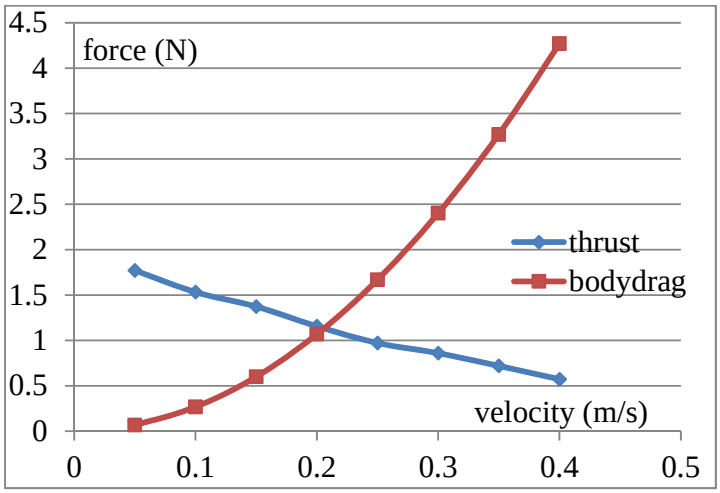

Figure 2.30 Average total thrust force and body drag force of Yu with actual flipper in different swimming velocities (the sign of both forces is set as plus here)

2.5.3 Hydrodynamic Analysis of Yu's Forelimbs With Prosthetic Flippers

Figure 2.31 shows the time variation of swimming velocity components of Yu with prosthetic flippers. Figure 2.32 gives the time variation of angles of attack of the 7th segment of Yu's left (left panel) and right prosthetic flippers (right panel). Figure 2.33 gives the time variation of total thrust force generated by Yu's both flippers and body drag force with prosthetic flippers. The average thrust force generated by left prosthetic flipper is -1.0399N, the average thrust force generated by the right one is -1.1661N, and the average body drag is 2.573N. The average thrust and body drag can be balanced.

The verification in different swimming velocities is shown in Figure 2.34. The velocity of the intersecting point is 0.268m/s and the actual swimming velocity is 0.293m/s. Although the discrepancy is a little bigger, almost it can be said that if installing prosthetic flippers, the method in this dissertation can also predict the hydrodynamic analysis of Yu's forelimb movements.

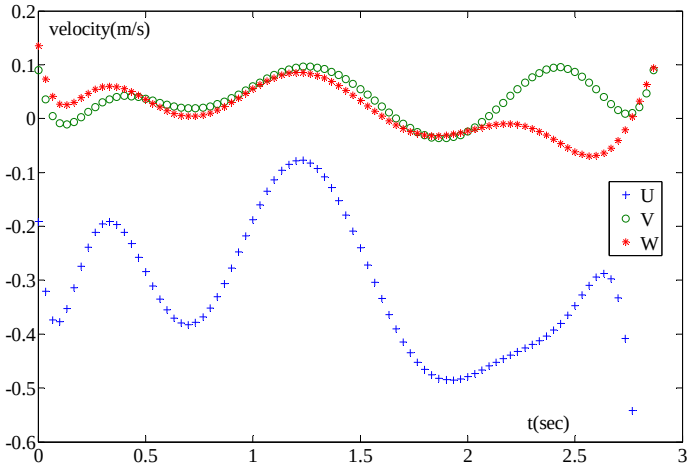

Figure 2.31 Time variation of swimming velocity components of Yu with prosthetic flippers

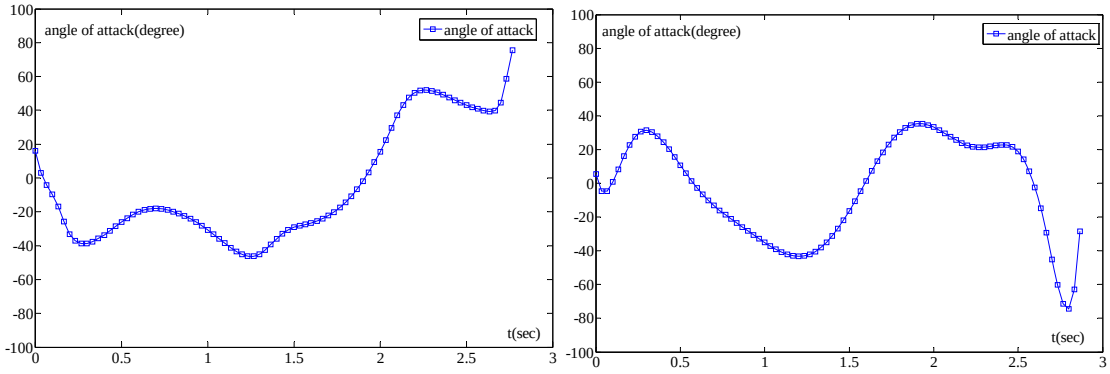

Figure 2.32 Time variation of angles of attack of the 7th segment of Yu's left forelimb (left panel) and right forelimb (right panel) with prosthetic flippers

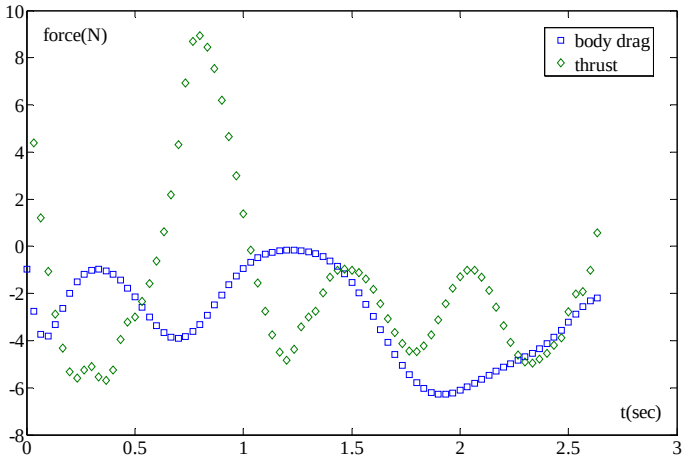

Figure 2.33 Time variation of total thrust force generated by Yu's both flippers and body drag of Yu with prosthetic flippers (Here the sign of body drag force is set as minus to compare easily with total thrust force)

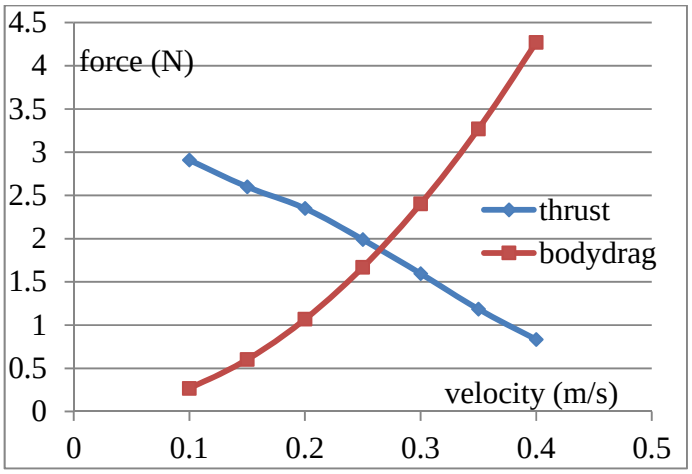

Figure 2.34 Average total thrust force and body drag force of Yu with prosthetic flippers in different swimming velocities (the sign of both forces is set as plus here)

2.5.4 Comparison Among Three Cases

a) The method in this dissertation can predict well the hydrodynamic characteristics in the case of Sho's flippers, Yu's actual flippers and Yu's prosthetic flippers;

b) Prosthetic flippers play a positive role in generating thrust force. But the thrust generated by the right prosthetic flipper is larger than that generated by the left one;

c) The angles of attack of Sho's left flipper stay in the large lift coefficient area for a long time in one period. But the angles of attack of Yu's actual flippers vary largely, and much of it is not in the large lift coefficient area. After installing the prosthetic flippers, the situation of angles of attack is improved;

d) From verification results, it can be seen that for Sho's case it shows good agreement but for Yu's cases with and especially without prosthetic flippers, there exist some discrepancies. The first reason is from the verification method itself: sea turtle's swimming velocity is not constant, but during the validation the relationship of average velocity and average forces (both thrust and body drag) was adopted to inspect the

validity of the method. And the asymmetry of Yu's real and prosthetic flippers aggravates this inconstancy of swimming velocities. The second reason may come from that when Yu swims with prosthetic flippers it cannot suit itself with the appendages and therefore cannot swim regularly, which increases the difficulty of taking high-quality videos.

2.6 Conclusion and Discussion

To contribute to design and development of prosthetic flippers, in this chapter it is contradistinguished the 3D kinematics and hydrodynamics of three cases of sea turtles' swimming and it is verified that the proposed method in this chapter can predict well the hydrodynamics of se turtles' forelimb motions.

Tries have been taken on finding some bijective correspondence between kinematics and propulsive force generation. One is that flipper flexibility plays a great role during the generation of thrust force. Flexible Sho's flippers and Yu's actual flippers behave curvilinear motions and can bend actively in both chordwise and spanwise directions, which correspondingly produce effective thrust force. But Yu's prosthetic flippers behave nearly linear motions and can only passively utilize the flexibility, which to some extent affect the effective generation of thrust.

From the viewpoint of making prosthetic flippers, it can be seen that the thrust generated by the right prosthetic flipper is larger than that generated by the left one. So in the future it is better to develop new prosthetic flippers or only install left prosthetic flipper, which can make both flippers generate equal thrust and therefore Yu's swimming motion will become smooth.

Chapter 3 Analysis of Flexible Pectoral Fin Propulsion on the Swimming Performance of Underwater Vehicle

3.1 Introduction

Pectoral fins of fish present great variability in shape, aspect ratio and structure, depending on the application they are intended for, resulting in different movement expressions. Also the flexibility of pectoral fins ranges greatly. They can flex along their spanwise and/or chordwise direction. Many studies show that a fin's oscillation parameters must be tuned to its stiffness for optimal performance [47, 48]. Kato et al. investigated the optimal parameters for rigid pectoral fin installed on BIRDFIN, a fixed compact three-motor-driven mechanical fin device with high-speed capacity and precise movement designed to assess the hydrodynamic characteristics of pectoral fin motions [49]. Following that, they developed a free biomimetic underwater vehicle PLATYPUS with two pairs of the same rigid mechanical pectoral fins to achieve dexterous hovering and low-speed maneuvering performance [50, 51, 52]. But the performance of PLATYPUS was limited as lift-based swimming mode was adopted to propel the vehicle but those rigid pectoral fins were designed as drag-based rigid ones.

This chapter introduces the research aiming at improving the swimming performance of PLATYPUS by designing and making new types of pectoral fins from the viewpoint of fin flexibility and chordwise crossection. The change of pectoral fin shapes and the use of flexibility necessitate the investigation of those effects on the hydrodynamic characteristics of the new pectoral fins.

Chapter 3. Analysis of Flexible Pectoral Fin Propulsion

3.2 PLATYPUS and Four Types of Pectoral Fins

3.2.1 PLATYPUS and Experimental System

3.2.1.1 Specifications of PLATYPUS

The specifications of PLATYPUS are 1.36m in length, 0.12m in diameter and 14.5kg in mass. The fore pair of pectoral fins is arranged in horizontal plane and the rear pair in vertical plane (Figure 3.1). Each pectoral fin is controlled by using Three-Motor-Driven Mechanical Fin system (3MDMPF), which will be explained in details in the pectoral fin kinematic part of this chapter. Each 3MDMPF has a maximum frequency of 3H with a rowing angle of -50° ~ 70°, flapping angle of -30° ~ 30° and feathering angle of -180° ~ 180°. A cylindrical float is attached to the fuselage to adjust its buoyancy. The vehicle has tilt sensor for pitching and rolling, an azimuth sensor, rate sensors for pitching, rolling and yawing, a depth sensor, an acoustic positioning measurement system and angular sensors on fin motion.

Figure 3.1 Photograph of PLATYPUS

3.2.1.2 Experimental System

The experiments of PLATYPUS were carried out in the towing tank of Osaka University (length 100 [m], width 7.8 [m], depth 4.35 [m]).

The power of PLATYPUS is supplied from the ground through a cable, and the data are transmitted through a cable between a computer on board and a computer on the ground. The computer on board has the functions of controlling the motions of two pairs of 3MDMPFs every 10ms, sending the data from sensors to the computer on the ground, and receiving the control command data from the computer on the ground. The computer on the ground has the functions of receiving the data from acoustic positioning measurement system, receiving and sending the data between the two computers every 100ms, and computing controlling parameters for each 3MDMPF every 100ms.

To measure the location of the vehicle, Long Baseline (LBL) Acoustic Positioning System is used to track the underwater vehicle. LBL systems are unique in that they use networks of seafloor mounted baseline transponders (receivers) as reference points for navigation. During our experiment three acoustic transponders were set up on the wall surface of the towing tank and one acoustic interrogator (pinger) at the bottom of PLATYPUS (Figure 3.2).

The vertical coordinate Z of the pinger is obtained directly from the depth sensor installed on PLATYPUS. The horizontal plane coordinate (X, Y) of the pinger is obtained through the geometrical relationship in Figure 3.3.

$$\begin{aligned} L1 &= \sqrt{(X1-X)^2+(Y1-Y)^2} \\ L2 &= \sqrt{(X2-X)^2+(Y2-Y)^2} \\ L3 &= \sqrt{(X3-X)^2+(Y3-Y)^2} \end{aligned} \tag{3.1}$$

If we assume the auxiliary parameters below:

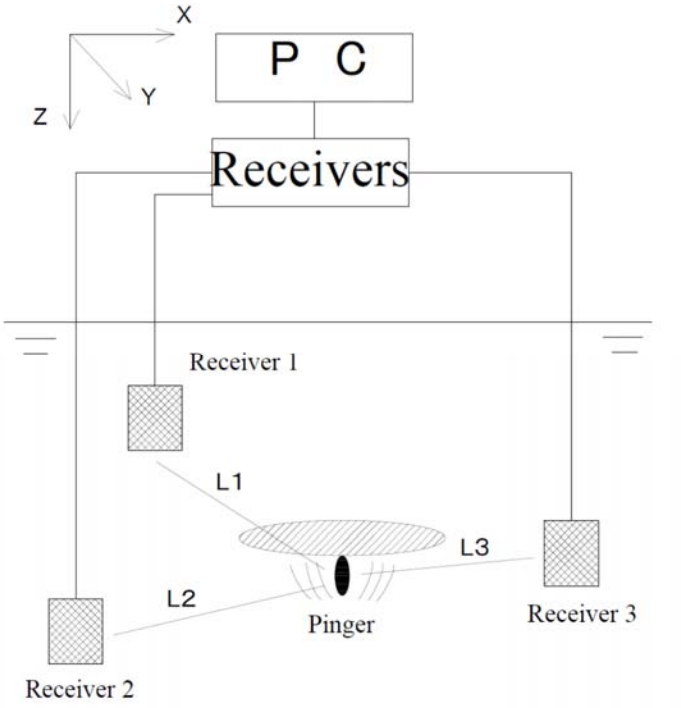

Figure 3.2 Positioning measurement system

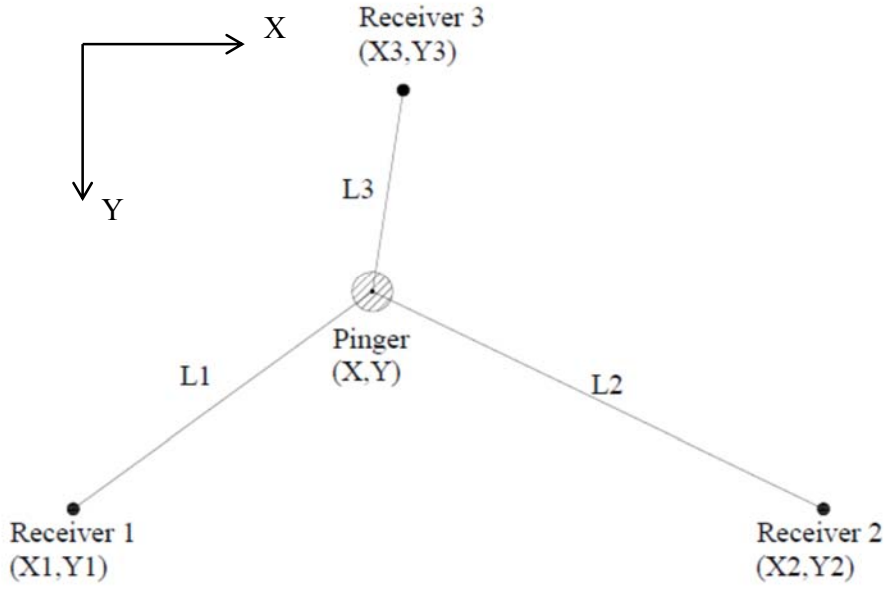

Figure 3.3 Horizontal plane of the positioning measurement system

$$\begin{aligned} A &= 2\times(-X1+X2) \\ B &= 2\times(-Y1+Y2) \\ C &= X1^2 - X2^2 + Y1^2 - Y2^2 \\ D &= 2\times(-X1+X3) \\ E &= 2\times(-Y1+Y3) \\ F &= C = X1^2 - X3^2 + Y1^2 - Y3^2 \end{aligned} \tag{3.2}$$

Thus the horizontal plane coordinates of the pinger can be obtained as:

$$\begin{aligned} X &= (L1^2 - L3^2 - F - E\times L1^2 / B + E\cdot L2^2 / B + E\times C / B) / (D - E\times A / B) \\ Y &= (L1^2 - L2^2 - C - A\times X) / B \end{aligned} \tag{3.3}$$

Up to now the coordinates of PLATYPUS are calculated.

3.2.2 Four Types of Pectoral Fins

3.2.2.1 Fabrication of Four Kinds of Pectoral Fins

In nature, the pectoral fins that employ drag-based mode usually have a short and round shape, for example largemouth bass (Microptepus salmoides); while those that use lift-based mode, usually have a narrow and long fin shape, Bluegill (Lepomis macrochirus) for example.

At present PLATYPUS employs lift-based swimming mode for propulsion but original fins were designed as drag-based ones. It is better to make some lift-based pectoral fins for PLATYPUS to improve its swimming performance. The original rigid fin is made from a stainless-steel plate with a thickness of 0.7mm. Specifications of the original fin are listed in Figure 3.4.

Two types of lift-based fin shapes are designed: symmetric and asymmetric. Symmetric fin has the elliptic cross section, while the cross section for asymmetric fins is NACA0015. They are given in Figure 3.5 and Figure 3.6 respectively.

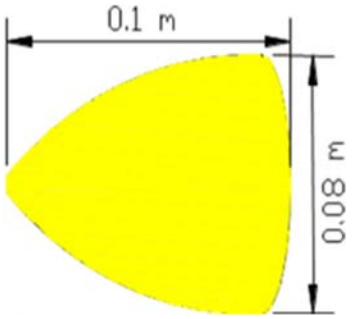

Span: 0.1m

Chord: 0.08m

Aspect ratio: 1.72

(AR=b^2/s, b: Span, S: Area)

Project area: 0.0058m^2

Young's modulus: $1.8\times10^{11}N/m^2$

Figure3.4 Specifications of original fin

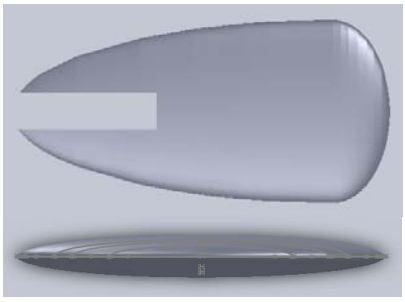

Span: 0.13m

Chord: 0.055m

Aspect ratio: 3.0

Project area: 0.005595m^2

Thickness: 0.00825m

Figure 3.5 Symmetrical fin (plan view and chordwise cross section)

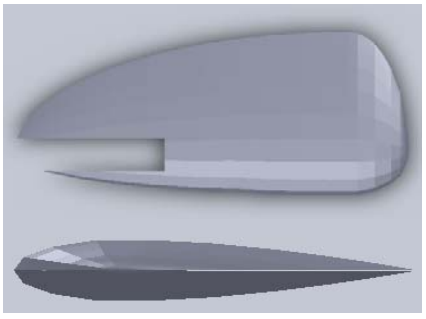

Span: 0.13m

Chord: 0.055m

Aspect ratio: 3.0

Project area: 0.005595m^2

Thickness: 0.00825m

Figure 3.6 Asymmetrical fin (plan view and chordwise cross section)

In total, four kinds of pectoral fins were made: Symmetric rigid fin, Asymmetric rigid fin, Asymmetric harder flexible fin, and Asymmetric softer flexible fin. The material of rigid fins is ABS resin (Young's modulus: $2.3\times10^9 N/m^2$) and flexible fins are made of two types of silicon gums, the properties of which will be given in the following section. As in nature most of pectoral fins show asymmetric properties, here only asymmetric flexible fins were made but symmetric flexible fins were not. Hereafter, "asymmetric softer flexible fin" is abbreviated to "Asym-softer", "asymmetric harder flexible fin" to "Asym-harder", "asymmetric rigid fin" to "Asym-rigid", and "symmetric rigid fin" to "sym-rigid".

3.2.2.2 Hyper Elastic Materials

The typical properties of silicone rubber include:

a) The ability to remain elastic even given large deformation;
b) A highly nonlinear relationship between load and extension;
c) Nearly incompressibility.

These characteristics can be generally defined as hyper elastic [53, 54]. Hyper-elasticity is defined as a material that has an elastic potential function W. A stress tensor is derived by differentiating W with respect to the conjugate strain tensor as

$$S_{ij} = \frac{\partial W}{\partial E_{ij}} \tag{3.4}$$

Where the following definitions can be applied:

$$\mathbf{E} = (\mathbf{C} - \mathbf{I})/2 \tag{3.5}$$

Where **E** denotes the Green-Lagrange strain tensor, **C** the right Cauchy-Green deformation tensor, and **S** the second Piola-Kirchhoff stress tensor. The elastic potential

function W is defined as the functions of the ratios of expansion and contraction, λ_1, λ_2, λ_3, in three dimensions.

$$W = f\left(\lambda_1, \lambda_2, \lambda_3\right) \tag{3.6}$$

In this analysis the Ogden model [55] for W was used since this model can represent the behavior of slightly compressible rubber, and Downhill-Simplex method was employed to obtain the values of the corresponding parameters in the following equation.

$$W = \sum_{n=1}^{N} \frac{\mu_n}{\alpha_n}\left[J^{\frac{-\alpha_n}{3}}\left(\lambda_1^{\alpha_n} + \lambda_2^{\alpha_n} + \lambda_3^{\alpha_n}\right) - 3 \right] + 4.5K\left(J^{\frac{1}{3}} - 1 \right)^2 \tag{3.7}$$

μ_n, α_n : material constants; K : initial bulk modulus;

$J = \lambda_1\lambda_2\lambda_3$: volumetric ratio; λ : principal stretch.

For practical purpose the sum in (3.7) is restricted to a finite number of terms, while, for consistency with the classical theory, the constants must satisfy the requirement below [56]:

$$\sum_{n=1}^{N} \mu_n\alpha_n = 2\mu \tag{3.8}$$

where μ is the shear modulus of the material in the undeformed stress-free (natural) configuration.

Tensile tests of two kinds of silicon gums give the stress-strain relationship (Figure 3.7). Table 3.1 and Table 3.2 show the values of corresponding parameters in (3.7). (Here N is set as 3).

According to (3.8), Table 3.1 and Table 3.2, it can be obtained below:

μ(Asym-softer) = 1.05×10^5, μ(Asym-harder) = 4.25×10^5

The shear modulus of the material of Asym-softer is smaller than that of Asym-harder, which validates that Asym-softer is more flexible than Asym-harder.

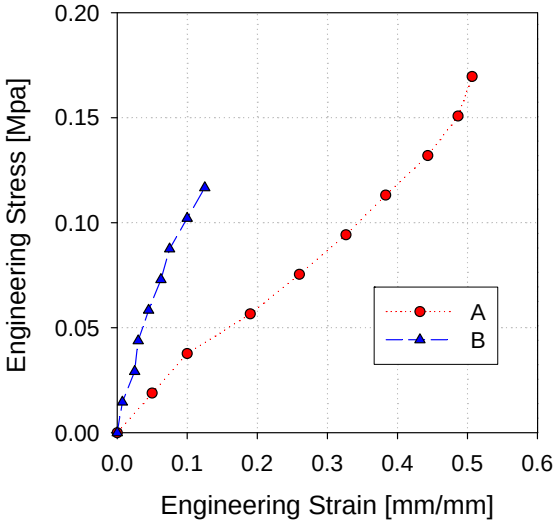

Figure 3.7 Relationship between stress and strain

(A: material of Asym-softer; B: material of Asym-harder)

Table 3.1 Ogden parameters of material of Asym-softer (N=3)

No.	Moduli μ_n	Exponents α_n	Initial modulus K
1	0.19e+02	0.228	0.67e+09
2	0.68e+02	0.17e+02	0.67e+09
3	0.11e+07	0.19	0.67e+09

Table 3.2 Ogden parameters of material of Asym-harder (N=3)

No.	Moduli μ_n	Exponents α_n	Initial modulus K
1	0.87e+07	0.14e-01	0.21e+10
2	0.15e+08	0.18e-01	0.21e+10
3	0.24e+08	0.19e-01	0.21e+10

3.3 Kinematic Expression of Mechanical Pectoral Fin System

There are five basic types of movements for pectoral fins of fish in real world: rowing motion (back-and-forth movement), feathering motion (twisting movement), flapping motion (up-and-down movement), bending motion and spanning motion as shown in Figure 3.8.

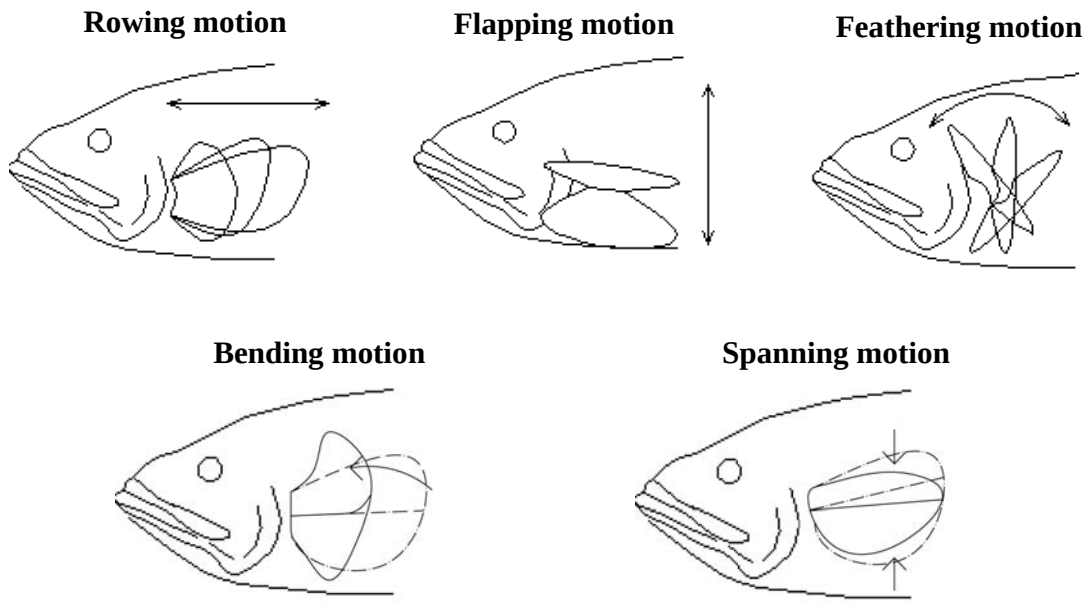

Figure 3.8 Basic motions of pectoral fin of fish

Based on the available literatures and previous demonstrations [57, 49], it is apparent that rigid pectoral fin motions can be expressed by the combination of flapping, rowing and feathering movements. Each fin of PLATYPUS is a compact Three-Motor-Driven Mechanical Fin (3MDMPF), which can generate combined rigid pectoral fin motions. The coordinate system of each 3MDMPF is shown in Figure 3.9 and the corresponding movement controlling equations are listed below.

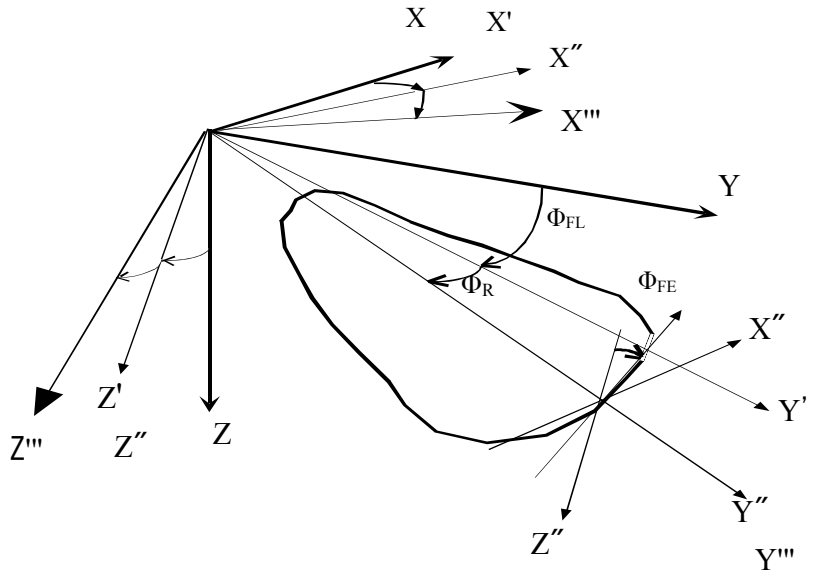

Figure 3.9 Coordinate system for each 3MDMPF

$$\begin{aligned}\Phi_R &= \Phi_{R0} - \Phi_{RA}\cdot\cos(\omega_{fin}\cdot t)\\ \Phi_{FL} &= \Phi_{FL0} - \Phi_{FLA}\cdot\cos(\omega_{fin}\cdot t + \Delta\Phi_{FL})\\ \Phi_{FE} &= \Phi_{FE0} - \Phi_{FEA}\cdot\cos(\omega_{fin}\cdot t + \Delta\Phi_{FE})\end{aligned} \tag{3.9}$$

$\Phi_R, \Phi_{FL}, \Phi_{FE}$ ---instant rowing angle, flapping angle and feathering angle of pectoral fin;

$\Phi_{R0}, \Phi_{FL0}, \Phi_{FE0}$ ---the initial value of rowing angle, flapping angle and feathering angle;

$\Phi_{RA}, \Phi_{FLA}, \Phi_{FEA}$ ---the amplitude of rowing angle, flapping angle and feathering angle;

$\Delta\Phi_{FL}$ ---phase difference between rowing and flapping movement;

$\Delta\Phi_{FE}$ ---phase difference between rowing and feathering movement;

$\omega_{fin} = 2\pi f$, t ---the angular frequency of pectoral fin motion and time, and f is the frequency of pectoral fin motion.

The flapping angle Φ_{FL} is defined as the rotation angle around the $O-X$ axis in Figure 3.9 along the longitudinal axis of the fuselage, by which coordinate $O-XYZ$ is transformed to coordinate $O-X'Y'Z'$. The rowing angle Φ_R is defined as the rotation angle around the $O-Z'$ axis in Figure 3.9, by which coordinate $O-X'Y'Z'$ is transformed to coordinate $O-X''Y''Z''$. The feathering angle is defined as the rotation angle around the $O-Y''$ axis in Figure 3.9, by which coordinate $O-X''Y''Z''$ is transformed to $O-X'''Y'''Z'''$.

3.4 Experimental Analysis of Flexible Pectoral Fin Propulsion

Generating the maximum propulsive force is an important factor for an underwater vehicle in near-shore, high-energy environments to achieve stable and precise hovering. Therefore this section focuses on optimization of the motion parameters of mechanical pectoral fin to generate maximum thrust force within the testing range. Here the maximum swimming speed of PLATYPUS is chosen as the indicator of the optimal combination of parameters within the testing range.

Because PLATYPUS was designed to perform high maneuverability in low speed under disturbances such as water currents and waves, the optimal combination of parameters of the new pectoral fins should be found from the aspect of maximizing the maneuverability in low speed under disturbances. Ideally speaking, it is better to enumerate all combinations of fin parameters to find the optimal one. But PLATYPUS has its own mechanical limitations. In this way no choice has been left but only to find the optimal combination under the given conditions. For example, the fin installed on PLATYPUS can perform the maximum flapping amplitude of 30°, and it was restricted to explore the optimal combination of fin parameters under these constraints.

3.4.1 Straight Forward Swimming

Straight forward swimming experiments of PLATYPUS using two pairs of fins were carried out to find the optimal forward combination of amplitudes for each type of fin within the testing range. Fin controlling parameters are listed in Table 3.3, where Φ_{FEA} was set as 20°, 30°, 40°, 50° and 60°, and Φ_{FLA} as 15°, 20°, 25°, 30°. The frequency of the fin motion was taken as 2.5Hz. Results are given in Figure 3.10. With the increment of flapping amplitudes, the speed of the vehicle increases under each feathering amplitude. Under constant flapping amplitude, the speed of the vehicle initially increases and then decreases with the increment of feathering amplitudes. It can be seen that the optimal parameters within the testing range for four types of pectoral fins are: $\Phi_{FLA} = 30^{\circ}$, $\Phi_{FEA} = 40^{\circ}$.

Table 3.3 Fin parameters for straight forward swimming

Φ_{R0}	Φ_{RA}	$\Delta\Phi_{R}$	Φ_{FE0}	Φ_{FEA}	$\Delta\Phi_{FE}$	Φ_{FL0}	Φ_{FLA}	$\Delta\Phi_{FL}$
0	0	0	-90	Var1	0	0	Var2	90

(Unit: degrees)

Table 3.4 Fin parameters for straight backward swimming

Φ_{R0}	Φ_{RA}	$\Delta\Phi_{R}$	Φ_{FE0}	Φ_{FEA}	$\Delta\Phi_{FE}$	Φ_{FL0}	Φ_{FLA}	$\Delta\Phi_{FL}$
0	0	0	90	Var1	0	0	Var2	-90

(Unit: degrees)

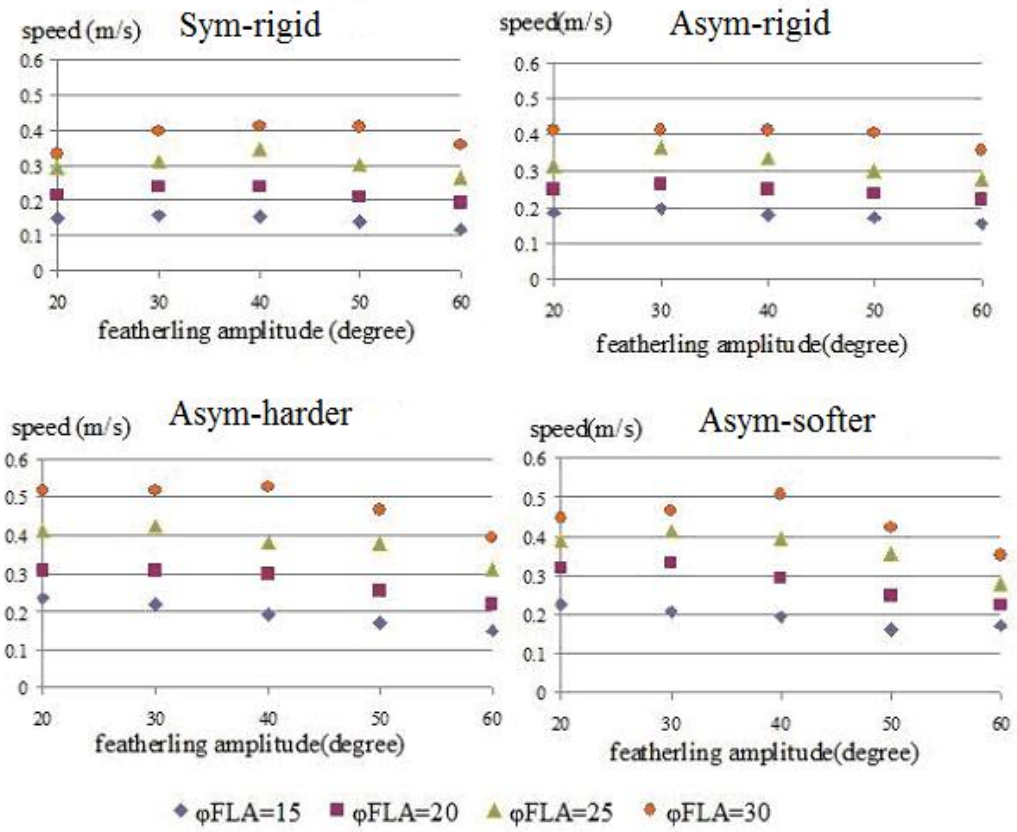

Figure 3.10 Results of straight forward swimming experiments of PLATYPUS

3.4.2 Straight Backward Swimming

Straight backward swimming experiments of PLATYPUS under two pairs of fins were carried out to find the optimal backward combination of amplitudes for each type of pectoral fins. Fin controlling parameters are listed in Table 3.4, where Φ_{FEA} was set as 20°, 30°, 40°, 50° and 60°, and Φ_{FLA} as 15°, 20°, 25°, 30°. The frequency of the fin motion was taken as 2.5Hz. Results are given in Figure 3.11. With the increment of flapping amplitudes, the speed of the vehicle increases under each feathering amplitude. Under constant flapping amplitude, the speed of the vehicle shows an almost decreasing tendency with the increment of feathering amplitudes (except the point of Sym-rigid

under $\Phi_{FLA} = 30^{\circ}$, $\Phi_{FEA} = 20^{\circ}$). It can be seen that the optimal parameters within the testing range for four types of fins are: $\Phi_{FLA} = 30^{\circ}$, $\Phi_{FEA} = 20^{\circ}$.

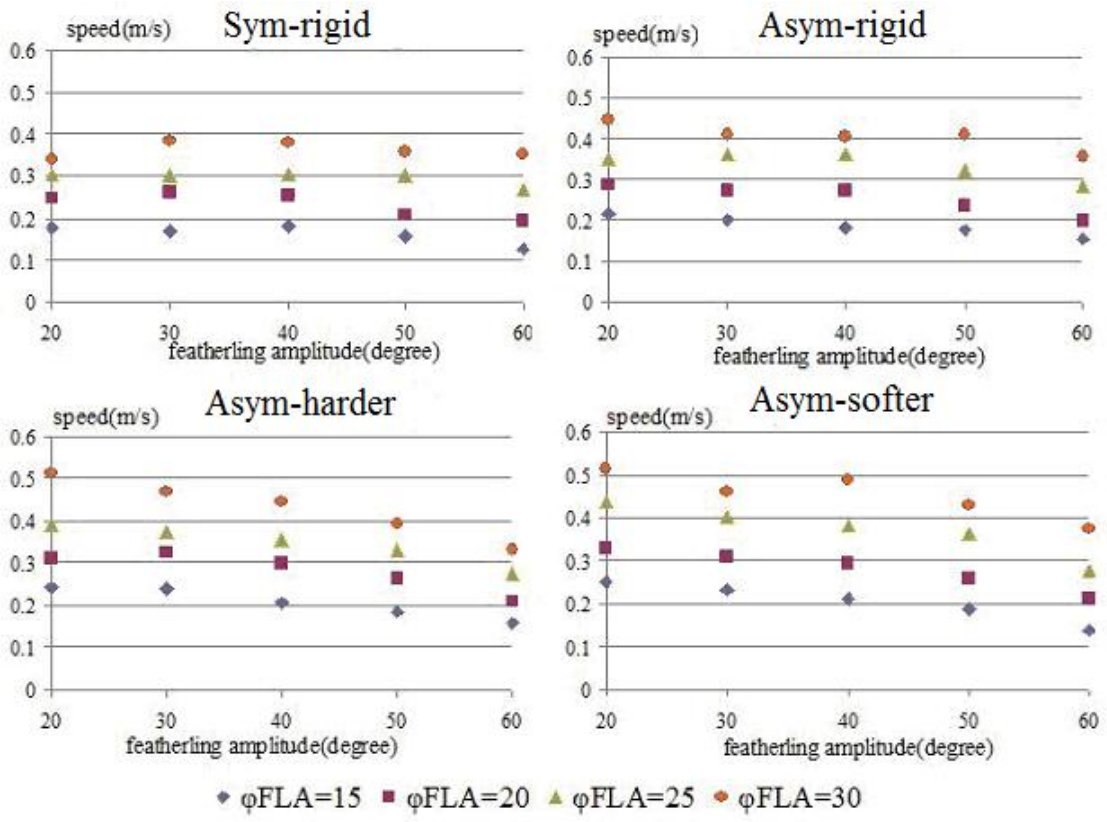

Figure 3.11 Results of straight backward swimming experiments of PLATYPUS

3.4.3 Discussion on Experiment Results

From the results in Figure 3.10 and Figure 3.11, the below items can be concluded:

a) Asymmetric rigid fin shows just a little superiority than that of symmetric rigid fin, although theoretically asymmetric rigid fin (NACA0015 cross section) is supposed to have a great advantage over symmetric rigid fin (elliptic cross section);

b) The performance of flexible pectoral fins is better than that of rigid ones, which verifies that flexibility takes a positive role in the generation of hydrodynamic forces;
c) Comparing two asymmetric elastic fins, the performance of harder one is almost the same as that of softer one in generating thrust force, although softer fin possesses much more flexibility than harder fin does.

3.5 Hydrodynamic Analysis of Flexible Pectoral Fin Propulsion

In last section based on the swimming experiments of PLATYPUS, some conclusions are listed just above. This section concentrates on elucidating the mechanism that lies behind the phenomena.

At first MSC.Marc software was used to calculate the natural frequency for the two kinds of elastic pectoral fins: f(Asym-softer) = 21.25Hz and F(Asym-harder) = 40Hz. They are relatively much larger compared to the frequency of fin motion (2.5Hz). So it can be said that natural frequency has little influence on the performance of pectoral fins during the swimming experiments.

Then it come the deformation and hydrodynamics analysis of flexible fins. Actually it is very difficult to investigate the whole deformation of the fin surface during fin movements, as spanwise and chordwise deformation would couple together, which causes a big problem during the calculation of hydrodynamics. To simplify the problem, firstly during the following calculation only the deformation along the spanwise direction is observed.

3.5.1 Method of Spanwise Deformation Calculation

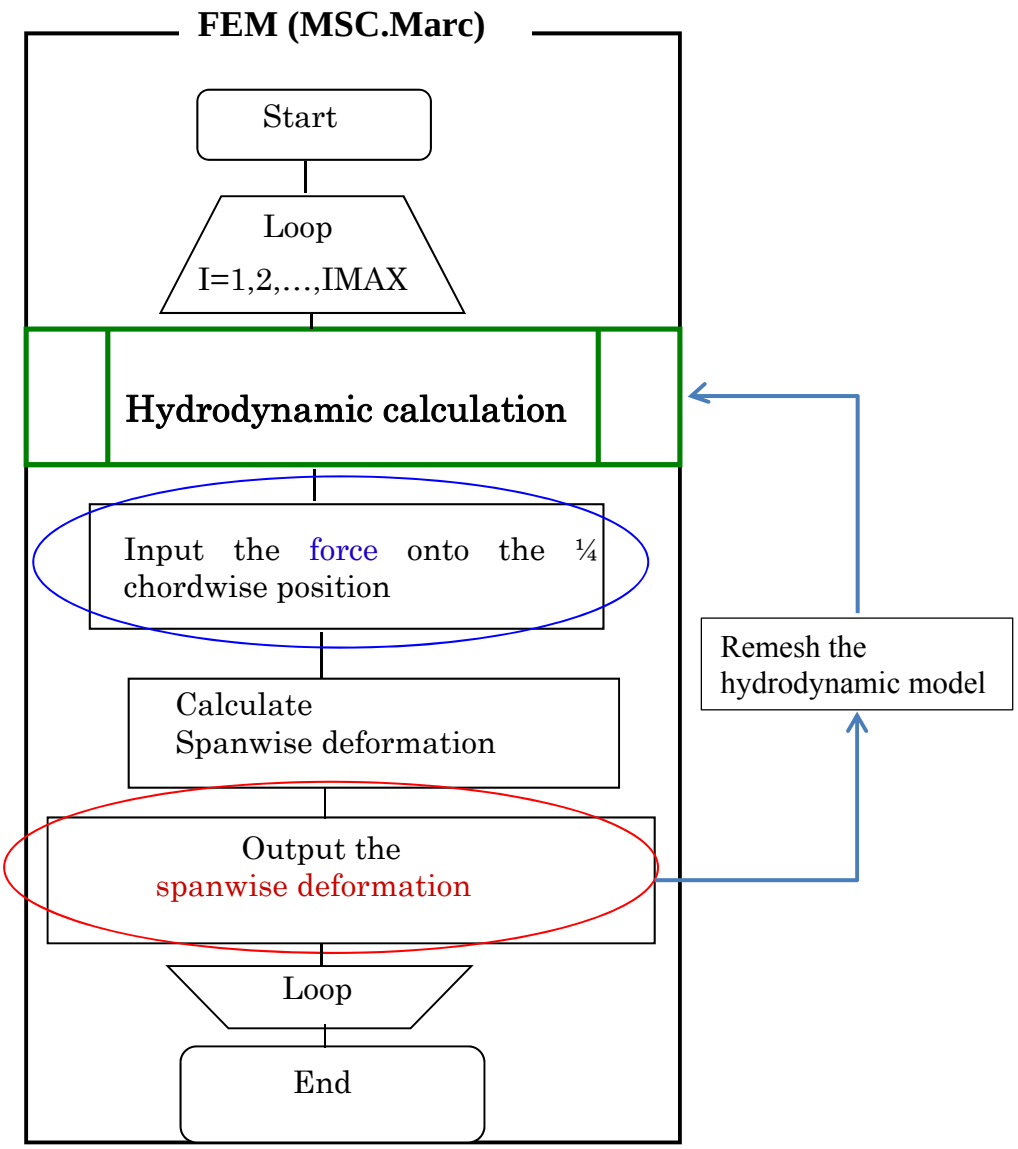

Figure 3.12 Flow chart of iterative calculation

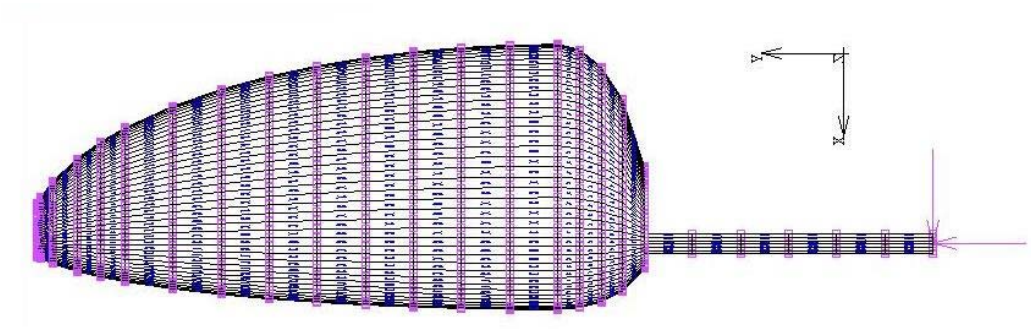

Figure 3.13 Segments of pectoral fin along spanwise direction

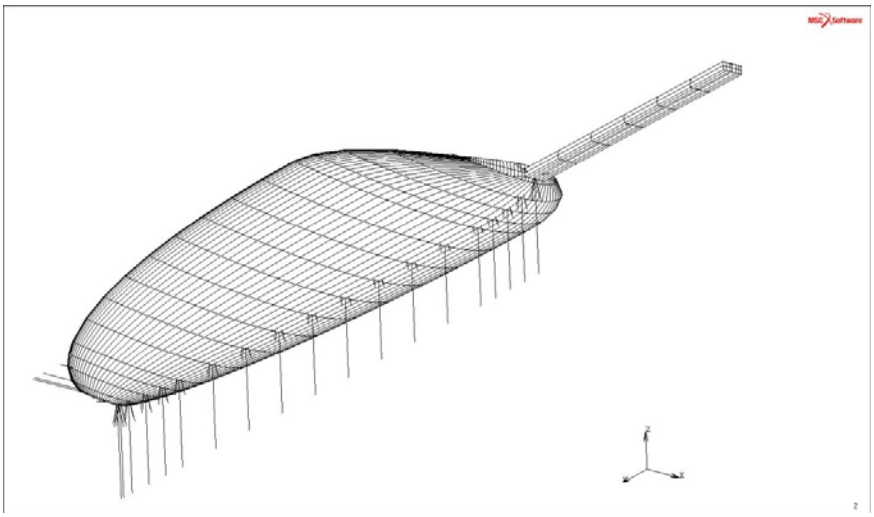

Figure 3.14 Point load applied on the one-quarter chordwise position for each segment

The calculation of spanwise deformation is an iterative process between MSC.Marc (Finite Element Method software) for structural computation and unsteady 2D wing element theory for hydrodynamic computation. The general calculating flow is given in Figure 3.12. The pectoral fin is divided into 18 segments along the spanwise direction (Figure 3.13). Inside each time step firstly theory of wing section is adopted to calculate the hydrodynamic force, which will be applied onto the one-quarter chordwise

position of each segment (Figure 3.14). And then MSC.Marc software is utilized for structural analysis, from which the spanwise deformation of elastic fins under each working condition can be obaserved.

3.5.2 Hydrodynamic Force in One Segment

During the calculation each fin is divided into eighteen segments. For each segment the 2-point hinge oscillating wing theory is adopted simulate the motion of the cross section, which is coupled with heaving and pitching movements.

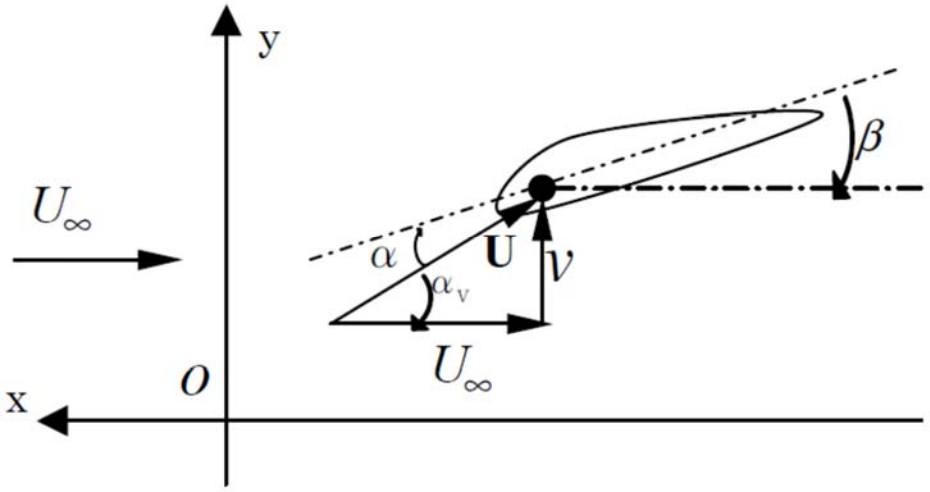

Figure 3.15 Compositions of velocities in one cross section

In Figure 3.15, the ordinate is along the linear velocity direction of flapping movement and the abscissa is along the chordwise direction assuming no feathering motion exists. Then the following relationships exist:

$$\begin{aligned} v &= -d\left(R\Phi_{FL}\right)/dt \\ \beta &= \Phi_{FE} \end{aligned} \tag{3.10}$$

Where R is the distance from the roof of shaft to that segment. The value of U_∞ is set as 0.45m/s during this calculation for three kinds of pectoral fins. Then it can be obtained below:

$$U = \sqrt{U_\infty^2 + v^2}$$
$$\alpha_v = \tan^{-1}\frac{v}{U_\infty} \tag{3.11}$$

The angle of attack is calculated as

$$\alpha = \alpha_v - \beta \tag{3.12}$$

Lift force, drag force and added mass force are obtained as follows:

$$L = 0.5C_L\rho U^2 S$$
$$D = 0.5C_D\rho U^2 S \tag{3.13}$$
$$F_n = (\pi/4)\rho bc^2\left(d\left(U\sin\alpha\right)/dt\right)$$

Here, C_L and C_D are lift and drag coefficients separately, the value of which can refer to the relationship curve between angle of attack and C_L and C_D [44], which is shown in Figure 3.16. S is the projecting area of each segment. b and c are the span and chord length of each segment separately.

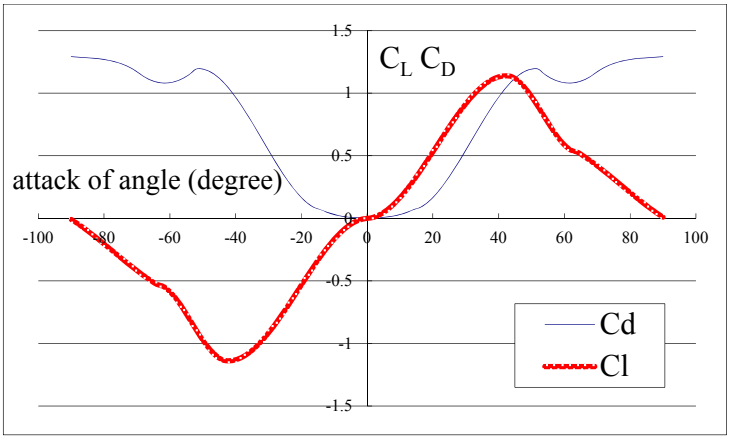

Figure 3.16 Relationships between C_L (C_D) and angles of attack

Finally the hydrodynamic force along x and y directions can be given as:

$$\begin{aligned} T &= L\sin\alpha_v - D\cos\alpha_v + F_n\sin\beta \\ Z &= L\cos\alpha_v + D\sin\alpha_v + F_n\cos\beta \end{aligned} \tag{3.14}$$

T is the force along the abscissa and Z is the force along the ordinate for each segment. Sequentially the hydrodynamic force applied onto each segment, which will be utilized during structural calculation on each time step, can be calculated.

3.5.3 Results of Spanwise Deformation Calculation

Here it should be mentioned ahead of time that during the following hydro-dynamic analysis, all forces are un-dimensionalized by $0.5\rho U_\infty^2 S$ except Figure 3.23.

Figure 3.17 shows that the non-dimensional average thrust force generated by each asymmetric pectoral fin first increases and then decreases with the increment of feathering amplitude under constant flapping amplitude $\Phi_{FLA} = 30^\circ$, reaching maximum at $\Phi_{FEA} = 30^\circ$. The thrust coefficient when $\Phi_{FEA} = 30^\circ$ is a little larger than that when $\Phi_{FEA} = 40^\circ$, which is different from the experimental results. (But in the following Point to Point control test in next chapter $\Phi_{FEA} = 40^\circ$ is still adopted based on the experiments' results). Another result is that the thrust forces produced by Asym-softer and Asym-harder are larger than that produced by Asym-rigid. Therefore, the forward speeds of PLATYPUS propelled by Asym-harder and Asym-softer are larger than that propelled by Asym-rigid, as shown in Figure 3.10. Comparing two elastic pectoral fins, it can be seen that Asym-softer has a little advantage over Asym-harder.

In order to find the reason why Asym-softer has an advantage over the other two asymmetric fins, it is analyzed that the spanwise distribution of mean thrust coefficients per segment for three asymmetric fins when $\Phi_{FLA} = 30^\circ$ and $\Phi_{FEA} = 40^\circ$ (Figure 3.18). It can be seen that for the segments nearer to the tip the average thrust coefficients of

Asym-softer are larger than those of Asym-harder and Asym-rigid. This result can be explained by the tip spanwise flexibility. Because the stiff shaft reaches up to the 12th segment, since the 13th segment flexibility can bring into effect along spanwise direction. Furthermore, the following are also analyzed: the spanwise distribution of the component of mean lift coefficients along x direction (namely the thrust direction), the component of mean drag coefficients along x direction and the component of mean added mass force coefficients along x direction, which are shown in Figure 3.19, Figure 3.20, and Figure 3.21 respectively. From three figures, it can be said that lift force component plays a great role in the generation of thrust force. The value of the component of added mass force coefficients along x direction can be negligible compared to those of lift coefficients and drag coefficients.

Furthermore, the variation of angles of attack and lift coefficients of No.17 segment in one period was investigated for three kinds of asymmetric fins (Figure 3.22 and Figure 3.23). It can be clearly seen that the angles of attack of Asym-softer vibrate between 30° and 50° during one period, which provides some advantage to the generation of lift force.

In order to clarify why thrust force reaches the maximum when $\Phi_{FEA} = 30^{\circ}$, we investigated the time variation of thrust force during one period in different feathering amplitudes for Asym-harder when $\Phi_{FLA} = 30^{\circ}$ (Figure 3.24). From these five curves it can be seen that the time variation of thrust force when $\Phi_{FEA} = 30^{\circ}$ has an advantage over those of other feathering amplitudes.

During the result analysis, tip deformation is used to describe the spanwise deformation in different feathering angle amplitudes for two flexible fins. It is defined as the maximum distance difference of fin tip between the elastic fin and rigid fin during fin motions. Figure 3.25 shows that the tip deformation of Asym-softer becomes larger when

the value of feathering amplitude increases, but the tip deformation of Asym-harder shows almost constant value. So it can be probably said that for our two kinds of elastic fins, spanwise deformation has positive influence on the thrust force generation.

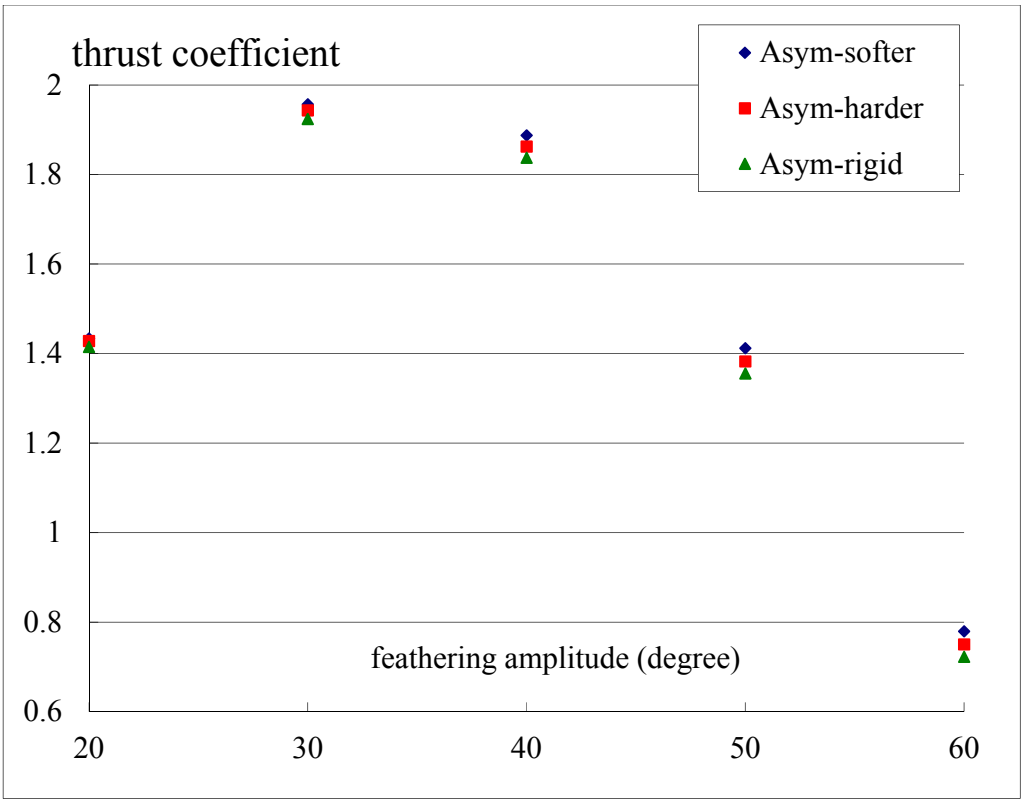

Figure 3.17 Thrust coefficients generated by asymmetric fins under different feathering amplitudes within flapping amplitude $\Phi_{FLA} = 30^{\circ}$

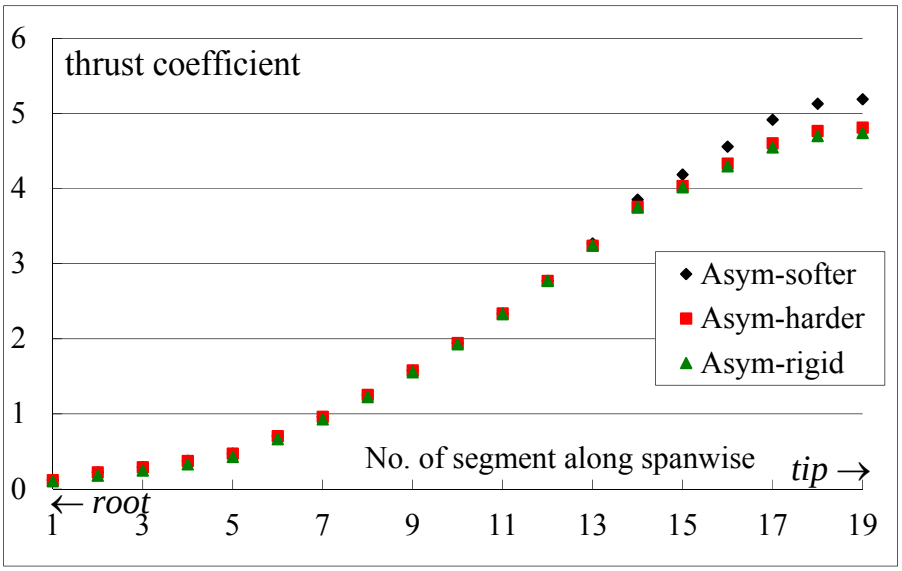

Figure 3.18 Spanwise distribution of mean thrust coefficients per segment for three asymmetric pectoral fins ($\Phi_{FLA} = 30^{\circ}$ and $\Phi_{FEA} = 40^{\circ}$)

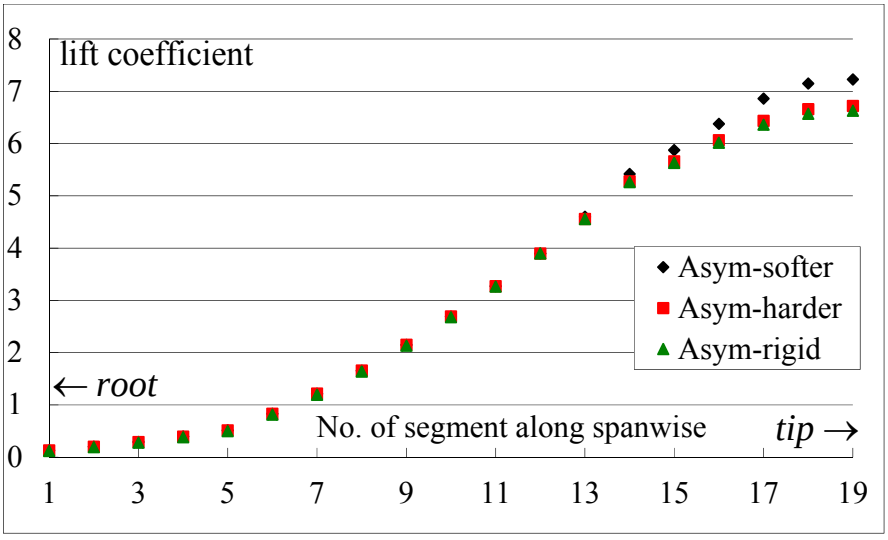

Figure 3.19 Spanwise distribution of mean lift coefficient component along x direction per segment for three asymmetric pectoral fins ($\Phi_{FLA} = 30^{\circ}$ and $\Phi_{FEA} = 40^{\circ}$)

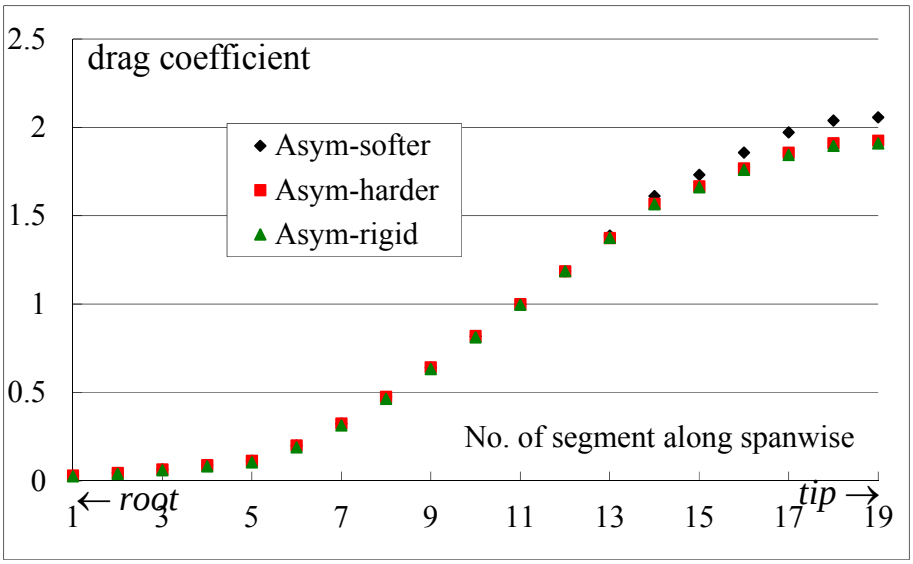

Figure 3.20 Spanwise distribution of mean drag coefficient component along x direction per segment for three asymmetric pectoral fins ($\Phi_{FLA} = 30^{\circ}$ and $\Phi_{FEA} = 40^{\circ}$)

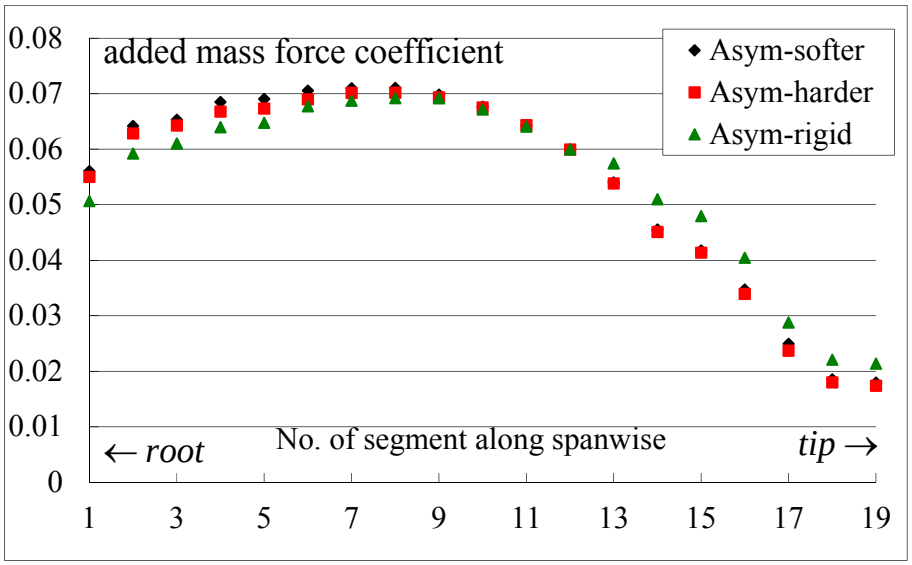

Figure 3.21 Spanwise distribution of mean added mass force coefficient component along x direction per segment for three asymmetric pectoral fins ($\Phi_{FLA} = 30^{\circ}$ and $\Phi_{FEA} = 40^{\circ}$)

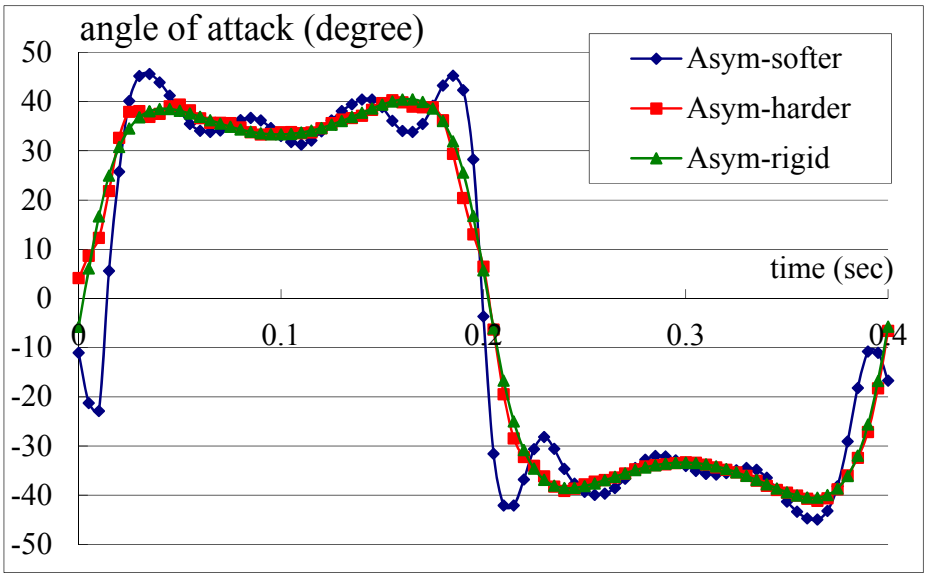

Figure 3.22 Variation of angles of attack of No.17 segment in one period ($\Phi_{FLA} = 30^{\circ}$ and $\Phi_{FEA} = 40^{\circ}$)

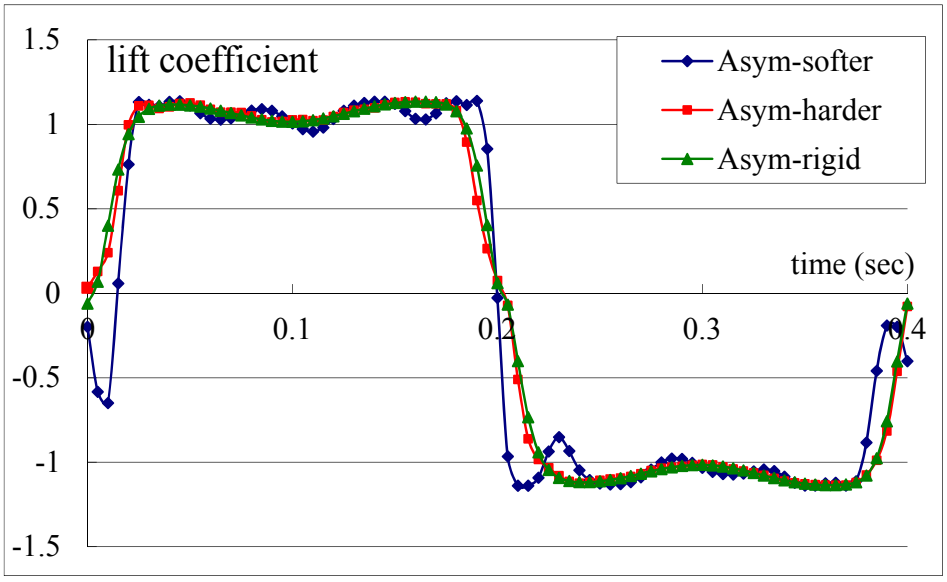

Figure 3.23 Variation of lift coefficients of No.17 segment in one period ($\Phi_{FLA} = 30^{\circ}$ and $\Phi_{FEA} = 40^{\circ}$)

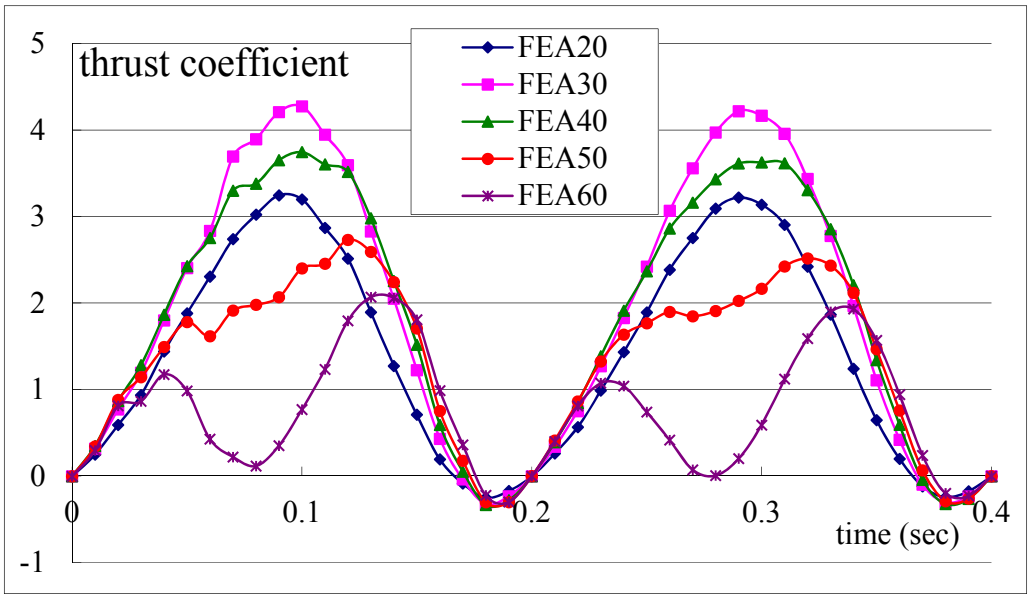

Figure 3.24 Time variation of thrust coefficients during one period in different feathering amplitudes for Asym-harder ($\Phi_{FLA} = 30^{\circ}$)

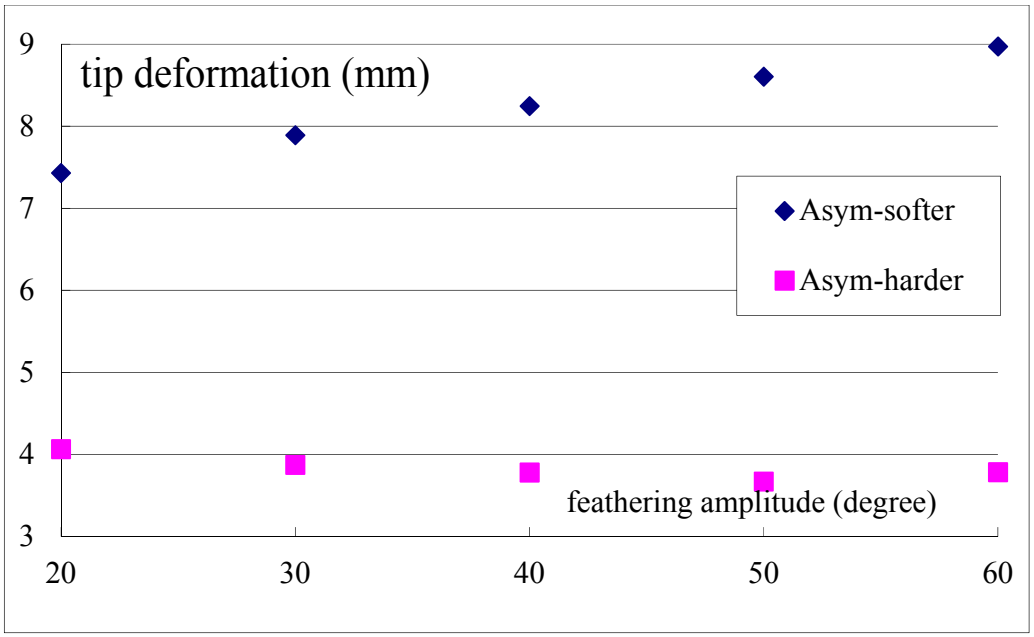

Figure 3.25 Relationship between tip deformation and feathering amplitude under flapping amplitude $\Phi_{FLA} = 30^{\circ}$

3.6 Conclusion and Discussion

Aiming at investigating the effects of flexibility and chordwise cross section of pectoral fins on the swimming performance of the biomimetic underwater vehicle PLATYPUS, two types of asymmetric elastic pectoral fins, one asymmetric rigid pectoral fin and one symmetric rigid pectoral fin were manufactured. The material properties of these pectoral fins are described in details and the kinematical controlling mechanism of mechanical pectoral fins is also introduced.

Fundamental experiments on the straight forward and backward swimming performance of PLATYPUS verify that asymmetric flexible pectoral fins have an advantage in propelling underwater robots over symmetric rigid fin and asymmetric rigid fin. The optimal combination of flapping movement amplitudes and feathering movement amplitudes within the testing range for each pectoral fin to propel PLATYPUS is obtained at the same time.

Iterative computation of spanwise deformation of asymmetric pectoral fins between Finite Element software and wing theory shows that asymmetric softer flexible fin can generate larger thrust force compared to asymmetric harder flexible fin and asymmetric rigid fin. Lift force plays an important role in generating the thrust force. The investigation of time variation of thrust force for three asymmetric pectoral fins in one period shows that the thrust force when the feathering amplitude is 30 degree has an advantage over those of other feathering amplitudes under constant flapping amplitude. Furthermore the investigation of tip deformation clarifies that spanwise deformation has positive influence on the generation of thrust force for the developed two kinds of elastic pectoral fins.

Because during iterative calculation simple wing theory was used to obtain the hydrodynamic force, only point loads were applied onto certain positions of pectoral fins,

which cannot describe the actual phenomena clearly. It is better to validate these results in the future by adopting computational fluid dynamics method to get the pressure distribution around the fin surface. Besides in order to clarify the mechanism more clearly, it is advisable to investigate what happens to the chordwise deformation. Finally The validation of the jointing effect of spanwise deformation and chordwise deformation of the flexible fins on hydrodynamics should be discussed.

Chapter 4 Effects of Pectoral Fin Form and Flexibility on the Motion Control of Underwater Vehicle

4.1 Introduction

Neurobiology studies have shown that the locomotion of animals is controlled hierarchically by the central nervous system, from the cerebral cortex level, the brainstem level to the spinal cord level [58]. During the controlling process, sense and feedback is important for different levels' central nervous systems to make the necessary and correct analysis and give the quick and efficient orders, which will affect the locomotion expression consequently. So are the biomimetic underwater vehicles. One challenge of underwater vehicle controlling lies in the need to consider the adjustment of the transient status of propulsors from the feedback information about surrounding environments. This adjustment process has close relationship with the selection of controlling mechanism of propulsors.

Many researches have been done on the controlling scheme for biomimetic underwater vehicles. Barret et al. developed a self-optimizing motion controller based on a generic algorithm in order to overcome two difficulties: that the overall intractability of the hydrodynamics of a flexible body precludes a purely analytical solution and that the immense size of the experimental variable space prevents a purely empirical one [59]. Harper et al. proposed the design of an optimal spring constant to actuate the oscillating foil [60]. Using discrete-time continuous feedback and iteration of motion planning step, Bullo et al. presented the motion control algorithms for an underactuated mechanical control system to solve the PTP reconfiguration, static interpolation, and exponential stabilization, which can typically be applied to the model of underwater vehicles [61].

Saimek et al. proposed a practical maneuvering control strategy for an aquatic vehicle that uses an oscillating foil as a propulsor, which consists of an off-line motion planning step and an on-line feedback control step [62]. Yu et al. developed an experimental closed-loop control system for a 4-link and free-swimming biomimetic robotic fish and the fish's motion control task is decomposed into online speed control and orientation control [63]. By using Central Pattern Generator-Based, Zhao et al. developed a flipper-actuated turtle-like underwater robot [20] and Zhou et al. developed a robotic manta ray (RoMan-II) [64].

Although much work on the controlling scheme of the propulsors for underwater vehicles, much of them are based on the rigid propulsors and little work has been done about the compatibility between underwater robots and flexible fins. Is it necessary to adjust the controlling mechanism of underwater vehicles if propelled by pectoral fins with different elastic properties? In real target mission carryout, what kind of flexible fins can achieve the best performance? Focusing on these questions, this chapter will explore the controlling schemes of paired oscillating pectoral fins.

Previous chapter describes the effect of flexible paired oscillating pectoral fins on the swimming performance of biomimetic underwater vehicle with the aspects of materials properties and manufacturing of the propulsors, kinematical expression of propulsor movement and the fluid dynamics evaluation. It shows that rigid and flexible pectoral fins can propel the underwater vehicle with different swimming velocities. This intrigues our curiosity that if rigid and flexible pectoral fins are used to propel PLATYPUS separately to achieve a prescribed mission, is there any difference about the controlling schemes and how about the results. This chapter could be thought of as an extension of the previous chapter, discussing the characteristics of flexible pectoral fins

from the viewpoint of the effect of their movements to the motion control of the attached underwater vehicles.

In this chapter Point-to-point (PTP) control, namely guiding an underwater vehicle move continuously and steadily from an initial point to a target point, is employed to verify the performance of different kinds of pectoral fins. PTP control is one of the basic problems concerning the robot's controllability. Many complex motions of the fish such as obstacle avoidance and formation control could be simplified into a series of PTP controls. In our case, the vehicle PLATYPUS is guided from a far point to a near target point and finally hovers around the target point with a prescribed attitude (Figure 4.1).

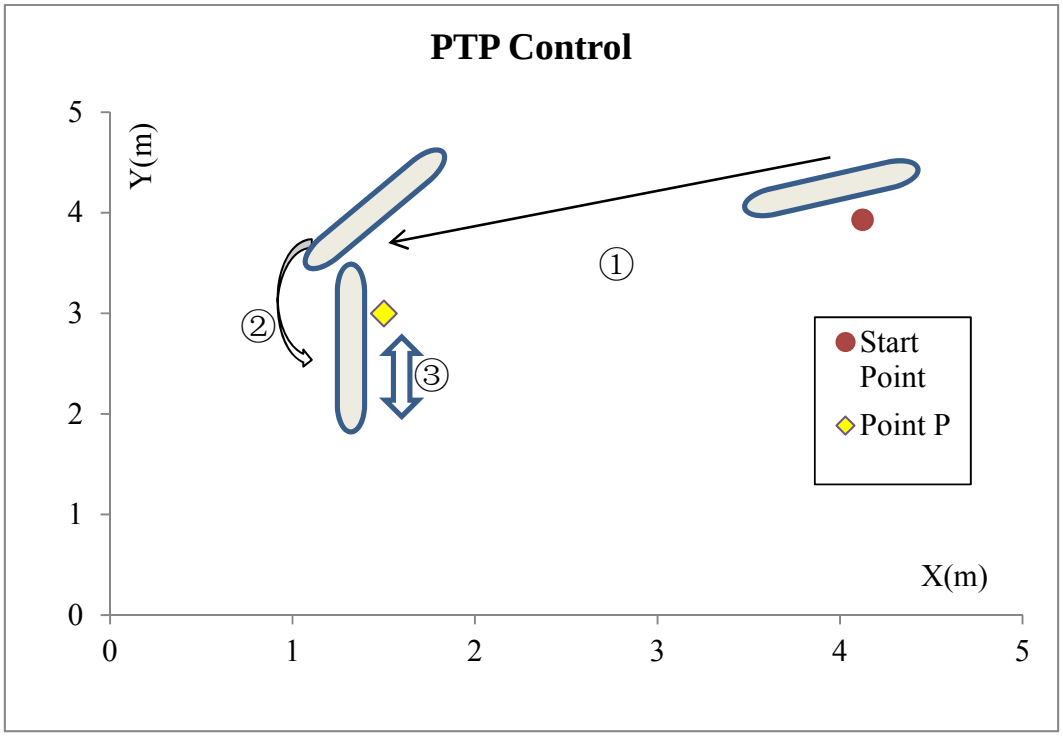

Figure 4.1 The trajectory of PLATYPUS in PTP control

4.2 Control Laws of PLATYPUS

Because the motion of vehicle is highly nonlinear about the control variables and also because it is difficult to express the equations of the motion explicitly in terms of control variables, fuzzy control algorithm is adopted here.

4.2.1 Fuzzy Control Theory

Fuzzy control systems are developed based on fuzzy mathematics, a branch of applied mathematics. While talking about fuzzy mathematics and its application, particularly in intelligent control systems, a typical question of common concern is first to be addressed: why is fuzzy mathematics necessary when there already exist well-developed deterministic as well as stochastic mathematics? Indeed, deterministic and stochastic mathematics has been developed for a long time. But both require precise knowledge and perfect information, such as certainty (crisp numbers, explicit functions, exact distributions, accurate means and variances, *etc.*), and when data information is not ideal (only partial, vague, or even conflict) they cannot be applied to formulate and solve any problems. Ironically, the majority of real-world problems are very often inexactly formulated and imperfectly described. Therefore fuzzy mathematics, beginning with the fundamental concept of fuzzy sets, come up to handle such abnormal and irregular problems [65].

Fuzzy set theory basically extends the classical set theory that has membership of its elements described by the classical characteristic function (either “is” or “is not” a member of the set), to allow for partial membership described by a membership function (both “is” and “is not” a member of the set at the same time, with a certain degree of belongings to the set). Roughly, fuzzy membership functions bridge the idealized, crisp, sharp, and discontinuous gap between “yes” and “no”, between “in” and “out”, between

"true" and "false", *etc*. As a result, it demonstrates great capabilities and flexibilities in solving many real-world problems which classical mathematics fails to handle.

Fuzzy systems are the application of fuzzy mathematics to control systems. In a sense, fuzzy systems can be "trained" and can "learn" how to perform throughout a control task, and to some extent fuzzy controllers can act in a humanlike fashion in making "decisions" to what actions to take under various conditions. Compared to classical mathematics and conventional control theory, fuzzy logic control theory has the advantage in modeling and controlling complex nonlinear dynamics systems, particularly ill-formulated and partially described physical systems.

The entire process of fuzzy control system can be decomposed into fuzzification, fuzzy operation and defuzzification. The overall structure of a fuzzy logic controller is shown in Figure 4.2. The key step—fuzzy operation—is executed by a logic rule base consisting some IF-THEN rules established by fuzzy logic and human analysis of the physical problem at hand.

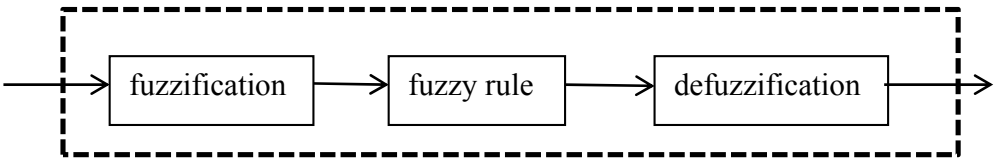

Figure 4.2 A typical fuzzy logic controller

4.2.1.1 Fuzzification

As mentioned earlier, the fundamental feature of fuzzy set theory that distinguishes itself from classical set theory is that it allows partial membership of an element with respect to a set: an element can partially belong to a set and, in the meantime, partially not belong to the same set. For example, Figure 4.3 shows grades of

an element, x, belonging to the set, X, specified by normalized triangle membership function, $\mu_X : X \to [0,1]$. There are two extreme cases: $\mu_X(x) = 0$ means $x \notin X$ and $\mu_X(x) = 1$ means $x \in X$ in the classical sense. But $\mu_X(x) = 0.3$ means x belongs to X only with grade 0.3, or equivalently, x does not belong to X with grade 0.7. A set, X, along with a membership function defined on it, $\mu_X(\cdot)$, is called a fuzzy set and is denoted (X, μ_X).

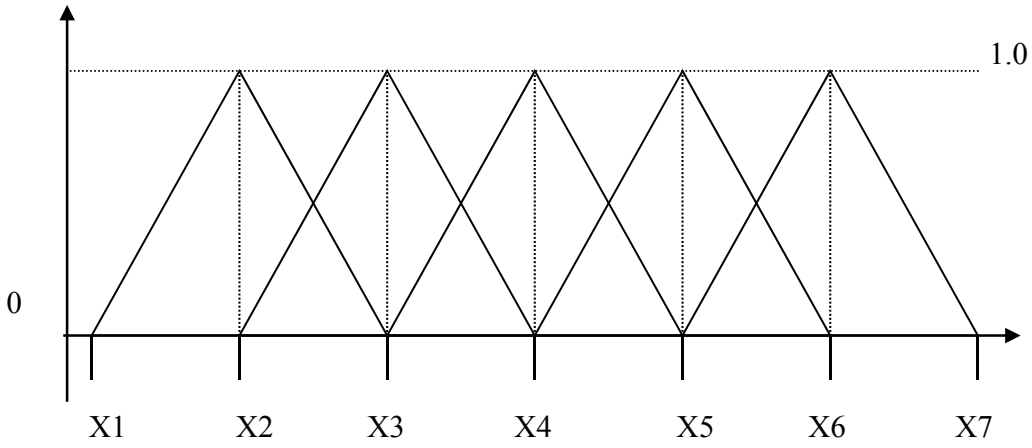

Figure 4.3 Normalized triangle membership function

Given a classical set of real numbers, $X = [-1,1]$, a point $x \in X$ assumes a real value, say $x = 0.4$, This is a crisp number without fuzzification. However, if a membership funtion $\mu_X(\cdot)$ is introduced to associate with the set X, then (X, μ_X) becomes a fuzzy set, and the same point $x = 0.4$ has a membership grade quantified by $\mu_X(x)$ (for instance, $\mu_X(x) = 0.9$). As a result, x has not one but two values associated with the point: $x = 0.4$ and $\mu_X(x) = 0.9$. In this sense, x is said to be fuzzied. For convenience, instead of saying that "x is in the set X with a membership value $\mu_X(x)$", in common practice it is usually said "x is X". If a member, x, belongs to two fuzzy sets, one says "x is X_1 AND x is X_2", and so on. Here, the relation AND needs a logical operation to

perform. As a result, this statement eventually yields only one membership value for the element x, denoted by $\mu_{X_1 \times X_2}(x)$. There are several logical operations to implement the logical AND; they are quite different but all valid within their individual logical system. A commonly used one is to take the minimum or maximum value between the two membership values of the same element x, namely,

$$\mu_{X_1 \times X_2}(x) = \min\left\{\mu_{X_1}(x), \mu_{X_2}(x)\right\} \quad \text{or} \quad \mu_{X_1 \times X_2}(x) = \max\left\{\mu_{X_1}(x), \mu_{X_2}(x)\right\} \qquad (4.1)$$

4.2.1.2 Fuzzy Logic Rule

The majority of fuzzy logic control systems are knowledge based systems. This means that either their fuzzy models or their fuzzy logic controllers are described by fuzzy logic IF-THEN rules, which can be expressed in the following languages (in the case of two input variables):

IF x1 is A1, AND x2 is B1	THEN y is C1
IF x1 is A1, AND x2 is B2	THEN y is C2
IF x1 is A2, AND x2 is B1	THEN y is C3
IF x1 is A2, AND x2 is B2	THEN y is C4
:	:
:	:
:	:
IF x1 is An, AND x2 is Bn	THEN y is Cn^2

Here, x1, x2 are input variables, y is output variable. And, A1, A2, …, An B1, B2, …, Bn C1, C2, …, Cn are fuzzy sets. The logic relationship is called fuzzy rule. If there are two input variables, fuzzy rule can be expressed as Table 4.1 below.

These rules have to be established based on human expert's knowledge about the system, the controller, and the performance specifications, *etc.*, and they must be implemented by performing rigorous logical operations.

Table 4.1 Fuzzy rule

x1 / x2	A1	A2	A3	…	An
B1	C1	C3	…	…	…
B2	C2	C4	…	…	…
B3	…	…	…	…	…
…	…	…	…	…	…
Bn	…	…	…	…	Cn^2

4.2.1.3 Defuzzification

After fuzzy reasoning a linguistic output variable is obtained, which needs to be translated into a crisp value. The objective is to derive a single crisp numeric value that best represents the inferred fuzzy values of the linguistic output variable. Defuzzification is such an inverse transformation which maps the output from the fuzzy domain back into the crisp domain. The result of defuzzication usually is a physical quality acceptable by the original real system. Whether or not this defuzzification result works well depends on the correctness and effectiveness of the logic rule base, while the latter depends on the designer's knowledge and experience about the physical system or process for control. A general weighted average formula for defuzzification is the following convex combination of the individual outputs, which tends to produce an integral output considering all the elements of the resulting fuzzy set with the corresponding weights.

$$output = \sum_{i=1}^{r} \alpha_i y_i := \sum_{i=1}^{r} \frac{w_i}{\sum_{i=1}^{r} w_i} y_i \tag{4.2}$$

with notation referred to the rule base above, where

$$w_i = \mu_{Y_i}(y_i), \qquad \alpha_i := \frac{w_i}{\sum_{i=1}^{r} w_i} \geq 0, \qquad i = 1, \cdots, r, \qquad \sum_{i=1}^{r} \alpha_i = 1.$$

4.2.2 Azimuth and Distance Control of PLATYPUS

The PTP control of PLATYPUS includes azimuth control and distance control during the guidance of the vehicle, which will be explained sequentially.

Then one problem comes up—how to define the range of control variables. From the point of carrying out specific task by underwater vehicles, sometimes the vehicle has to swim fast and turn quickly in order to reach the prescribed location, and in this case large velocity is required. But sometimes the vehicle has to finely adjust its gesture to hover or track certain trajectory, and here it means the vehicle can be able to slow down itself by offsetting initial motions or achieve zero velocity freely.

So it is better to investigate the direct relationship between control variables and vehicle locomotion expression. Then range of control variables can be chosen by the standard that the vehicle can achieve from low to high velocities monotonically.

4.2.2.1 Azimuth Control of PLATYPUS

In water currents, dexterous turning ability is necessary to keep the posture of underwater vehicles. As for PLATYPUS, azimuth control is performed by using the upper and below rear pectoral fins through controlling the rowing angles of the 3MDMPFs on the basis of motion parameters shown in Table 4.2, where $\Delta\Phi_{FE}$ is set as a control variable for azimuth control. As Figure 4.4 shows, the azimuth fuzzy control of

PLATYPUS is adopted in a range of ±20° to the target azimuth. If it is out of this range, the maximum turning force is output to adjust the gesture of PLATYPUS as quickly as possible.

Table 4.2 Basic parameters for azimuth control

Φ_{R0}	Φ_{RA}	$\Delta\Phi_{R}$	Φ_{FE0}	Φ_{FEA}	$\Delta\Phi_{FE}$	Φ_{FL0}	Φ_{FLA}	$\Delta\Phi_{FL}$
0	30	0	0	40	Var	0	0	0

(Unit: degree)

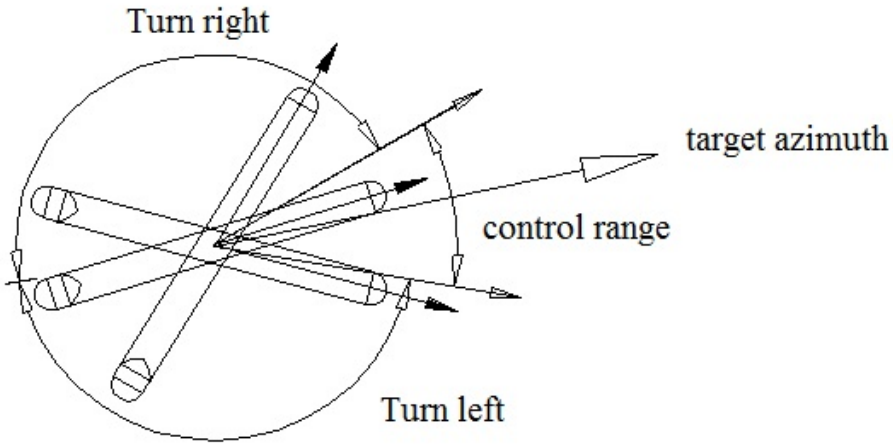

Figure 4.4 Azimuth control of PLATYPUS

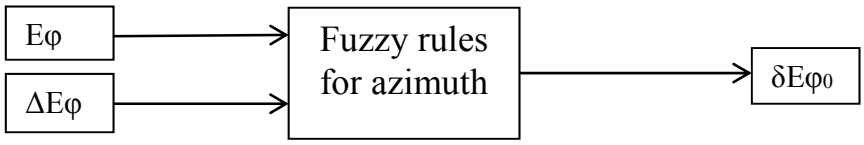

Figure 4.5 Azimuth fuzzy controller for PLATYPUS

As shown in Figure 4.5, two input variables $E\varphi$ and $\Delta E\varphi$ are defined from the azimuth φ of the vehicle and the target azimuth φ_0 as follows:

$$E\varphi = \varphi_0 - \varphi \qquad \Delta E\varphi = -\dot{\varphi} \tag{4.3}$$

where $\dot{\varphi}$ denotes the yaw rate. Each value is transformed into five fuzzy sets of Negative Big (NB), Negative Small (NS), Zero (Z), Positive Small (PS), Positive Big (PB) using continuous triangle membership functions (Figure 4.3). The output variable $\delta E\varphi$ is also represented by five fuzzy sets. Here the i-th fuzzy rule is expressed as below:

$$\text{IF} \quad \Delta E\varphi = Ai, E\varphi = Bi \quad \text{THEN} \quad \delta E\varphi = Ci \tag{4.4}$$

where Ai , Bi and Ci denote the corresponding fuzzy sets to the i-th fuzzy rule in Table 4.3. The values of the parameters of membership function in azimuth control are given in Table 4.4.

The membership fuction $\mu(\delta E\varphi)$ is obtained as:

$$\mu(\delta E\varphi) = \max_{1\le i\le 25}\left\{\min\left\{\mu Ai(\Delta E\varphi), \mu Bi(E\varphi)\right\}\cdot \mu Ci(\Delta E\varphi)\right\} \tag{4.5}$$

The crisp value of the output variable $\delta E\varphi$, denoted by $\delta E\varphi_0$ is given by:

$$\delta E\varphi_0 = \int \mu(\delta E\varphi)\cdot \delta E\varphi \cdot d\delta E\varphi \,/ \int \mu(\delta E\varphi)\cdot d\delta E\varphi \tag{4.6}$$

Finally the phase angle $\Delta\Phi_{FE}\_ur(t)$ and $\Delta\Phi_{FE}\_lr(t)$ for the upper-rear feathering phase angle and the low-rear feathering phase angle are given as follows:

$$\begin{aligned} \Delta\Phi_{FE}\_ur(t) &= \Delta\Phi_{FE}\_ur(t-\Delta t) - \delta E\varphi_0 \\ \Delta\Phi_{FE}\_lr(t) &= \Delta\Phi_{FE}\_lr(t-\Delta t) - \delta E\varphi_0 \end{aligned} \tag{4.7}$$

Table 4.3 Fuzzy rule for azimuth control

		$\Delta E\varphi$				
		NB	NS	ZO	PS	PB
$E\varphi$	NB	NB	NB	NB	NS	ZO
	NS	NB	NB	NS	ZO	PS
	ZO	NB	NS	ZO	PS	PB
	PS	NS	ZO	PS	PB	PB
	PB	ZO	PS	PB	PB	PB

Table 4.4 Values of the parameters of membership function in azimuth control

	X1	X2	X3	X4	X5	X6	X7
$E\varphi$ (degree)	-100	-20	-10	0	10	20	100
$\Delta E\varphi$ (degree/s)	-100	-5.0	-1.0	0	1.0	5.0	100
$\delta E\varphi$ (degree)	-15	-10	-5	0	5	10	15

In order to confirm the control range of $\Delta\Phi_{FE}$, basic experiments were carried out to test the turning ability using only rear fins by changing $\Delta\Phi_{FE}$ from -110° to 110° for four types of fins. During the turning ability test, both fore fins were set into no motion. The results are given in Figure 4.6. From the graph, it can be seen that the control range of $\Delta\Phi_{FE}$ can be chosen in the range from -90° to 90° for Sym-rigd, in the range from -70° to 90° for Asym-rigid and Asym-harder. Asym-softer cannot be used in fuzzy control because it could not drive PLATYPUS to turn in counter-clockwise direction.

Chapter 4. Effects of Pectoral Fin Form and Flexibility

Due to a mechanical limitation of PLATYPUS, asymmetric fins have to employ their trailing edge as leading edge to generate the force to rotate the vehicle. It shows that among three asymmetric fins, Asym-harder shows the best performance in turning.As for Asym-softer, it cannot turn in counter-clockwise direction. From experiment videos, it was observed that the thin and soft trailing edge of Asym-softer fin swings freely underwater, which does not act in harmony with the motion of fins and therefore impairs the generation of thrust force. Consequently, fin flexibility can improve hydrodynamic performance; however, too much softness may have a negative effect.

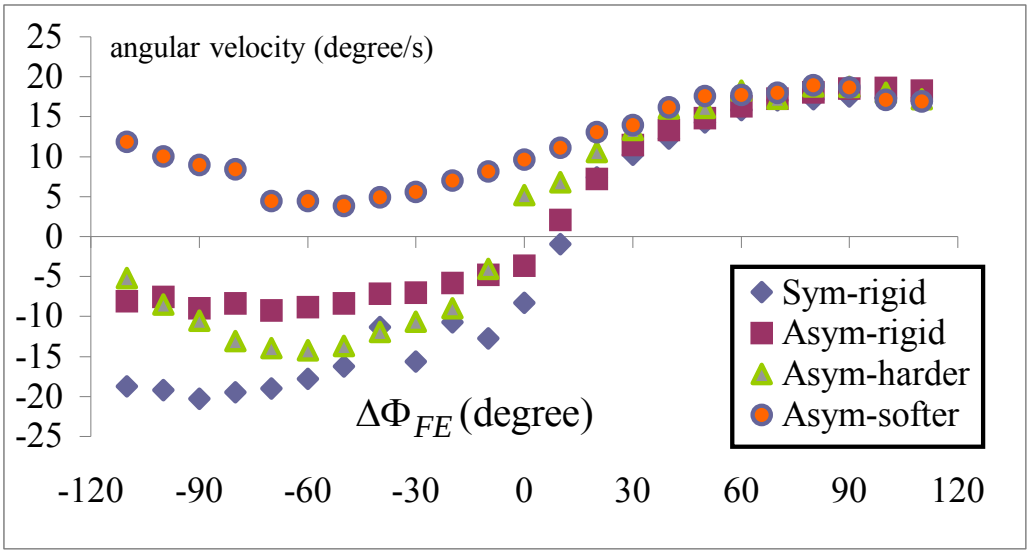

(sign of angular velocity: + clockwise; - counter-clockwise)

Figure 4.6 Turning ability test of PLATYPUS using only rear fins

4.2.2.2 Distance Control of PLATYPUS

Distance control is performed by using the right and left fore pectoral fins through controlling the flapping angles of the 3MDMPFs on the basis of motion parameters in Table 4.5.

Table 4.5 Basic parameters for distance control

Φ_{R0}	Φ_{RA}	$\Delta\Phi_{R}$	Φ_{FE0}	Φ_{FEA}	$\Delta\Phi_{FE}$	Φ_{FL0}	Φ_{FLA}	$\Delta\Phi_{FL}$
0	0	0	-90	40	0	0	30	Var

(Unit: degree)

X_0 and X are defined as the target distance and the current distance respectively. Then two input variables are defined as:

$$Ex = X_0 - X \quad \Delta Ex = -(Ex(t) - Ex(t-\Delta t))/\Delta t \tag{4.8}$$

where t and Δt denote time and time step. The fuzzy control rule used in distance control is shown in Table 4.6. $\mu(\delta Ex)$, the membership function of the output variable δEx, and the crisp value of the output variable, denoted by δEx_0 are calculated as:

$$\mu(\delta Ex) = \max_{1\le i\le 25}\left\{\min\left\{\mu Ai(\Delta Ex), \mu Bi(Ex)\right\}\cdot \mu Ci(\Delta Ex)\right\} \tag{4.9}$$

$$\delta Ex_0 = \int \mu(\delta Ex)\cdot \delta Ex\cdot d\delta Ex \Big/ \int \mu(\delta Ex)\cdot d\delta Ex \tag{4.10}$$

The values of the parameters of membership function in distance control are given in Table 4.7.

Then the flapping phase angle $\Delta\Phi FL\_lf$ and $\Delta\Phi FL\_rf$ for the left-forward flapping phase angle and the right-forward flapping phase angle can be calculates as:

$$\begin{aligned}\Delta\Phi_{FL\_lf}(t) &= \Delta\Phi_{FL\_lf}(t-\Delta t) - \delta Ex_0\\ \Delta\Phi_{FL\_rf}(t) &= \Delta\Phi_{FL\_rf}(t-\Delta t) - \delta Ex_0\end{aligned} \tag{4.11}$$

Table 4.6 Fuzzy rule for distance control

		ΔEx				
		NB	NS	ZO	NS	PB
Ex	NB	NB	NB	NB	NS	ZO
	NS	NB	NB	NS	ZO	NS
	ZO	NB	NS	ZO	NS	PB
	PS	NS	ZO	NB	PB	PB
	PB	ZO	PS	PB	NS	PB

Table 4.7 Values of the parameters of membership function in distance control

	X1	X2	X3	X4	X5	X6	X7
Ex (m)	-100	-1.0	-0.3	0	0.3	1.0	100
ΔEx (m/s)	-100	-0.1	-0.05	0	0.05	0.1	100
δEx (m)	-15	-10	-5	0	5	10	15

In order to confirm the control range of $\Delta\Phi_{FL}$, basic experiments were carried out to test the straight swimming ability using only fore fins for four types of fins. During swimming ability test, both rear fins were set into no motion. The results are given in Figure 4.7. From the graph, it can be seen that the control range of $\Delta\Phi_{FL}$ can be chosen from -130° to 60° for four types of fins.

From the graph, it can also be seen that Asym-harder can achieve larger working range compared to the other three pectoral fins, which is a very important advantage in precise control of underwater vehicles.

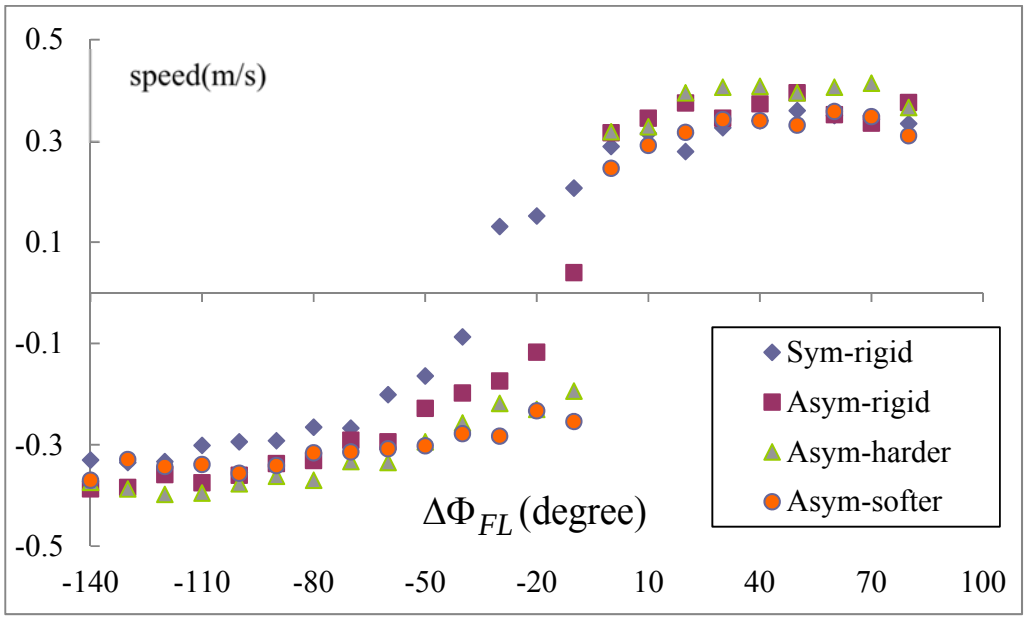

Figure 4.7 Swimming ability test of PLATYPUS using only fore fins

4.2.3 Determination of the Azimuth Value

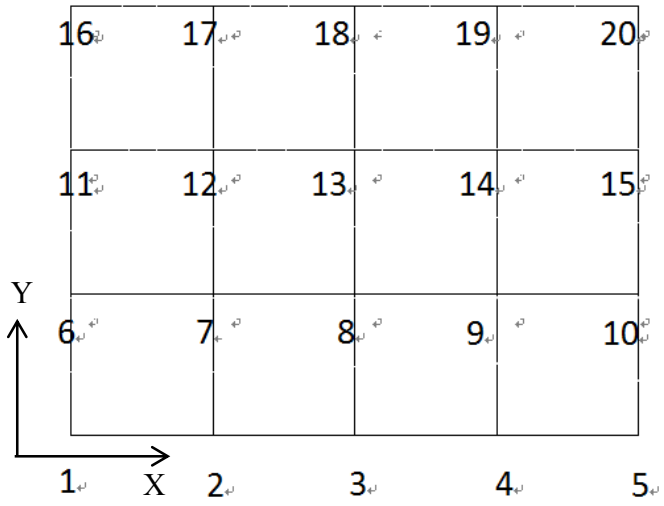

Figure 4.8 The azimuth map in the experimental area

Table 4.8 Coordinates and azimuth value parallel to X axis of each peak of azimuth map

		X (m)				
		0.54	1.54	2.54	3.54	4.54
Y (m)	1.505	133.93(1)	111.12(2)	154.94(3)	127.75(4)	129.2(5)
	2.505	125.95(6)	111.63(7)	125.39(8)	130.79(9)	126.97(10)
	3.505	106.1(11)	122.98(12)	135.78(13)	128.5(14)	152.62(15)
	4.505	111.27(16)	124.49(17)	131.73(18)	90.13(19)	114.38(20)

(Unit of azimuth: degree)

We constructed an azimuth map (including twelve 1m×1m squares, Figure 4.8) in the experimental area and measured the azimuth value $\Theta(X,Y)$ of each node parallel to X axis. Table 4.8 shows the coordinates and the azimuth value parallel to X axis of every node in the azimuth map.

With the azimuth map measured in Table 4.8, the azimuth of PLATYPUS $\Theta(X,Y)$ can be calculated from its location. At first, the nearest nodes to the location of PLATYPUS should be picked up and be numbered clockwise from (i) to (iv) as shown in Figure 4.9. Then by interpolating in the X direction, it can be obtained that:

$$\begin{aligned}\Theta(X,Y)_{(\mathrm{i})(\mathrm{ii})} &= \Theta(X_k,Y_k)+\{\Theta(X_k,Y_k)-\Theta(X_{k+1},Y_k)\}/(X_k-X_{k+1})\times(X-X_k)\\ \Theta(X,Y)_{(\mathrm{iii})(\mathrm{iv})} &= \Theta(X_k,Y_{k-1})+\{\Theta(X_k,Y_{k-1})-\Theta(X_{k+1},Y_{k-1})\}/(X_k-X_{k+1})\times(X-X_k)\end{aligned} \quad (4.12)$$

Next by interpolating in the Y direction, the azimuth value of PLATYPUS parallel to X axis can be calculated.

$$\Theta(X,Y)=\Theta_{(\mathrm{i})(\mathrm{ii})}+\{\Theta_{(\mathrm{i})(\mathrm{ii})}-\Theta_{(\mathrm{iii})(\mathrm{iv})}\}/(Y_k-Y_{k-1})\times(Y-Y_{k-1}) \quad (4.13)$$

However, due to the method in defining the numbers from (i) to (iv), sometimes the value of X_k-X_{k+1}, Y_k-Y_{k-1} will be zero. In that case, the numbers are adjusted as:

{(i)→(iv), (ii)→(i), (iii)→(ii), (iv)→(iii)}.

Furthermore, if PLATYPUS is outside the azimuth map, its azimuth value is defined as $\Theta = 110.15^{\circ}$.

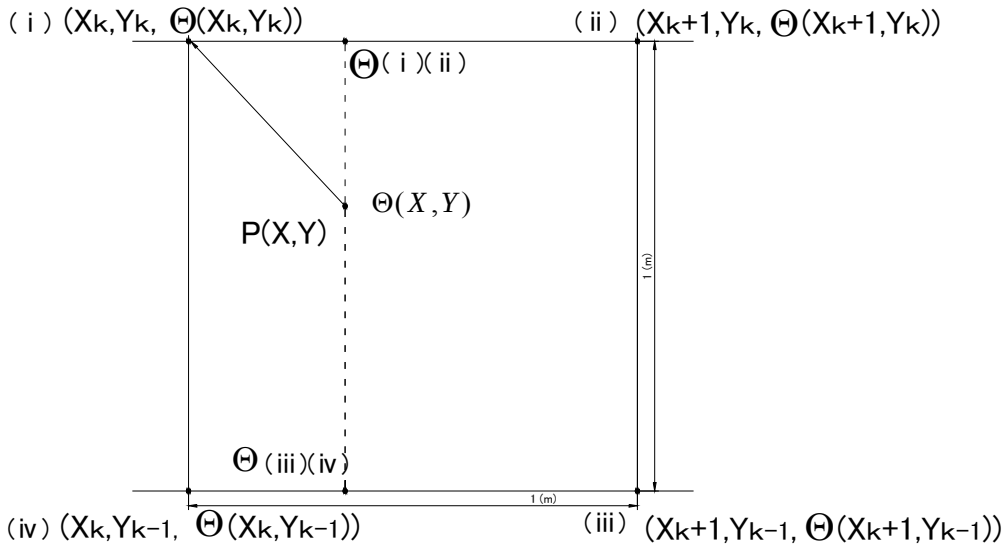

Figure 4.9 Surrounding nodes to the location of PLATYPUS

4.3 Control Strategy during Point-to-Point Test

The PTP control strategy consists of two modes:

Mode1: The center of the vehicle is located outside of the circle with the radius R_0. The fore pair of mechanical pectoral fins play a role in distance control about $Dist$ and the rear pair of mechanical pectoral fins play a role in azimuth control about $E\phi$ defined in Figure 4.10.

Mode2: The center of the vehicle is located inside the circle with the radius R_0. The fore pair of mechanical pectoral fins play a role in distance control about $Dist$ and

the rear pair of mechanical pectoral fins play a role in azimuth control about $E\phi$ defined in Figure 4.11.

The switch between two modes in PTP control test is given in Figure 4.12.

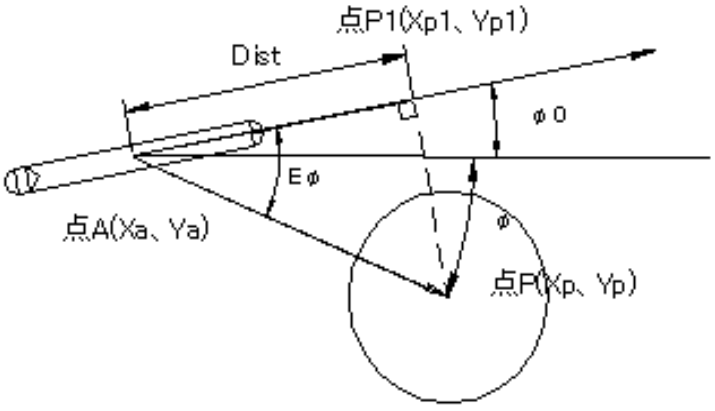

Figure 4.10 Notations for Mode1

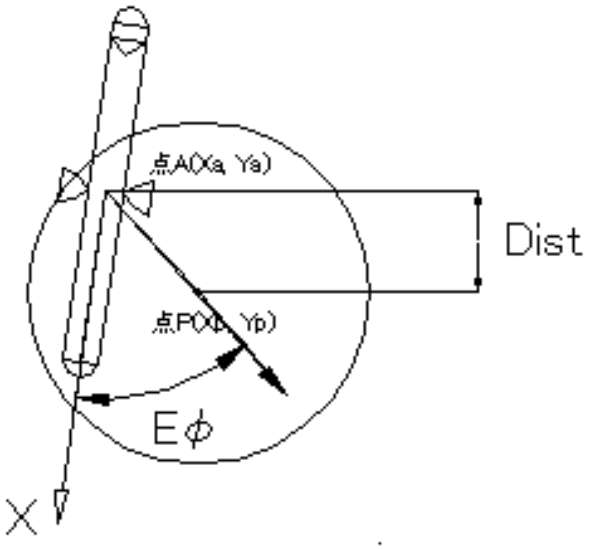

Figure 4.11 Notations for Mode2

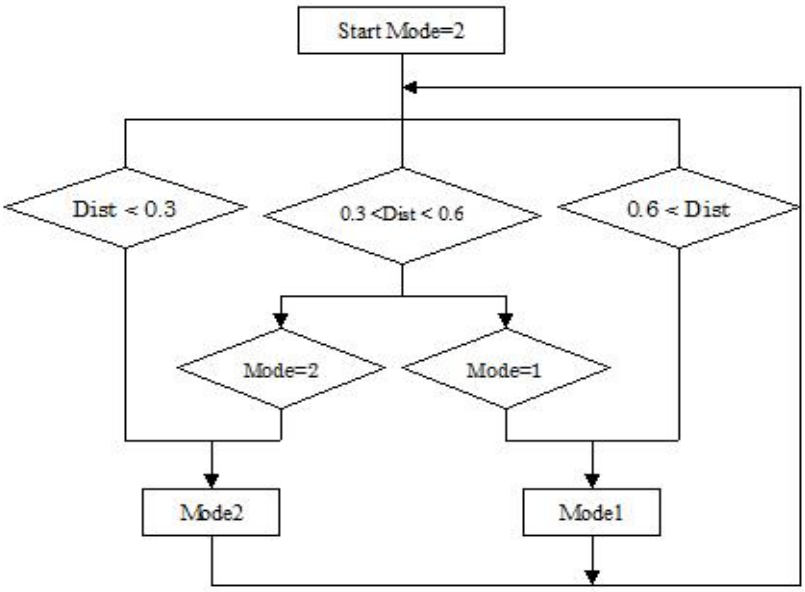

Figure 4.12 Switch of two modes in PTP control

4.4 PTP Control Test in Still Water

4.4.1 Evaluation Criteria of the Performance of Pectoral Fins in PTP Control

The performance of PTP control propelled by different pectoral fins can be evaluated quantitatively by the following three criteria:

a) Time that PLATYPUS spends in approaching the target point. The shorter the time, the faster the speed;

b) The average value of distance and azimuth difference between the current location of PLATYPUS and the target point. The smaller the difference, the more precise the control;

c) The standard deviation of distance and azimuth difference between the current location of PLATYPUS and the target point. The smaller the deviation, the more stable the control.

4.4.2 PTP Control for Three Kinds of Pectoral Fins in Still Water

Experiments were carried out at the towing tank of Osaka University (100m long, 7.8m wide and 4.35m deep).

During this stage we tried finding out the most appropriate fuzzy control rule for each asymmetric fin, namely the control rule that can minimize the distance and the change of azimuth to the target point. The reason lies in that original fuzzy rule was developed based on the properties of symmetric fins but during PTP experiments Asym-rigid and Asym-harder are also employed to propel the vehicle as well as Sym-rigid. Therefore different kinds of fuzzy rules were tested to find out the most appropriate one for each fin.

4.4.2.1 Fuzzy Rule Revision for Asymmetric Rigid Fin

The original and modified fuzzy control rules in azimuth control for Asym-rigid are given in Figure 4.13. Because Asym-rigid is not good at counterclockwise turning, the original azimuth control rule was modified strengthen its turning ability in the counterclockwise direction. For example, $E\varphi = NS$ and $\Delta E\varphi = PS$ mean that the vehicle is now a little over the target direction and turning slowly in the counterclockwise direction to the target azimuth from the definition in (4.3). According to the original azimuth control rule in Figure 4.13, the output is $\delta E\varphi = ZO$ at this stage, which means the vehicle will keep the previous state from the definition of (4.7). But in the modified azimuth control rule, the output is $\delta E\varphi = PS$ at this stage, which means the vehicle will strengthen its counterclockwise rotation from the definition of (4.7).

The original and modified control rules in distance control for Asym-rigid are given in Figure 4.14. Because the vehicle swims fast when inside the target circle, the

original distance control rule was modified to slow down the speed when the vehicle is near around the target point.

The corresponding real-time azimuth and distance comparisons of PTP control tests under original and modified fuzzy rules are given in Figure 4.15 and Figure 4.16 separately. It can be seen that modified fuzzy control rule can improve the performance of Asym-rigid in PTP control.

Azimuth

Eø \ △Eø	NB	NS	ZO	PS	PB
NB	NB	NB	NB	NS	ZO
NS	NB	NB	NS	ZO	PS
ZO	NB	NS	ZO	PS	PB
PS	NS	ZO	PS	PB	PB
PB	ZO	PS	PB	PB	PB

Eø \ Δ Eø	NB	NS	ZO	PS	PB
NB	NB	NB	NB	NS	ZO
NS	NB	NB	NS	***PS***	***PB***
ZO	NB	NS	ZO	PS	PB
PS	NS	ZO	PS	PB	PB
PB	ZO	PS	PB	PB	PB

Figure 4.13 Original and modified fuzzy rules for azimuth control of Asym-rigid

Distance

Ex \ △Ex	NB	NS	ZO	PS	PB
NB	NB	NB	NB	NS	ZO
NS	NB	NB	NS	ZO	PS
ZO	NB	NS	ZO	PS	PB
PS	NS	ZO	PS	PB	PB
PB	ZO	PS	PB	PB	PB

Ex \ Δ Ex	NB	NS	ZO	PS	PB
NB	NB	NB	NB	NS	ZO
NS	NB	NB	NS	***PS***	PS
ZO	NB	NS	ZO	PS	PB
PS	NS	***NS***	PS	PB	PB
PB	ZO	PS	PB	PB	PB

Figure 4.14 Original and modified fuzzy rules for distance control of Asym-rigid

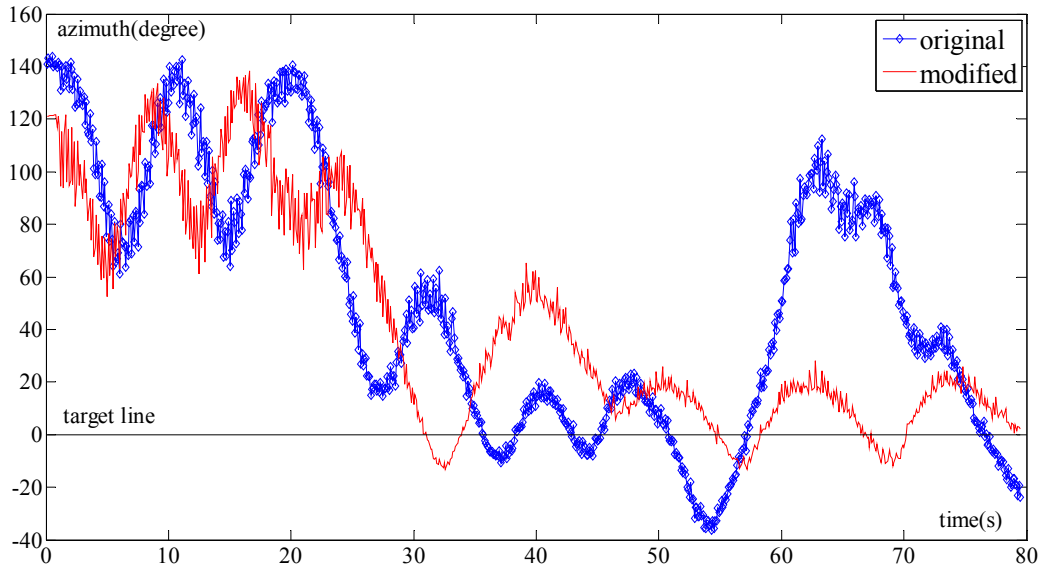

Figure 4.15 Comparison of azimuth in PTP control in still water for Asym-rigid under original and modified fuzzy rules

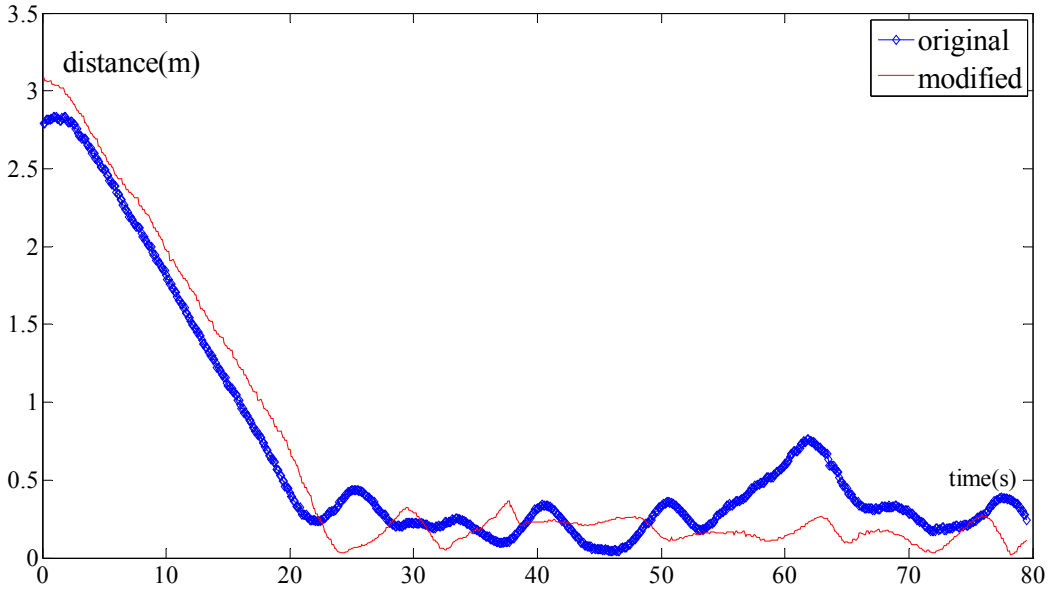

Figure 4.16 Comparison of distance in PTP control in still water for Asym-rigid under original and modified fuzzy rules

4.4.2.2 Fuzzy Rule Revision for Asymmetric Harder Flexible Fin

The original and modified fuzzy control rules in azimuth control and distance control for Asym-harder are given in Figure 4.17 and Figure 4.18. Because Asym-harder is not good at turning counterclockwise, the azimuth control rule was modified to strengthen its turning ability in the counterclockwise direction. And also because the vehicle swims fast when inside the target circle, the distance control rule was modified to slow down the speed when the vehicle is near around the target point.

The corresponding real-time azimuth and distance comparisons of PTP control tests under original and modified fuzzy rules are given in Figure 4.19 and Figure 4.20 separately. It can be seen that modified fuzzy control rule can improve the performance of Asym-harder in PTP control.

Eø \ △Eø	NB	NS	ZO	PS	PB
NB	NB	NB	NB	NS	ZO
NS	NB	NB	NS	ZO	PS
ZO	NB	NS	ZO	PS	PB
PS	NS	ZO	PS	PB	PB
PB	ZO	PS	PB	PB	PB

Azimuth

E \ Δ Eø	NB	NS	ZO	PS	PB
NB	NB	NB	NB	NS	ZO
NS	NB	NB	NS	***PS***	PS
ZO	NB	NS	ZO	PS	PB
PS	NS	***NS***	PS	PB	PB
PB	ZO	PS	PB	PB	PB

Figure 4.17 Original and modified fuzzy rules for azimuth control of Asym-harder

Distance

Ex \ △Ex	NB	NS	ZO	PS	PB
NB	NB	NB	NB	NS	ZO
NS	NB	NB	NS	ZO	PS
ZO	NB	NS	ZO	PS	PB
PS	NS	ZO	PS	PB	PB
PB	ZO	PS	PB	PB	PB

Ex \ ΔEx	NB	NS	ZO	PS	PB
NB	NB	NB	NB	NS	ZO
NS	NB	NB	NS	***PS***	***PB***
ZO	NB	NS	ZO	PS	PB
PS	***NB***	***NS***	PS	PB	PB
PB	ZO	PS	PB	PB	PB

Figure 4.18 Original and modified fuzzy rules for distance control of Asym-harder

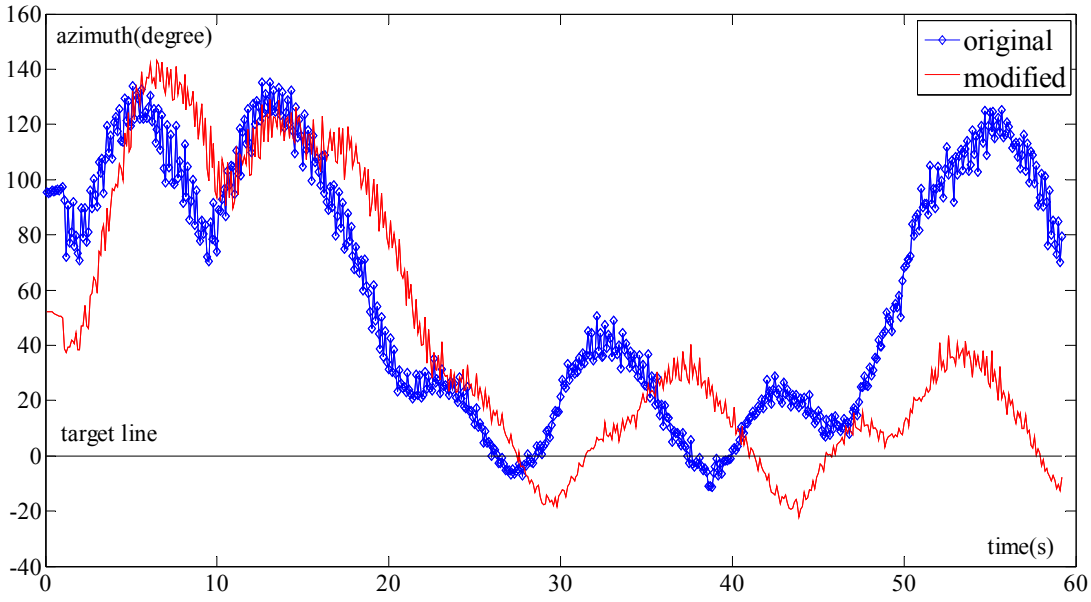

Figure 4.19 Comparison of azimuth in PTP control in still water for Asym-harder under original and modified fuzzy rules

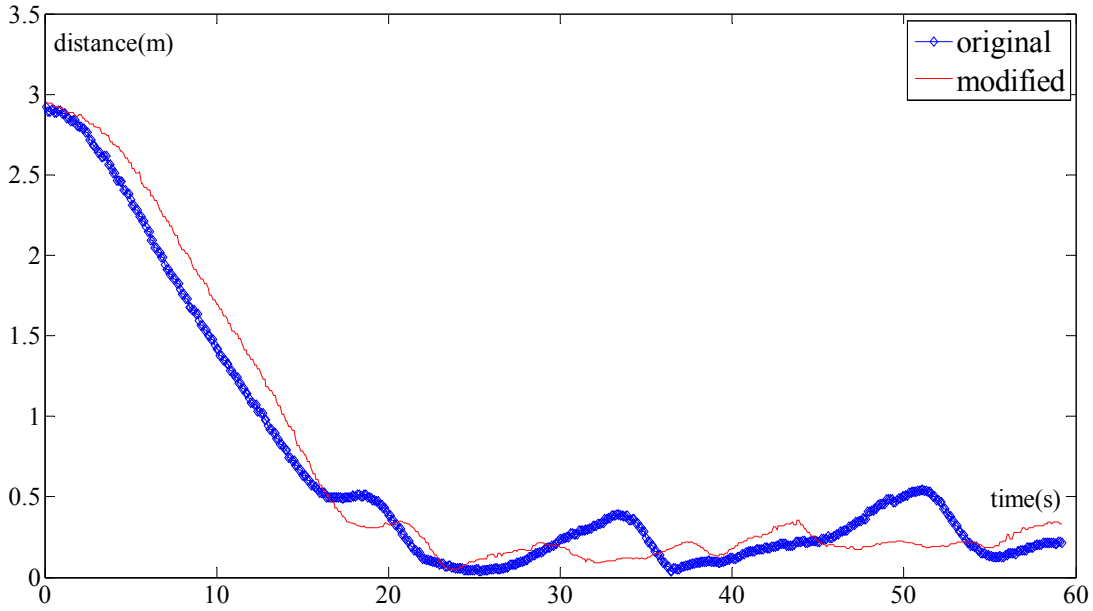

Figure 4.20 Comparison of distance in PTP control in still water for Asym-harder under original and modified fuzzy rules

4.4.2.3 Comparisons of PTP Control Under Three Types of Fins in Still Water

Comparisons among the results of PTP control for three kinds of pectoral fins under modified control rules are shown in Figure 4.21 and Figure 4.22. Statistical comparison is given in Table 4.9 (The statistics sample was taken from t=30s to the end moment). It can be seen that in still water the performances of the distance control are almost the same for three kinds of fins. But from the viewpoint of the performance of the azimuth control, Asym-harder exerts the best control performance in terms of standard deviation of offset azimuth from target azimuth, because fluctuation of azimuth decreases workability of the robot like observation by cameras.

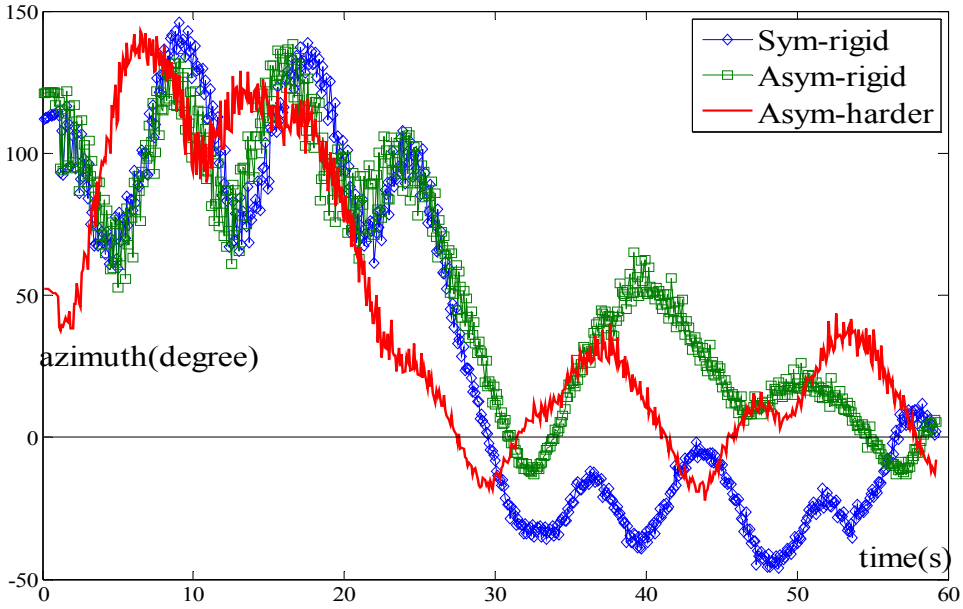

Figure 4.21 Comparison of azimuth in PTP control in still water for three pectoral fins under modified control rules

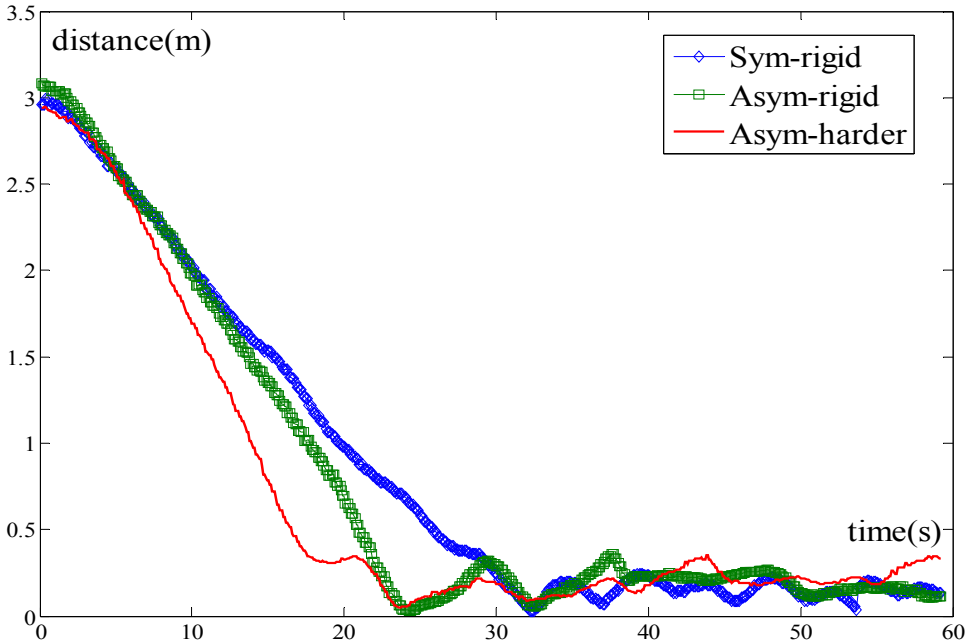

Figure 4.22 Comparison of distance in PTP control in still water for three pectoral fins under modified control rules

Table 4.9 Statistical comparison of PTP control in still water

Category	Azimuth (degree)		Distance (m)	
Properties	Average	Standard-deviation	Average	Standard-deviation
Sym-rigid	-10.76	27.68	0.15	0.108
Asym-rigid	18.99	22.47	0.17	0.069
Asym-harder	10.18	8.01	0.21	0.065

4.5 PTP Control Test in Water Currents

Three thrusters were set up at the water depth of 0.55m to generate water currents in the lateral direction of the towing tank. Figure 4.23 gives the positions of the thrusters, start point and target point within experimental area and Figure 4.24 shows the distribution of water currents at the water depth of 0.55m. The mean value of water currents is 0.095m/s.

Comparisons among the results of PTP control under three kinds of pectoral fins in water currents are shown in Figure 4.25 and Figure 4.26 separately. Statistical comparison is shown in Table 4.10 (the statistics sample was taken from t=30s to the end moment). Generally speaking, the performance of three pectoral fins in water currents is worse than that in still water. From Figure 4.23 it can be seen that the target point is located very near to one thruster and from Figure 4.24 we can also know that the water currents along the axes of thrusters are stronger than those in other areas. Both reasons above cause the underwater vehicle difficult to hover stably around the target point.

It is found that there is not so much difference in distance control among three types of pectoral fins, but Sym-rigid is superior to other two asymmetric fins in fluctuation of azimuth. Asymmetric fins cannot produce enough force to turn against

water currents, especially for the flexible one. Sometimes the robot can turn to the target azimuth only when it is pushed away from the thrusters. The reason lies in that due to the mechanical limitation of PLATYPUS, symmetric fin can use both edges of the fin effectively during both clockwise and counterclockwise rotation, but asymmetric fins can use their leading edge for production of lift force more effectively in clockwise rotation than in counterclockwise rotation.

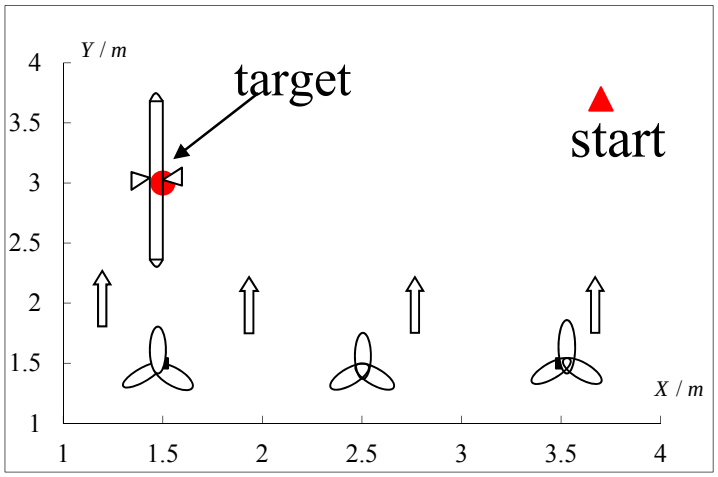

Figure 4.23 Allocation of thrusters, start point and target point

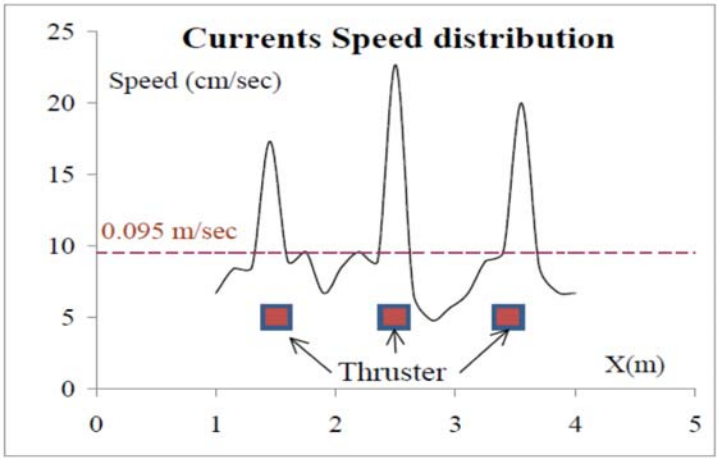

Figure 4.24 Distribution of water currents

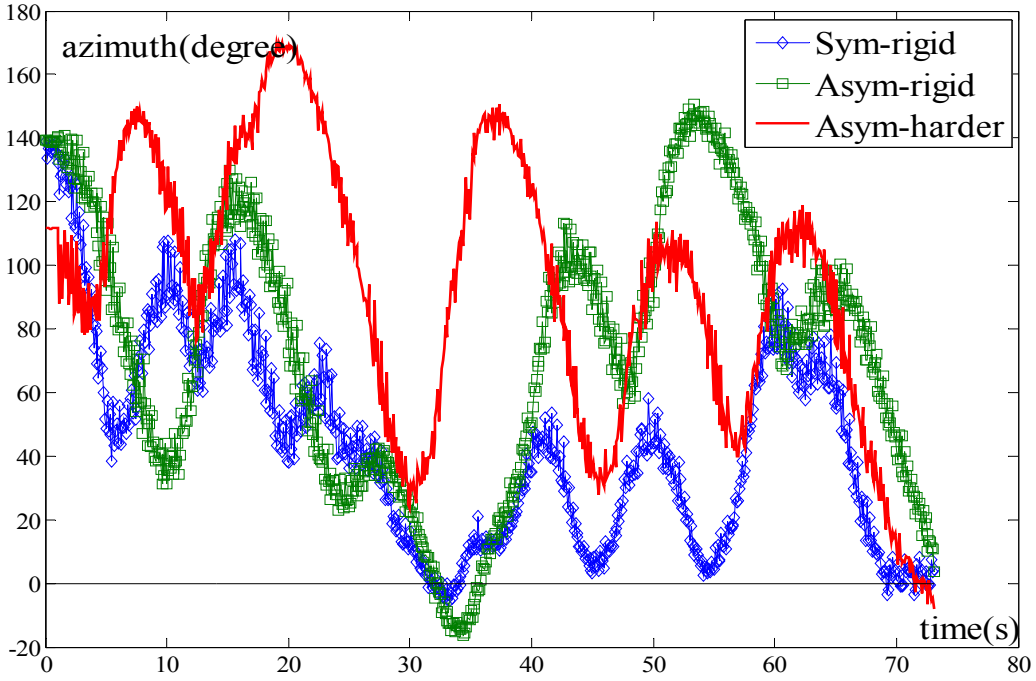

Figure 4.25 Comparison of azimuth in PTP control in water currents for three fins

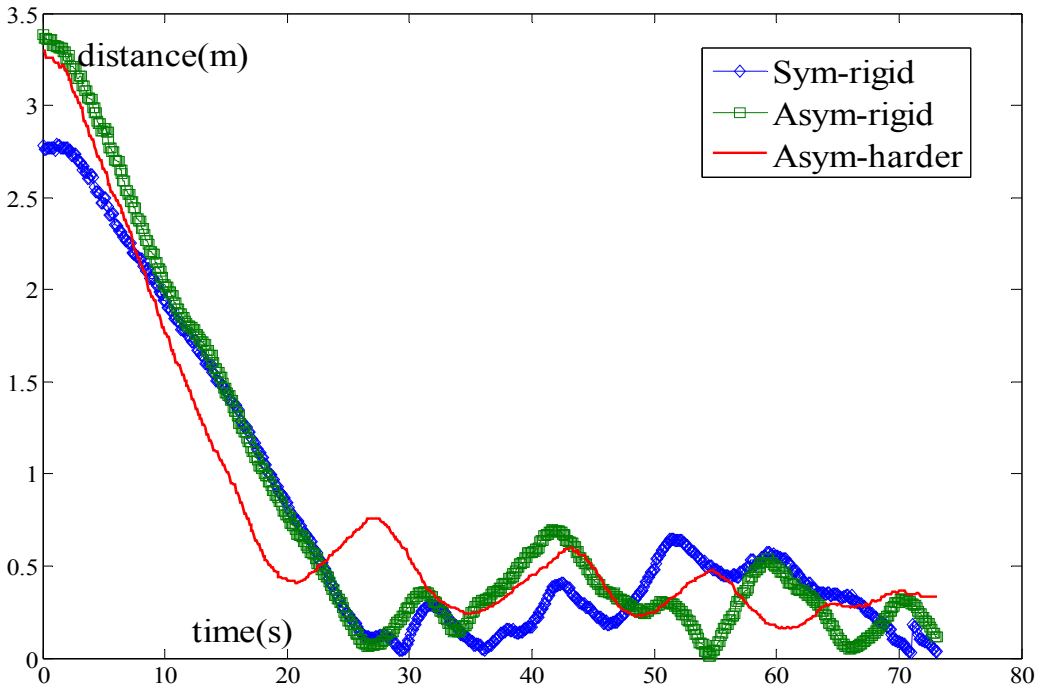

Figure 4.26 Comparison of distance in PTP control in water currents for three fins

Table 4.10 Statistical comparison of PTP control in water currents

Category	Azimuth (degree)		Distance (m)	
Properties	Average	Standard-deviation	Average	Standard-deviation
Sym-rigid	28.25	23.31	0.31	0.17
Asym-rigid	58.91	46.58	0.29	0.16
Asym-harder	60.78	33.21	0.32	0.11

4.6 Conclusion and Discussion

In this chapter PTP control tests were employed to check the performance of different kinds of pectoral fins and verify its effect to the controlling mechanism of underwater vehicles in real target mission carryout.

First of all, from turning ability test of PLATYPUS using only rear fins the azimuth fuzzy control range is selected and it also shows asymmetric flexible softer fin cannot be used in PTP control because it could not propel PLATYPUS to turn in counter-clockwise direction; from swimming ability test of PLATYPUS using only fore fins the distance fuzzy control range is selected. Secondly, during the PTP control test in still water, fuzzy control rules for asymmetric fins are improved to find the most suitable one for each fin; asymmetric flexible harder fin behaves better compared to asymmetric rigid fin and symmetric rigid fin. Thirdly, during the PTP control test in water currents symmetric rigid fin does better compared to the other two asymmetric fins. This is due to the feathering motion limitation of PLATYPUS, leading to asymmetric fins have to employ their trailing edges as leading edges to generate force to rotate the vehicle.

The work in this chapter shows that compatibility between underwater vehicles and pectoral fins and fin design process is a series of try-and-trial stages. During this

process different factors may dominate the performance in different working conditions. For instance, flexibility plays a positive role during swimming test, but during rotation test of PLATYPUS flexibility instead becomes a disadvantage factor because of the mechanical limitation of the vehicle itself.

Therefore it can be said that the performance of the fin is limited to the mechanical workout and depends on the working conditions of the vehicle. During fin design, it is advisable to take into account the matching among many factors: fin shape, fin flexibility, mechanical workout probability, working conditions and so on. Then according to the specific characteristics of each fin, the designers have to find out the suitable controlling mechanism for each one to achieve certain prescribed mission.

Chapter 5 Conclusion

5.1 Conclusion

In this dissertation centering on how to apply paired flexible biomimetic flapping appendages onto and how to investigate the effects of their locomotion on the swimming performance of their attached bodies, a united methodology is tentatively narrated to evaluate the performance of flexible artificial pectoral fins and prosthetic fore flippers from the aspects of (1) material properties and manufacturing of the propulsors; (2)3D kinematics of propulsor movement; (3) the fluid dynamics effects of propulsor motion on the attached bodies. Furthermore, as an extension, this dissertation also discusses the characteristics of pectoral fins from the viewpoint of the effect of fin form and flexibility on the motion control of the attached underwater vehicles by allowing the vehicle to carry out a specific task. The repeating of these steps would allow for further experimental and computational investigation of changes to propulsor design and for testing of hypothesized relationships between movement and force generation. The accumulation of such a comprehensive suite of data would possibly provide some references for other researchers in this area.

a) Material Properties and Manufacturing of Flexible Propulsors

Although in the past research elastic fin rays and webs or shape memory alloy are always employed to construct flexible pectoral fins or flippers, in this dissertation elastic materials only are used directly to manufacture paired flexible oscillating limbs. The prosthetic flippers are made of a kind of copolymer and the flexible pectoral fins are

made of silicon gums. The manufacturing processes for different pectoral fins and flippers are also different because of their special material properties and locomotion workout. The results show these elastic pectoral fins and prosthetic flippers can perform the corresponding movements well.

b) 3D Kinematics of Propulsor Movement

On the one hand, by observing the motion trajectories of fore flippers of sea turtles, it can be seen that on the horizontal plane parallel to the body of sea turtles, the fore flippers of Sho and Yu depict a circular arc with large curvature in both the power stroke and the recovery stroke, but in case of Yu equipped with prosthetic flippers, the projecting trajectory on this plane is a circular arc with small curvature; on the vertical plane from the side view of sea turtles, the projecting trajectories of the fore flippers of Sho and Yu are ovals but in the case of Yu equipped with prosthetic flippers the trajectory is similar to an oval with twist at the posterior position for the left prosthetic flipper and at the middle position for the right prosthetic flipper. On the other hand as for the mechanical pectoral fin system, the fin controlling equations and parameters are explained in details.

Actually the fore flippers of marine turtles and the pectoral fins of fish relying on labriform propulsion for sustained cruising adopt the similar swimming kinematic mode—flapping locomotion, during which the propulsive appendages reciprocate upward and downward in a stroke plane largely orthogonal to swimming direction of aquatic animals. This provides a new sight in the future development of flexible paired flapping limbs for biomimetic underwater vehicles—to absorb and merge the advantages of both propulsors considering the concrete conditions.

c) Hydrodynamic Effects of Propulsor Motion on the Attached Body

The 3D hydrodynamic analysis method based on quais-steady wing element theory proposed in this dissertation can to some extent evaluate the hydrodynamic characteristics of sea turtles' forelimb motion. It shows prosthetic flippers play a positive role in generating thrust force but the thrust generated by the right flipper is larger than that generated by the left one. Another finding is that flipper flexibility plays a great role during the generation of thrust forces. Flexible Sho's flippers and Yu's actual flippers behave curvilinear motions and can bend actively in both the chordwise and spanwise directions, which correspondingly produce effective thrust force. But Yu's prosthetic flippers behave nearly linear motions and can only passively utilize the flexibility, which to some extent affect the effective generation of thrust.

Fundamental experiments on the straight forward and backward swimming performance of PLATYPUS verify that: (1) asymmetric rigid fin shows a little superiority than symmetric rigid fin although they possess different cross-sections; (2) the performance of flexible pectoral fins is better than that of rigid ones, which is a proof that flexibility plays a positive role in the generation of hydrodynamic forces; (3) the performance of two asymmetric elastic fins is almost the same, although softer fin possesses more flexibility than harder fin does. Iterative computation of spanwise deformation of asymmetric pectoral fins between Finite Element software and wing theory shows that asymmetric flexible softer fin can generate larger thrust force compared to asymmetric flexible harder fin and asymmetric rigid fin; lift force plays an important role in generating the thrust force; the investigation of tip deformation clarifies that spanwise deformation has positive influence on the generation of thrust force for elastic pectoral fins.

Two things have to be noted here. One is that wing element theory can be employed to roughly calculate the hydrodynamics of flapping-based swimming modes of both fishes and sea turtles, or probably even other aquatic animals (needing verification). The other is that the positive influence of fin or flipper flexibility on the thrust generation can be clearly seen from both the experiment and calculation results.

d) Effect of Fin Form and Flexibility on Motion Control of Underwater Vehicles

Point-to-point control tests in still water and water currents are employed to investigate the effects of pectoral fin movements to the motion control of PLATYPUS. From turning ability test of PLATYPUS using only rear fins the azimuth fuzzy control range is selected and it also shows asymmetric flexible softer fin cannot be used in PTP control because it could not propel PLATYPUS to rotate in counterclockwise direction; from swimming ability test of PLATYPUS using only fore fins the distance fuzzy control range is selected. During the PTP control tests it can be said that for different flexible pectoral fins it is advisable to adjust the controlling scheme of the propulsor and asymmetric flexible harder fin behaves better compared to asymmetric rigid fin and symmetric rigid fin. During the PTP control test in water currents symmetric rigid fin does better compared to the other two asymmetric fins. This is due to the feathering motion limitation of PLATYPUS, leading to asymmetric fins have to employ their trailing edges as leading edges to generate force to rotate the vehicle.

5.2 Future Works

1) One important thing that needs to be done in the future is to improve the hydro-dynamic calculation method. 2D wing element theory is adopted in both the hydro-

dynamics prediction of sea turtles' forelimb propulsion and the iterative computation of spanwise deformation of asymmetric pectoral fins. But from this method only concentrated point loads can be obtained on the one quarter position of the chord for each cross-section of the pectoral fin or fore flipper. In the future it is advisable to employ more precise computational fluid dynamic method to calculate the hydrodynamic pressure around the surface of the fore flipper or pectoral fin, by which the hydrodynamic prediction of sea turtles' forelimb motion would become much more accurate and the whole deformation both in the spanwise and chordwise direction of flexible pectoral fins can be investigated.

2) From the viewpoint of making prosthetic flippers for Yu, it can be seen that the thrust generated by the right flipper is larger than that generated by the left one. So in the future it is better to develop new prosthetic flippers or only install left prosthetic flipper, which maybe can make both flippers generate equal thrust and therefore Yu's swimming motion can become smooth.

3) During PTP control tests in water currents, it can be seen that asymmetric flexible pectoral fins do not behave very well due to the mechanical limitation of PLATYPUS itself and the special properties of the fin. In the future it is advisable to improve the shape and flexibility of pectoral fins to let them perform better in water currents or even more complicated environments.

Bibliography

[1] A. Azuma. The Biokinematics of Flying and Swimming Second Edition. Published by American Institute of Aeronautics and Astronautics, Inc., Reston, Virginia. ISBN: 1-56347-781-5 (2006).

[2] J. J. Videler. Fish Swimming, Chapman and Hall. ISBN: 978-0-412-40860-1 (1993).

[3] D. S. Barrett and M. S. Triantafyllou. The Design of a Flexible Hull Undersea Vehicle Propelled by an Oscillating Foil. Proceedings of the 9th International Symposium on Unmanned Untethered Submersible Technology, pp.111-123 (1995).

[4] J. M. Anderson and P. A. Kerrebrock. The Vorticity Control of an Unmanned Undersea Vehicle (VCUUV) Performance Results. Proceedings of the 11th International Symposium on Unmanned Untethered Submersible Technology, pp.360-369 (1999).

[5] D. Lachat, A. Crespi and A. J. Ijspeert. BoxyBot, the Fish Robot, Design and Realization. EPFL—Semester Project Report, Biologically Inspired Robotics Group (BIRG) (2005).

[6] D. S. Barrett, M. S. Triantafyllou, D. K. P. Yue, M. A. Grosenbaugh and M. J. Wolfgang. Drag Reduction in Fish-like Locomotion. Journal of Fluid Mechanics, Vol.392, pp.183-212 (1999).

[7] M. S. Triantafyllou, G. S. Triantafyllou and D. K. P. Yue. Hydrodynamics of Fishlike Swimming. Annual Review of Fluid Mechanics, Vol.32, pp.33-53 (2000).

[8] B. J. Borrell, J. A. Goldbogen and R. Dudley. Aquatic Wing Flapping at Low Reynolds Numbers: Swimming Kinematics of the Antarctic Pteropod, Clione Antarctica. The Journal of Experimental Biology, Vol.208, pp.2939-2949 (2005).

[9] S. Vogel. Life in Moving Fluid. Princeton: Princeton University Press (1994).

[10] W. F. Walker, Jr. Swimming in Sea Turtles of the Family Cheloniidae. Copeia, Vol.1971, No.2, pp.229-233 (1971).

[11] J. Davenport, S. A. Munks and P. J. Oxford. A Comparison of the Swimming of Marine and Freshwater Turtles. Proceedings of the Royal Society of London B, Vol.220, No. 1221, pp.447-475 (1984).

[12] S. Renous and V. Bels. Comparison Between Aquatic and Terrestrial Locomotions of the Leatherback Sea Turtle (Dermochelys Coriacea). Journal of Zoology, Vol.230, Iss.3, pp.357-378 (1993).

[13] J. Wyneken. Sea Turtle Locomotion: Mechanisms, Behavior and Energetics. The Biology of Sea Turtles, edited by P. Lutz and J. Musick, Boca Raton Florida: CRC Press, pp.165-198 (1997).

[14] J. A. Walker and M. W. Westneat. Mechanical Performance of Aquatic Rowing and Flying. Proceedings of The Royal Society of London B: Biological Science, Vol.267, No.1455, pp.1875-1881 (2000).

[15] C. M. Pace, R. W. Blob and M. W. Westneat. Comparative Kinematics of the Forelimb During Swimming in Red-eared Slider (Trachemys Scripta) and Spiny Softshell (Apalone Spinifera) Turtles. The Journal of Experimental Biology, Vol.204, pp.3261-3271 (2001).

[16] A. Konno, T. Furuya, A. Mizuno, K. Hishinuma, K. Hirata and M. Kawada. Development of Turtle-like Submergence Vehicle. Proceedings of the 7th International Symposium on Marine Engineering, Tokyo, pp.1-5 (2005).

[17] J. H. Long, J. Schumacher, N. Livingston and M. Kemp. Four Flippers or Two? Tetrapodal Swimming with an Aquatic Robot. Bioinspiration & BIomimetics, Vol.1, No.1, pp.20-29 (2006).

[18] S. Licht, M. Wibawa, F. S. Hover and M. S. Triantafyllou. Towards Amphibious Robots: Asymmetric Flapping Foil Motion Underwater Produces Large Thrust Efficiently. Proceedings of the 16th Annual International Symposium on Unmanned Untethered Submersible Technology, Durham, USA, pp.128-133 (2009).

[19] Y. Kawamura, J. Shimoya, E. Yoshida, N. Kato, H. Suzuki and H. Senga. Design and Development of Amphibious Robot with Fin Actuators. International Journal of Offshore and Polar Engineering, Vol.20, No.3 pp.175-180 (2010).

[20] W. Zhao, Y. Hu and L. Wang. Construction and Central Pattern Generator-Based Control of a Flipper-Actuated Turtle-like Underwater Robot. Advanced Robotics, Vol.23, No.1-2, pp.19-43 (2009).

[21] H. J. Kim, S. H. Song and S. H. Ahn. A Turtle-like Swimming Robot Using a Smart Soft Composite (SSC) Structure. Smart Materials and Structures, Vol.22, No.1, Paper No.014007 (2012).

[22] D. Font, M. Tresanchez, C. Siegentahler, T. Palleja, M. Teixido, C. Pradalier and J. Palacin. Design and Implementation of a Biomimetic Turtle Hydrofoil for an Autonomous Underwater Vehicle. Sensors (Basel, Switzerland), Vol.11, No.12, pp.11168-11187 (2011).

[23] C. C. Lindsey. Form, Function and Locomotory Habits in Fish. Fish Physiology Volume VII: Locomotion, edited by W. S. Hoar and D. J. Randall, New York, Academic Press, Inc., pp.1-100 (1978).

[24] R. W. Blake. The Mechanism of Labriform Locomotion I. Labriform Locomotion in the Angelfish (Pterphyllum Eimekei): An Analysis of the Power Stroke. The Journal of Experimental Biology, Vol.82, pp.255-271 (1979).

[25] G. V. Lauder, P. G. A. Madden, R. Mittal, H. Dong and M. Bozkurttas. Locomotion with Flexible Propulsions: I. Experimental Analysis of Pectoral Fin Swimming in Sunfish. Bioinspiration & BIomimetics, Vol.1, No.4, pp.S25-S34 (2006).

[26] N. Kato, Y. Ando, T. Ariyoshi, H. Suzuki, K. Suzumori, T. Kanda and S. Endo. Elastic Pectoral Fin Actuators for Biomimetic Underwater Vehicles. Bio-mechanisms of Swimming and Flying, edited by N. Kato and S. Kamimura, Springer-Verlag, pp.271-282 (2008).

[27] H. Suzuki, N. Kato and K. Suzumori. Load Characteristics of Mechanical Pectoral Fin. Experiments in Fluids, Vol.44, No.5, pp.759-771 (2008).

[28] J. Palmisano J. Geder, R. Ramamurti and et al.. Design, Development and Testing of Flapping Fins with Actively Controlled Curvature for an Underwater Vehicle. Bio-mechanisms of Swimming and Flying, edited by N. Kato and S. Kamimura, Springer-Verlag, pp.283-294 (2008).

[29] J. L. Tangorra, G. V. Lauder, P. G. Madden, R. Mittal, M. Bozkurttas and I. W. Hunter. A Biorobotic Flapping Fin for Propulsion and Maneuvering. Proceedings of IEEE International Conferences on Robotics and Automation, pp.700-705 (2008).

[30] J. D. Geder, J. S. Palmisano, R. Ramamurti, M. Pruessner, B. Ratna and W. C. Sandberg. Bioinspired Design Process for an Underwater Flying and Hovering Vehicle. Marine Technology Society Journal, Vol.45, No.4 pp.74-82 (2011).

[31] P. Liu and N. Bose. Propulsive Performance From Oscillating Propulsors With Spanwise Flexibility. Proceedings of the Royal Society of London A8, Vol.453, No.1963, pp.1763-1770 (1997).

[32] N. Bose. Performance of Chordwise Flexibility Oscillating Propulsors Using a Time-domain Panel Method. International Shipbuilding Progress, Vol.42, No.432, pp.281-294 (1995).

[33] P. Prepraneerach, F. S. Hover and M. S. Triantafyllou. The Effect of Chordwise Flexibility on the Thrust and Efficiency of a Flapping Foil. Proceedings of the 13th International Symposium on Unmanned Untethered Submersible Technology, Durham, USA, pp.120-128 (2003).

[34] K. Shoele and Q. Zhu. Fluid-structural Interactions of Skeleton-reinforced Fins: Performance Analysis of a Paired Fin in Lift-based Propulsion. The Journal of Experimental Biology, Vol.212, pp.2679-2690 (2009).

[35] N. K. Taft, G. V. Lauder and P. G. A. Madden. Functional Regionalization of the Pectoral Fin of the Benthic Longhorn Sculpin during Station Holding and Swimming. Journal of Zoology, Vol.276, No.2, pp.159-167 (2008).

[36] S. Ramakrishnan, M. Bozkurttas, R. Mittal and G. V. Lauder. Thrust Production in Highly Flexible Pectoral Fins: A Computational Dissection. Marine Technology Society Journal, Vol.45, No.4, pp.56-64 (2011).

[37] J. L. Tangorra, T. Gericke and G. V. Lauder. Learning From the Fins of Ray-finned Fish for the Propulsors of Unmanned Undersea Vehicles. Marine Technology Society Journal, Vol.45, No.4, pp.65-73 (2011).

[38] A. K. Elwaleed, N. A Mohamed, M. J. M. Nor and M. M. Mustafa. A New Concept of A linear Smart Actuator. Sensors and Actuators A: Physical, Vol.135, No.1, pp.244-249 (2007).

[39] J. Davenport, S. A. Munks and P. J. Oxford. A Comparison of the Swimming of Marine and Freshwater Turtles. Proceedings of the Royal Society of London B, Vol.220, No. 1221, pp.447-475 (1984).

[40] J. A. Walker and M. W. Westneat. Labriform Propulsion in Fishes: Kinematics of Flapping Aquatic Flight in the Bird Wrasse Gomphosus Varius (Labridae). The Journal of Experimental Biology, Vol.200, pp.1549-1569 (1997).

[41] E. G. Drucker and G. V. Lauder. Locomotior Forces on a Swimming Fish: Three-dimensional Vortex Wake Dynamics Quantified Using Digital Particle Image Velocimetry. The Journal of Experimental Biology, Vol.202, pp.2393-2412 (1999).

[42] Y. Isobe, N. Kato, H. Suzuki and others. Motion Analysis of Sea Turtle with Prosthetic Flippers. Proceedings of The International Society of Offshore and Polar Engineers 2010 Conference, Vol.2, pp.335-342 (2010).

[43] M. Nagai, I. Teruya, K. Uechi and T. Miyazato. Study on an Oscillating Wing Propulsion Mechanism. Transactions of the Japan Society of Mechanical Engineers. B, 62 (593), pp.200-206 (1996).

[44] M. Okamoto and Y. Jinba. Experimental Study on Aerodynamic Characteristics of Wing Platforms at Low Reynolds Number. Research Reports of Akita National College of Technology, 44, pp.42-50 (2009).

[45] K. Kato, A. Ooya and K. Karasawa. Introduction to Aerodynamics. University of Tokyo Press, ISBN: 978-4-13-061043-0, pp.41-42 (1982).

[46] K. P. Watson, R. A. Granger. Hydrodynamic Effect of a Satellite Transmitter on Juvenile Green Turtle. The Journal of Experimental Biology, Vol.201, No.17, pp.2497-2505 (1998).

[47] S. Heathcot and I. Gursul. Flexible Flapping Airfoil Propulsion at Low Reynolds Numbers. AIAA Journal, Vol.45, No.5, pp.1066-1079 (2007).

[48] P. Prepraneerach, F. S. Hover and M. S. Triantafyllou. The Effect of Chordwise Flexibility on the Thrust and Efficiency of a Flapping Foil. Proceedings of the 13th International Symposium on Unmanned Untethered Submersible Technology: Special Session on Bioengineering Research related to Autonomous Underwater Vehicles, New Hampshire (2003).

[49] N. Kato, H. Liu and H. Morikawa. Biology-inspired Precision Maneuvering of Underwater Vehicles. Proceedings of the 12th International Offshore and Polar Engineering Conference, pp.269-276 (2002).

[50] N. Kato, H. Liu and H. Morikawa. Biology-inspired Precision Maneuvering of Underwater Vehicle (Part 2). Proceedings of the 13th International Offshore and Polar Engineering Conference, pp.178-185 (2003).

[51] N. Kato, H. Liu and H. Morikawa. Biology-inspired Precision Maneuvering of Underwater Vehicle (Part 3). International Journal of Offshore and Polar Engineering, Vol.15, No.2, pp.81-87 (2004).

[52] N. Kato, Y. Ando and T. Shigetomi. Biology-inspired Precision Maneuvering of Underwater Vehicle (Part 4). International Journal of Offshore and Polar Engineering, Vol.16, No.3, pp.81-85 (2005).

[53] T. Ariyoshi, N. Kato, H. Suzuki, Y. Ando, K. Suzumori, T. Kanda and S. Endo. Elastic Pectoral Fin Actuators for Biomimetic Underwater Vehicle. Journal of The Japan Society of Naval Architects and Ocean Engineers, Vol.5, pp.15-25 (2007).

[54] T. Hisada and H. Noguchi. Essentials of Nonlinear Finite Element Method, Maruzen Publishing Co. Ltd, pp.54-63, ISBN: 9784621041253 (1972).

[55] R. W. Ogden. Large Deformation Isotropic Elasticity: On the Correlation of Theory and Experiment for Incompressible Rubber-like Solids. Proceedings of the Royal Society of London, Series A, Mathematical and Physical Sciences, Vol.326, No.1567, pp.565-584 (1972).

[56] R. W. Ogden, G. Saccomandi and I. Sgura. Fitting Hyperelastic Models to Experimental Data. Computational Mechanics, Vol.34, No.6, pp.484-502 (2004).

[57] N. Kato. Hydrodynamic Characteristics of Mechanical Pectoral Fin. Journal of Fluids Engineering, Transactions of The American Society of Mechanical Engineers, Vol.121, No.3, pp.605-613 (1999).

[58] S. Delcomyn. Neural Basis for Rhythmic Behavior in Animals. Science, Vol.210, No.4469, pp.492-498 (1980).

[59] D. Barrett, M. Grosenbaugh and M. Triantafyllou. The Optimal Control of a Flexible Hull Robotic Undersea Vehicle Propelled by an Oscillating Foil. Proceedings of the 1996 Symposium on Autonomous Underwater Vehicle Technology, pp.1-9 (1996).

[60] K. A. Harper, M. D. Berkemeier and S. Grace. Modeling the Dynamics of Spring-driven Oscillating-foil Propulsion. IEEE Journal of Oceanic Engineering, Vol.23, No.3, pp.285-296 (1998).

[61] F. Bullo, N. E. Leonard and A. D. Lewis. Controllability and Motion Algorithms for Underactuated Lagrangian Systems on Lie Groups. IEEE Transactions on Automatic Control, Vol.45, No.8, pp.1437-1454 (2000).

[62] S. Saimek and P. Y. Li. Motion Planning and Control of a Swimming Machine. The International Journal of Robotics Research, Vol.23, No.1, pp.27-53 (2004).

[63] J. Yu, M. Tan, S. Wang and E. Chen. Development of a Biomimetic Robotic Fish and Its Control Algorithm. IEEE Transactions on Systems, Man, and Cybernetics—Part B: Cybernetics, Vol.34, No.4, pp.1798-1810 (2004).

[64] C. Zhou and K. H. Low. Design and Locomotion Control of a Biomimetic Underwater Vehicle with Fin Propulsion. IEEE/ASME Transactions on Mechatronics, Vol.17, No.1 pp.25-35 (2012).

[65] L. A. Zadeh. Fuzzy Sets. Information and Control, Vol.8, pp.338-353 (1965).